

S-inflation: a testable, minimal model of
inflation and dark matter

Rose Natalie Lerner
MPhys (Hons)



August 2010

This thesis is submitted for the degree of Doctor of Philosophy.

Rose Natalie Lerner *MPhys (Hons)*

S-inflation: a testable, minimal model of inflation and dark matter

August 2010

This thesis is submitted to Lancaster University in partial fulfilment of the requirements for the degree of Doctor of Philosophy.

Abstract

This thesis describes work on inflationary cosmology, specifically in relation to observations. After reviewing the theory of inflation and dark matter, we introduce a model, ‘*S*-inflation’, in which a gauge singlet scalar *S* (with quartic self-coupling λ_s) is both thermal relic dark matter and the inflaton. This is made possible by its non-minimal coupling ξ_s to gravity, where $\frac{\xi_s}{\sqrt{\lambda_s}} \sim 4.6 \times 10^4$ at tree level. Reheating occurs primarily through a stochastic resonance to Higgs bosons, which then annihilate to relativistic particles. Primary importance is given to the predictions the model makes for the Higgs mass (m_h), spectral index (n) and *S* mass (m_s). Under reasonable assumptions, $130 \text{ GeV} < m_h < 170 \text{ GeV}$, $50 \text{ GeV} < m_s < 1 \text{ TeV}$ and $n > 0.966$. All of these are in principle within reach of the LHC, Planck and direct detection dark matter experiments, such as XENON100.

We then show that the renormalization group improved effective potential is a superior method to the standard Coleman Weinberg potential for calculating inflation observables. Then, we compare the predictions of *S*-inflation to those of pure Higgs inflation and Higgs inflation with an additional scalar. For $m_h \gtrsim 130 \text{ GeV}$, the models are in general distinguishable through the spectral index n , with $n > n_{cl}$ for *S*-inflation models and $n < n_{cl}$ for Higgs inflation. For \tilde{N} e-foldings of inflation, $n_{cl} \approx 1 - \frac{2}{\tilde{N}} - \frac{3}{2\tilde{N}^2} \approx 0.966$.

We next explain the origin of the apparent violation of unitarity at energy scales greater than $\Lambda \sim \frac{M_p}{\xi_s}$ (M_p is the reduced Planck mass). As we demonstrate, the calculation of the unitarity bound is done perturbatively, while the theory is non-perturbative at the energy of unitarity violation. Therefore, it is not possible to conclude whether or not unitarity is violated in the model. The model may instead be strongly coupled, meaning that the calculation of scattering amplitudes at $E \sim \Lambda$ becomes non-perturbative, while the analysis of inflation is unchanged.

If unitarity is shown to be violated in the original model, a new, unitarity conserving version

of the model can be considered. This has a simple form in the Einstein frame, and predicts a larger spectral index ($n \approx 0.975$) than the original model.

I dedicate this thesis to two of my grandparents
Dr. Natalie Hope Lerner and Professor Laurence David Lerner
for their continued support, encouragement and interest in my education.

Acknowledgements

I first wish to thank my supervisor, Dr. John McDonald, for always making time for me, and for patiently encouraging and supporting me during my three years in Lancaster. I have benefited hugely from many stimulating and thought-provoking discussions about cosmology. I look forward to collaborating in the future!

It is also a pleasure to thank members of the Cosmology and Astroparticle Physics Group, past and present, who have been the source of many interesting discussions. I owe particular thanks to the technical and administrative staff in the Department of Physics, who have made my time here run so smoothly.

While writing this thesis, I was supported by the Science and Technology Facilities Council (STFC) through a postgraduate studentship. I also acknowledge the generous support of the European Union, through the Marie Curie Research and Training Network “UniverseNet” (MRTN-CT-2006-035863).

Finally, I wish to thank those close to me for their encouragement and support. I extend particular thanks to my mum, my dad, Ele and Ros.

Declaration

The contents of Chapter 3 were previously published in [1]. The chapter results from original work done mainly by myself, under the guidance of my supervisor, John McDonald (with the exception of Sections 3.2.4 and 3.2.5, which were a collaborative effort between myself and John McDonald). Chapters 4 and 5 are mainly my own work and have not previously been published. The work in Chapter 6 was done in collaboration with John McDonald and is partially based on a published paper [2] and a paper in press [3].

Except where otherwise declared, this thesis is my own work and has not been submitted for the award of a higher degree elsewhere.

Rose Lerner

John McDonald

Contents

1	Introduction	1
1.1	Status of Cosmology	2
1.2	Inflation	4
1.2.1	Problems of the Hot Big Bang	4
1.2.2	Friedman and fluid equations	6
1.2.3	The scalar inflaton	7
1.2.4	Slow roll approximation	7
1.3	The primordial curvature perturbation	8
1.3.1	Fluctuations during inflation	8
1.3.2	The curvature perturbation	9
1.3.3	Parameters of the spectrum	10
1.3.4	Relationship to observations: the CMB spectrum	10
1.4	After Inflation	11
1.4.1	Reheating	11
1.4.2	Baryogenesis	13
1.5	Dark Matter	13
1.6	Minimal extensions to the Standard Model	16
1.7	Inflation with the Standard Model	17
2	Effective potential, renormalization group and bounds on field theories	19
2.1	Field theory	19
2.1.1	The concept of a field theory	19
2.1.2	The Standard Model	21
2.1.3	The effective action	22
2.1.4	Scattering amplitudes	23
2.1.5	Radiative corrections, regularisation and renormalization	24
2.1.6	The Callan-Symanzik equation	26

2.1.7	The Standard Model Coleman-Weinberg effective potential	27
2.1.8	The RG improved effective action	28
2.2	Bounds on the theory	29
2.2.1	Vacuum stability	29
2.2.2	Perturbativity	31
2.2.3	Unitarity	31
3	Connecting inflation and dark matter	34
3.1	The S -Inflation Model	34
3.1.1	Non-minimally Coupled Gauge Singlet Scalar Extension of the Standard Model	34
3.1.2	Conformal transformation	35
3.1.3	Jordan and Einstein Frames	37
3.1.4	Slow Roll Inflation	38
3.2	Radiative corrections	39
3.2.1	Coleman-Weinberg Potential	39
3.2.2	Suppression of Scalar Propagators	40
3.2.3	Initial conditions	42
3.2.4	RG equations for scalar couplings	43
3.2.5	RG equations for ξ_s and ξ_h	44
3.2.6	RG equations for gauge and Yukawa couplings	46
3.3	Constraints	47
3.3.1	Vacuum stability and perturbativity	47
3.3.2	Constraints from slow-roll inflation	48
3.4	Thermal relic dark matter	51
3.5	Parameter space for S -inflation	52
4	Reheating in S-inflation	59
4.1	Evolution of the oscillating inflaton	61
4.2	Reheating via stochastic resonance	62
4.2.1	Evolution of the Higgs boson modes	62
4.2.2	Stochastic resonance	66
4.3	An alternative mechanism of reheating	67
4.4	Relic density of the inflaton	68
4.5	Determining the temperature of radiation domination	71
4.5.1	Obtaining \tilde{N} from T_R	71

5	Comparing the predictions of S-inflation and Higgs inflation	75
5.1	Differing approaches to calculating the effective potential	75
5.2	A Comparison of two approaches to calculating the effective potential in pure Higgs inflation	78
5.2.1	The standard Coleman-Weinberg potential	79
5.2.2	The RG improved effective action	80
5.3	RG improved effective action is a more complete method	83
5.4	Distinguishing S -inflation from Higgs-inflation through observations	86
5.4.1	Defining the models	86
5.4.2	Theoretical differences	88
5.4.3	Higgs inflation in the presence of an additional scalar	88
5.4.4	S -inflation	90
5.4.5	Distinguishing the models observationally	92
5.4.6	Dependence on \tilde{N}	94
6	Naturalness and Unitarity	95
6.1	Unitarity violation in Higgs inflation models	96
6.1.1	The singlet scalar case	98
6.1.2	Non-polynomial potential	98
6.2	Breakdown of perturbation theory and strong coupling	100
6.2.1	Breakdown of perturbation theory <i>before</i> unitarity violation	100
6.2.2	Tree level unitarity violation can be misleading	101
6.3	The future of non-minimally coupled models of inflation	102
6.3.1	Avoiding the unitarity bound with small λ_s	102
6.3.2	Strong coupling as an alternative to unitarity violation	104
6.4	A Unitarity conserving model of Higgs inflation	104
6.4.1	The unitarity-conserving action	105
6.4.2	Cosmology of the unitarity conserving model	106
6.4.3	Radiative corrections favour S -type inflation model	107
7	Conclusions	109
	Appendix: Deriving the RG equations for scalar couplings	113
	Bibliography	117

List of Figures

3.1	Einstein frame potential, in limit $s \gg M_P/\sqrt{\xi}$ (dashed) and exact (solid). This figure is plotted for real S with $m_h = 160$ GeV, $\lambda_s(m_t) = 0.01$ and $\lambda_{hs}(m_t) = 0$	38
3.2	Showing the running of the scalar couplings λ_h (solid red), λ_s (green dashed) and λ_{hs} (blue dashed) and the suppression factor c_s (black dotted). The figure is plotted for real S with $m_h = 150$ GeV, $\lambda_s(m_t) = 0.2$, $\lambda_{hs}(m_t) = 0.1$ and $x_{is}(m_t) \approx 16500$ (chosen to match COBE normalisation of curvature perturbation). The figure is plotted in terms of $t = \ln(\mu/m_t)$, from $\mu = m_t$ to $\mu = M_p$. The suppression factor becomes important at the scale $\Lambda \sim \frac{M_p}{\xi_s}$	43
3.3	Showing the running of the non-minimal couplings ξ_h (solid red) and ξ_s (green dashed). The figure is plotted for real S with $m_h = 150$ GeV, $\lambda_s(m_t) = 0.2$, $\lambda_{hs}(m_t) = 0.1$, $\xi_h(m_t) = 0$ and $x_{is}(m_t) \approx 16500$ (chosen to match COBE normalisation of curvature perturbation). The figure is plotted in terms of $t = \ln(\mu/m_t)$, from $\mu = m_t$ to $\mu = M_p$	44
3.4	Showing the running of the gauge and Yukawa couplings: g (solid red), g' (green dashed), g_3 (blue dashed) and y_t (black dotted). The suppression factor c_s does not directly affect these couplings. The figure is plotted with $m_h = 150$ GeV, with $t = \ln \mu/m_t$ (from $\mu = m_t$ to $\mu = M_p$).	46
3.5	The value of m_s as a function of $\lambda_{hs}(m_t)$ necessary to produce the correct density of thermal relic dark matter. In this example $m_h = 150.0$ GeV. The solid line indicates real S and the dashed line complex S	51
3.6	Allowed region for inflation in the s -direction for $\lambda_s = 0.025$. Excluded regions are shown in grey. Limits from couplings in the s -direction are shown with dashed lines, those from the couplings running in the h -direction have solid lines and the $1\text{-}\sigma$ upper limit on n is dot-dashed. In (a) we also show the line $n = 0.981$ (dot-dot-dash) demonstrating the variation of n	53
3.7	Allowed region for inflation in the s -direction for $\lambda_s = 0.2$. Excluded regions are shown in grey. Limits from couplings in the s -direction are shown with dashed lines, those from the couplings running in the h -direction have solid lines and the $1\text{-}\sigma$ upper limit on n is dot-dashed.	54
3.8	Showing the variation of n with m_h for $\lambda_s(m_t) = 0.025$ and $\lambda_{hs}(m_t) = 0.16$. The WMAP central value and $1\text{-}\sigma$ upper bound are shown with short dashed lines; classical n for S -inflation is shown with a dashed line.	55

3.9	Allowed region for inflation in the s -direction, with a $1\text{-}\sigma$ upper limit on n . Excluded regions are shown in grey and all masses are in GeV. The dashed line shows $m_h = 2m_s$. Below this line, production of S -particles at the LHC (via $h \rightarrow S^\dagger S$ decay) is possible. There is no allowed region in (d).	56
3.10	Figure showing dark matter cross sections (a) predicted for this model and (b) projected for the XENON1T detector.	58
4.1	Showing the value of $\frac{X_{sto}}{X_{CR}}$ for regions of the parameter space where reheating via stochastic resonance can complete before X_{CR}	66
4.2	Showing the value of $\frac{X_{ex}}{X_{CR}}$ for regions of the parameter space where reheating via production of S excitations can complete before X_{CR} . Note that the scale has a much smaller range than Fig. (4.1).	68
4.3	Showing the regions of the λ_s and λ_{hs} parameter space allowed by the constraints of reheating. The shaded region is excluded. In most of the region marked ‘both’, $X_{sto} > X_{ex}$ (as can be seen by comparing Fig. (4.1) and Fig. (4.2)), therefore reheating via stochastic resonance is expected to dominate for the majority of this region.	72
5.1	Showing n as a function of m_h for Higgs inflation, taken from papers in the literature — see text for details of each method. Although general features are in agreement between some figures (particularly (b) and (c)), it is not apparent which prediction is to be trusted.	76
5.2	Spectral index n versus Higgs mass m_h for Coleman-Weinberg (solid red) and RG improved (green dashed) methods.	84
5.3	Tensor to scalar ratio r versus Higgs mass m_h for Coleman-Weinberg (solid red) and RG improved (green dashed) methods.	85
5.4	Spectral index n versus Higgs mass m_h for inflation in the Higgs direction with $\lambda_s = 0$ and varying λ_{hs} : $\lambda_{hs} = 0$ (pure Higgs inflation; red), $\lambda_{hs} = 0.1$ (green), $\lambda_{hs} = 0.3$ (pink) and $\lambda_{hs} = 0.5$ (blue).	89
5.5	Spectral index n versus Higgs mass m_h for inflation in the Higgs direction, with $\lambda_s = 0.0$ (solid red) and $\lambda_s = 0.15$ (green dashed).	90
5.6	Spectral index n versus Higgs mass m_h for inflation in the S-direction with $\lambda_{hs} = 0.0$: $\lambda_s = 0.01$ (solid red) and $\lambda_s = 0.25$ (green dashed). ‘Pure’ Higgs inflation is shown for comparison (solid black)	91
5.7	Spectral index n versus Higgs mass m_h for inflation in the S -direction, with $\lambda_s = 0.1$ (solid) and $\lambda_s = 0.01$ (dashed). Various values of λ_{hs} are shown: $\lambda_{hs} = 0.0$ (black), $\lambda_{hs} = 0.01$ (blue), $\lambda_{hs} = 0.1$ (red), $\lambda_{hs} = 0.3$ (green) and $\lambda_{hs} = 0.5$ (pink).	91

5.8	Spectral index n versus Higgs mass m_h for inflation in the S-direction (pink circles), for inflation in the H-direction (blue circles) and pure Higgs inflation (solid green line). Couplings have been varied by 0.1 and required to remain less than 100.	92
5.9	Tensor to scalar ratio r (log scale) versus Higgs mass m_h for inflation in the S-direction (pink circles), for inflation in the H-direction (blue circles) and pure Higgs inflation (solid green line). Couplings have been varied by 0.1 and required to remain less than 100.	93
6.1	Feynman diagram for the scattering of two scalars: $\phi_1\phi_2 \rightarrow \phi_1\phi_2$	97
6.2	Showing the ratio $\frac{U^{\frac{1}{4}}}{\Lambda}$ (solid black line). The ratio becomes less than 1 for $\lambda_s < 4.3 \times 10^{-5}$. . .	103

Chapter 1

Introduction

This thesis deals with the connection between the beginning of the observable Universe and particle physics. Specifically, we will consider the observational predictions and theoretical basis of ‘ S -inflation’ — a minimal model of inflation where the inflaton also serves as dark matter. This model will be tested by future cosmological observations and particle physics experiments.

We use this introductory chapter to motivate the work contained in this thesis. First, in Section 1.1, we outline the status of cosmology at present. Section 1.2 introduces inflation and the slow roll formalism, which is developed in Section 1.3 to describe the primordial curvature perturbation and its connection to observations. Consideration of the transition between the end of inflation and the current Universe is essential and will be discussed in Section 1.4. Our work concerns the connection between inflation and dark matter — so in Section 1.5 we discuss the evidence for dark matter and the Lee-Weinberg approximation, used to calculate the current density of dark matter. Many (often well motivated) extensions to the Standard Model are complicated — such as supersymmetry (SUSY). However, in this thesis we consider a very minimal extension of the Standard Model. In Section 1.6 we discuss this philosophy of minimalness and review a particular minimal model known as the ν MSM. Finally, Section 1.7 discusses inflation in the context of minimal models. Further background — mainly field theory and renormalization — is contained in the following chapter.

Conventions

In this thesis, M_p is the reduced Planck mass, defined by $M_p = (8\pi G)^{-\frac{1}{2}}$. The constants c , k_B and \hbar are set to 1 unless explicitly stated. Unless otherwise defined, a dot (e.g. $\dot{\phi}$) is a derivative with respect to cosmic time t and a dash (e.g. V') is a derivative with respect to the relevant field. Our sign convention is $(+, -, -, -)$.

1.1 Status of Cosmology

In general, cosmology is a discipline of observation rather than experiment — we cannot recreate the formation of the Universe. Fortunately, these observations are becoming extremely precise — specifically, observations of the cosmic microwave background (CMB) radiation and of the distribution of large scale structure in the Universe. High energy particle physics and high energy astroparticle physics experiments also contribute towards our understanding of the Universe. The Large Hadron Collider (LHC) at CERN should reach a centre of mass energy of 14 TeV in the next few years — much lower than the energy of the big bang, but hopefully high enough to discover new particles. The Planck satellite, launched in May 2009, will measure the anisotropy of the CMB radiation over the whole sky, improving on earlier observations by WMAP (Wilkinson Microwave Anisotropy Probe) and COBE (COsmic Background Explorer). This will provide precise measurements of the spectral index of the CMB anisotropy, as well as measurements or improved upper bounds for the ratio of scalar to tensor modes and the running of the spectral index, all of which should help to constrain models of inflation. Just as important are direct and indirect dark matter detection experiments such as CDMSII (Cryogenic Dark Matter Search), XENON100 and DAMA/LIBRA (DARK MATter / Large sodium Iodide Bulk for RARE processes). The model presented in this thesis, *S*-inflation, could easily be ruled out or favoured by any of these experiments.

Hot Big Bang

In 1929, Hubble published measurements of the velocities (v) and separations (r) of a selection of galaxies [4]. This gave the relationship $v \simeq H_0 r$ (where H_0 is known as the Hubble constant), which means that each galaxy is receding from each other galaxy at a speed proportional to the separation of the two galaxies. Assuming the cosmological principle, which states that the Universe is homogeneous and isotropic on large scales, we can draw the conclusion that all space is expanding, carrying the non-expanding gravitationally-bound structures (such as galaxies and galaxy clusters) along with it. Extrapolating backwards from this, we can suppose that the Universe was once very hot and very dense — this is the Hot Big Bang. Inflation, discussed in Section 1.2, provides the necessary initial conditions for the hot big bang (the initial conditions for inflation then become the important issue).

Starting from this hot and dense period, the Universe expanded and cooled. It became energetically favourable to form protons and neutrons, and then atoms. Different particle species stopped interacting with each other and began to evolve separately. The CMB was formed (approximately 380,000 years after the beginning of the hot big bang) when photons could no

longer interact with atoms and so travelled unhindered¹. As the Universe expanded, CMB photons cooled to a current temperature of 2.73 K [5]. The CMB radiation was discovered by Penzias and Wilson [6], who observed microwave radiation (at one wavelength) with the same effective temperature at each point in the sky. It has now been confirmed (by COBE, WMAP and Earth-based experiments) that the radiation is blackbody radiation with a temperature in each direction in the sky which is the same to one part in 10^5 (once the dipole has been subtracted).

Robertson-Walker metric

The metric $g_{\mu\nu}$ relates coordinates to the invariant interval,

$$ds^2 = g_{\mu\nu} dx^\mu dx^\nu. \quad (1.1)$$

The cosmological principle states that the Universe is homogeneous and isotropic on large scales. This has not been conclusively proven by observations and is an assumption that we will use throughout this thesis. The cosmological principle greatly restricts the form of the metric. Assuming the cosmological principle, the Universe can be described by the Robertson-Walker metric in either physical coordinates ($a(t)x_i$ and t) or comoving coordinates (x_i and τ), where the expansion of the Universe has been factored out. If the Universe is flat (the main evidence for this is given by CMB observations [5, 7], for example), it is

$$\begin{aligned} ds^2 &= -dt^2 + a^2(t) \sum_{i=1}^3 dx_i^2 \\ &= a^2(\tau) \left(-d\tau^2 + \sum_{i=1}^3 dx_i^2 \right) \end{aligned} \quad (1.2)$$

where $a(t)$ is the scale factor (which must only be a function of time because of the assumed homogeneity and isotropy). For fixed t , spatial slicings are homogeneous and isotropic; the threading is orthogonal to this slicing. Eq. (1.2) is only valid for the *background* homogeneous and isotropic evolution of the Universe, not for the evolution of perturbations.

Energy density of the Universe

The amount of matter in the Universe is usually measured in terms of the density parameter

$$\Omega = \sum_i \Omega_i = \frac{\sum_i \rho_i}{\rho_c}, \quad (1.3)$$

¹Almost... small effects such as the Sunyaev-Zeldovich effect do involve interactions with CMB photons.

where ρ_c is the critical density of the Universe:

$$\rho_c = \frac{3H^2}{8\pi G} \quad (1.4)$$

and the Hubble parameter H is

$$H = \frac{\dot{a}}{a}. \quad (1.5)$$

Components contributing to Ω include relativistic matter, non-relativistic baryons, dark matter and dark energy.

1.2 Inflation

Inflation is a short period of extremely rapid (nearly exponential) expansion of space defined by the acceleration of the scale factor:

$$\ddot{a} > 0. \quad (1.6)$$

In contrast, the expansion of the Universe in the Hot Big Bang is *decelerating* ($\ddot{a} < 0$). Equivalently, inflation is any period of time when the *comoving* Hubble radius (the event horizon), $H(t)^{-1}$, is decreasing. We believe that the entire (observable) Universe has grown from a tiny, causally connected patch. Inflation sets the initial conditions for the hot big bang as a flat, homogeneous, isotropic and hot Universe in thermal equilibrium.

Since the beginning of the hot big bang, light could have travelled a distance equal to the *particle horizon*. Events separated by more than the particle horizon could never have had a common causal root. The particle horizon X_{ph} in comoving coordinates (assuming the metric Eq. (1.2)) is [8]

$$X_{ph}(t) = \int_{t_0}^t \frac{dt}{a}, \quad (1.7)$$

where t_0 is some early time where the metric is valid. The event horizon X_{event} is

$$X_{event}(t) = \int_t^\infty \frac{dt}{a}. \quad (1.8)$$

1.2.1 Problems of the Hot Big Bang

Various observations are not easily explained purely within the Hot Big Bang model. Inflation provides an explanation for these observations — and this is discussed below. However, inflation also raises questions of its own, particularly questions about how inflation could begin. It is beyond the scope of this thesis to discuss the initial conditions for inflation in detail.

The Universe is flat

While the Universe is decelerating (most of its history), $|\Omega - 1|$ increases². The current measured value of Ω is very close to 1. Therefore, at the beginning of the big bang, Ω must have been even closer to 1. This is considered to be a very finely tuned initial condition and in need of an explanation. Inflation offers the explanation: in an accelerating Universe, Ω is driven *towards* 1 — so any initial Ω before inflation would still lead to our currently observed value.

The Universe is homogeneous

We mentioned above that the CMB is the same temperature in all directions, to high accuracy. From the beginning of the hot big bang until now, opposite sides of the sky could never have been in causal contact as they are separated by much more than the current particle horizon (Eq. (1.7))³. Therefore, without inflation, there is no clear way to explain how the temperatures are the same. The inflation explanation is that the entire observable Universe *was* originally in causal contact. During inflation, the comoving Hubble radius decreases. Therefore, at the end of inflation, the entire Universe is no longer in causal contact although it is at the same temperature due to the fact that it *was* once in causal contact.

We do not observe monopoles

We do not observe monopoles, topological defects or various other particles which could (in theory) be produced at high enough energies. Inflation explains this: any particle species existing before inflation would be diluted out of existence in only a few e-foldings. The hot big bang begins after inflation at a finite temperature (the exact temperature depends on the particular model of inflation and reheating) which can be low enough to avoid thermal production of the particles which we do not observe. However, this is not a strong motivation for inflation on its own, as it can be explained if the Hot Big Bang had a maximum temperature much lower than the GUT (Grand Unified Theory) temperature (10^{16} GeV). In that case we would not expect monopoles (which are GUT particles) to be produced in thermal equilibrium, thus removing the problem. Monopoles would only be produced anyway if the GUT group is semi-simple.

Perturbations are the seeds for galaxies

This is the most important motivation for inflation. The CMB is measured by COBE and WMAP to have small perturbations in its blackbody spectrum ($\frac{\delta T}{T}$ is approximately 10^{-5}). The perturbations have a clear, oscillating power spectrum over a wide range of angular scales. These

²Unless $|\Omega - 1|$ is initially *exactly* equal to zero.

³It is important to note that we have no real understanding of physics at the Planck scale, so for example the Universe could have some strange causal structure at the Planck scale.

temperature perturbations are due to perturbations in the energy density (through the Sachs-Wolfe effect). The density perturbations are due to perturbations in a field during inflation according to the inflationary paradigm. As the density perturbations evolved after the time of decoupling, gravitational collapse occurred and structure in the Universe began to form. A power spectrum of the large scale structure (LSS) can be made, and its features mapped onto the CMB power spectrum⁴. Inflation can explain the fluctuations in the CMB as random quantum fluctuations which are ‘frozen in’ during inflation as each scale leaves the horizon. Perturbations produced during inflation are mostly Gaussian (matching observation) and naturally occur on superhorizon scales (again matching observation). It is difficult to produce Gaussian superhorizon perturbations by any other mechanism.

1.2.2 Friedman and fluid equations

Einstein’s field equation is

$$R_{\mu\nu} - \frac{1}{2}g_{\mu\nu}R = \frac{1}{M_p^2}T_{\mu\nu} \quad (1.9)$$

where $T_{\mu\nu}$ is the energy-momentum tensor, $R_{\mu\nu}$ is the Ricci tensor and R is the Ricci scalar. In a homogeneous and isotropic Universe, the 0-0 component of Eq. (1.9) is known as the Friedmann equation:

$$H^2 = \frac{\rho}{3M_p^2} - \frac{K}{a^2} \quad (1.10)$$

where $H = \frac{\dot{a}}{a}$. We only consider a flat geometry in this thesis (according to observation), so $K = 0$ from here onwards.

A second useful equation is known as the fluid equation:

$$\dot{\rho} + 3H(\rho + p) = 0 \quad (1.11)$$

where ρ is energy density and p is pressure. This is derived using the expression $\nabla_\mu T^{\mu\nu} = 0$. A third equation, not independent of the Friedmann or fluid equations, can be derived by differentiating the Friedmann equation (Eq. (1.10)) and using the fluid equation (Eq. (1.11)):

$$\frac{\ddot{a}}{a} = -\frac{1}{6M_p^2}(\rho + 3p). \quad (1.12)$$

This is known as the acceleration equation.

⁴The features of the LSS power spectrum are less clear than for the CMB due to many non-linear processes occurring between the formation of the CMB and structure formation.

1.2.3 The scalar inflaton

To achieve $\ddot{a} > 0$ necessary for inflation, according to Eq. (1.12) we require $p < -\frac{\rho}{3}$. The simplest way to achieve this is for the Universe to be dominated by a homogeneous scalar condensate with energy density

$$\rho = \frac{1}{2}\dot{\phi}^2 + V(\phi) \quad (1.13)$$

and pressure

$$p = \frac{1}{2}\dot{\phi}^2 - V(\phi). \quad (1.14)$$

Provided that $\dot{\phi}^2 \ll V(\phi)$, then $p \simeq -\rho$. The condition $p < -\frac{\rho}{3}$ must hold for long enough to create the flat, homogeneous Universe that we observe.

1.2.4 Slow roll approximation

Considering a homogeneous single field ϕ (called the inflaton) which dominates the Universe, the Friedmann equation is

$$3M_p^2 H^2 = V(\phi) + \frac{1}{2}\dot{\phi}^2 \quad (1.15)$$

and field equation (derived in Section 2.1.1), is

$$\ddot{\phi} + 3H\dot{\phi} + \frac{dV}{d\phi} = 0. \quad (1.16)$$

Most models of inflation satisfy the slow roll approximation which assumes

- the $\dot{\phi}$ term in Eq. (1.15) is negligible, so

$$3M_p^2 H^2 \simeq V(\phi), \quad (1.17)$$

- the $\ddot{\phi}$ term in the field equation (Eq. (1.16)) is negligible, so

$$3H\dot{\phi} \simeq -\frac{dV}{d\phi} \equiv -V' \quad (1.18)$$

- and that differentiating Eq. (1.18) is valid, so

$$\ddot{\phi} \simeq -\frac{\dot{H}}{H}\dot{\phi} - \frac{V''}{3H}\dot{\phi}. \quad (1.19)$$

These can equivalently be written in terms of the slow roll parameters η and ϵ :

$$\epsilon \equiv \frac{M_p^2}{2} \left(\frac{V'}{V} \right)^2 \ll 1 \quad (1.20)$$

$$|\eta| \equiv \left| M_p^2 \frac{V''}{V} \right| \ll 1. \quad (1.21)$$

Subsequent slow roll parameters can be defined. We will use⁵

$$\vartheta \equiv M_p^4 \frac{V'V'''}{V^2} \ll 1. \quad (1.22)$$

1.3 The primordial curvature perturbation

Quantum mechanics dictates that a field will always have fluctuations about its classical value. The fluctuations during inflation are frozen as they leave the horizon. Under suitable conditions, the spectrum of the fluctuations of certain fields can form the curvature perturbation, which is constant on superhorizon scales⁶. The curvature perturbation gives the perturbation in the total energy density and can be seen imprinted on the CMB and the spectrum of structure in the Universe. Other forms of primordial perturbation include the tensor perturbation and the isocurvature perturbation; however our main concern is the curvature perturbation.

1.3.1 Fluctuations during inflation

Well before a particular scale exits the horizon, fluctuations of the inflaton field are vacuum fluctuations in a flat space-time background because these subhorizon scales are less than the curvature radius H^{-1} (the scalar curvature is $R \sim H^2$). In conformal time τ , the perturbation of ϕ is

$$\psi_k \equiv a\delta\phi_k \quad (1.23)$$

which obeys the mode equation [8]

$$\frac{d^2\psi_k(\tau)}{d\tau^2} + \omega_k^2(\tau)\psi_k(\tau) = 0 \quad (1.24)$$

where

$$\omega_k^2 = k^2 - \frac{2}{\tau^2}. \quad (1.25)$$

⁵This is usually denoted by ξ but we use ϑ to avoid confusion with the non-minimal coupling.

⁶It is constant provided that pressure depends only on the energy density.

Well after horizon exit, the solution is [8]

$$\psi_k(\tau) = -\frac{i}{\sqrt{2k}} \frac{1}{k\tau}. \quad (1.26)$$

The spectrum is the two-point correlator, and is defined as

$$\langle \delta\phi_{\vec{k}} \delta\phi_{\vec{k}'} \rangle = \frac{2\pi^2}{k^3} \mathcal{P}_{\delta\phi} \delta^3(\vec{k} + \vec{k}'). \quad (1.27)$$

The spectrum of $\delta\phi$ (conformal time for $H \sim \text{constant}$ is $\tau = (aH)^{-1}$) is therefore

$$\mathcal{P}_{\delta\phi} = \left(\frac{H}{2\pi} \right)^2 \Big|_{k=aH}. \quad (1.28)$$

This is evaluated at ‘horizon crossing’ when the wavelength of the perturbations becomes equal to the size of the event horizon. After this, the perturbations are frozen in and do not change (in comoving coordinates). Due to the above, the typical perturbation of the field is $\delta\phi \approx \sqrt{\mathcal{P}_{\delta\phi}} = \frac{H}{2\pi}$.

1.3.2 The curvature perturbation

On a flat slicing⁷, the first order curvature perturbation is [8]

$$\zeta = H\delta t = -H \frac{\delta\phi}{\phi}. \quad (1.29)$$

The curvature perturbation spectrum is given by

$$\langle \zeta_{\vec{k}} \zeta_{\vec{k}'} \rangle = \frac{2\pi^2}{k^3} \mathcal{P}_{\zeta} \delta^3(\vec{k} + \vec{k}'). \quad (1.30)$$

Given that the spectrum of $\delta\phi$ is given by Eq. (1.28), the curvature perturbation spectrum is therefore

$$\mathcal{P}_{\zeta} = \frac{1}{4\pi^2} \left(\frac{H^2}{\phi} \right)^2 \Big|_{k=aH}. \quad (1.31)$$

Using the slow roll approximations (Section 1.2.4) we can write this as

$$\mathcal{P}_{\zeta} = \frac{1}{24\pi^2 M_p^4} \frac{V}{\epsilon} \Big|_{k=aH}. \quad (1.32)$$

⁷A slicing of spacetime is defined by considering hypersurfaces with fixed x^0 . A flat slicing has zero spatial curvature.

The tensor perturbation

In the slow roll approximation, the primordial tensor perturbation spectrum is [8]

$$\mathcal{P}_h(k) = \frac{8}{M_p^2} \left(\frac{H}{2\pi} \right)^2 \Big|_{k=aH}. \quad (1.33)$$

The tensor to scalar ratio is given using Eq. (1.32) and Eq. (1.33):

$$r \equiv \frac{\mathcal{P}_h}{\mathcal{P}_\zeta} \approx 16\epsilon. \quad (1.34)$$

1.3.3 Parameters of the spectrum

Assuming the spectrum of the curvature perturbation can be parameterised as a power law

$$\mathcal{P}_\zeta \propto k^{n-1}, \quad (1.35)$$

the spectral index is given by

$$n(k) - 1 = \frac{d \ln \mathcal{P}_\zeta}{d \ln k} \Big|_{k=aH} \quad (1.36)$$

where $d \ln(aH) \simeq H dt$ (assuming \dot{H} is negligible). Using the slow roll approximations and the spectrum Eq. (1.32), the spectral index can be written in terms of ϵ and η as

$$n = 1 + 2\eta - 6\epsilon. \quad (1.37)$$

Similarly, the running of the spectral index is given by

$$\alpha \equiv \frac{dn}{d \ln k} \Big|_{k=aH} = -16\eta\epsilon + 24\epsilon^2 + 2\vartheta. \quad (1.38)$$

1.3.4 Relationship to observations: the CMB spectrum

We observe the CMB anisotropy and the distribution of galaxies. This allows us to reconstruct the curvature perturbation, $\mathcal{P}_\zeta(k)$ and compare with predictions. The quantities $\mathcal{P}_\zeta(k_0)$, n , r and α are calculated from the theory at horizon exit during inflation. Ignoring the monopole and dipole moments⁸), the brightness function Θ is [8]

$$\frac{\delta T}{T} \equiv \Theta(\tau, \vec{x}, \vec{n}) = \sum_{lm} (-1)^l Y_{lm}(\vec{n}) \Theta_{lm}(\tau, \vec{x}). \quad (1.39)$$

⁸The dipole moment has $\frac{\delta T}{T} \sim 10^{-3}$ and is probably due to the Earth's motion in the CMB rest frame.

This has been expanded in terms of spherical harmonics Y_{lm} , where \vec{n} is the direction of the photon momentum and τ is conformal time.

Now considering the fourier component of the brightness function for scalar modes only, we see that [8]

$$\Theta(\tau, \vec{k}, \vec{n}) = \sum_l (-i)^l \sqrt{4\pi(2l+1)} Y_{l0}(\vec{n}) \Theta_l(\tau, \vec{k}), \quad (1.40)$$

where

$$\Theta_l(\vec{k}) = T_l(k) \zeta_k. \quad (1.41)$$

Eq. (1.41) defines the transfer function, T_l , which encodes the effects of the physical processes between horizon exit during inflation and photon decoupling. The spectrum of the CMB anisotropy is then

$$C_l = \langle |\Theta_{lm}|^2 \rangle = 4\pi \int_0^\infty T_l^2(k) \mathcal{P}_\zeta(k) \frac{dk}{k}. \quad (1.42)$$

1.4 After Inflation

Inflation needs to last for only a brief moment and usually ends when the inflaton field rolls quickly towards the minimum of the potential, violating the slow roll conditions. Reheating is the transfer of energy from the inflaton field to a relativistic radiation-like gas. This is the beginning of the transition to low energy particle physics described by the Standard Model. Some time later, electroweak symmetry breaking occurs (in the Standard Model this is a crossover process) followed by chiral symmetry breaking (when QCD becomes strong enough to form a quark condensate). Around this time, the quarks form into hadrons.

It is assumed that the net baryon number in the Universe is initially zero, because leptons are formed in pairs with anti-leptons and hadrons with anti-hadrons. Thus we need a mechanism to create a net baryon number; this is known as ‘baryogenesis’. Baryogenesis could also take place through leptogenesis, where a net lepton number is generated and transformed into a net baryon number by non-perturbative processes which violate $B + L$. Nucleosynthesis — the formation of nuclei (particularly hydrogen and helium) begins at $T \sim 1$ MeV, about 3 seconds after the end of inflation.

1.4.1 Reheating

As the inflaton ϕ nears the minimum of its potential it begins to oscillate with a frequency ω and amplitude ϕ_{end} . A simple reheating mechanism is for the inflaton to decay to Standard Model particles as it oscillates; other mechanisms usually fall under the category of ‘preheating’. For simple reheating, the decay rate is $\Gamma \sim \frac{g^2}{4\pi} m$ where the decay could be through gauge couplings

($g \sim 0.1$), gravitational strength couplings ($\sim \frac{m}{M_p}$) or anything else in between. For this decay to be effective we need $\Gamma \sim H$ and $\Gamma \lesssim \omega$ (in order to have time for the inflaton to oscillate). In most models of inflation, the coupling of the inflaton to the Standard Model is unknown, so the precise details of reheating cannot be calculated. In a realistic model it is likely that a combination of mechanisms contribute towards reheating the Universe.

It is not sufficient only to produce relativistic particles. These must then *thermalise* in order to complete the process of reheating. This is not trivial and requires $2 \rightarrow 3$ process to occur.

We can usually ignore the expansion of the Universe, as the production of relativistic particles occurs in a time much shorter than the characteristic timescale of the expansion, H^{-1} . Inflation gives the initial condition that the occupation number of all states (except the zero mode of the inflaton) is small: $n_k \ll 1$. This is because the inflaton is a homogeneous condensate and all other particle species have been diluted to tiny occupation numbers by inflation.

Preheating

While standard reheating requires a small vacuum expectation value (vev) or oscillations of the inflaton, this is not required for preheating. In general, preheating produces a non-equilibrium gas which should decay or scatter to produce thermal radiation. Assuming the inflaton vev is at zero and that it couples to another field χ (with negligible mass), the potential is

$$V = \frac{1}{2}m_\phi^2\phi^2 + \frac{1}{2}g^2\phi^2\chi^2 + \dots$$

The equation of motion for the modes of χ is

$$\ddot{\chi}_k + E_k(t)^2\chi_k = 0$$

where $E_k^2(t) = \left(\frac{k}{a}\right)^2 + m_\chi^2(t)$. There are no χ particles during inflation, because E_k only varies adiabatically. After inflation, ϕ oscillates and $m_\chi^2(t) = g^2\phi_{end}^2 \sin^2(m_\phi t)$. This gives a Mathieu equation

$$\frac{d^2\chi_k}{dz^2} + [A(k) - 2q \cos(2z)]\chi_k = 0 \tag{1.43}$$

where $A = \frac{k^2}{m_\phi^2} + 2q$, $q = \frac{g^2\phi_{end}^2}{4m_\phi^2}$ and $z = m_\phi t$. For particular values of A and q , χ_k can grow rapidly, giving a parametric resonance which quickly drains energy from the inflaton field.

Other mechanisms of preheating exist and include instant preheating [9] and tachyonic preheating [10]. Instant preheating occurs very quickly and the inflaton only passes through zero once. This is because a strong coupling to fermions means that ϕ can decay very quickly at its oscillation maximum, draining energy almost instantly from the inflaton field. Tachyonic

preheating produces excitations of the inflaton. The background inflaton has a negative mass-squared, becoming more negative with time. Excitations of ϕ are created when the mass-squared becomes negative, as it is non-adiabatic at this point. The excitations can then annihilate or decay to produce thermal radiation, through $2 \rightarrow 3$ processes.

1.4.2 Baryogenesis

In order for baryogenesis to occur, three conditions (known as the Sakharov conditions [11]) must be met. These are

- (i) baryon number must be violated in some process(es),
- (ii) C (charge) and CP (charge-parity) symmetries must be broken (otherwise any baryons created would be cancelled by an equal number of anti-baryons) and
- (iii) the processes must be out of equilibrium, otherwise everything is just as likely to occur in reverse, producing no net baryon number (equivalent to CPT (where T is time) violation).

There are a number of scenarios where baryogenesis occurs. Particularly interesting for this thesis are Electroweak baryogenesis which occurs at the electroweak transition, and baryogenesis via resonant leptogenesis.

1.5 Dark Matter

If the Universe is at the critical density, $\Omega = 1$, then it has a flat geometry ($K = 0$ in Eq. (1.10)). CMB fluctuations [5, 12] and data from distant supernovae [13, 14] confirm that this is true (it is also a consequence of any inflation model). The amount of baryonic matter that we observe in clusters and dust is not sufficient to account for $\Omega = 1$ today; it only gives $\Omega_B \simeq 0.04$. There are two components to the remaining 96% of the energy density — dark matter and dark energy. Dark energy has a negative pressure and if it dominates, it causes acceleration expansion of the Universe. It makes up the proportion of Ω which is not accounted for by baryonic matter or dark matter, but is only dominant at late times, so will not concern us in this thesis. Dark matter makes up about 23% of Ω . A number of observations are explained by dark matter and these include the following.

- Bullet cluster — a collision between two galaxies clusters provides direct observational evidence for dark matter. Visible matter is mostly in the centre of the system as observed by x-rays (when the clusters collided, visible matter was slowed by electromagnetic inter-

actions). However weak gravitational lensing shows most of the mass to be further away (dark matter was not slowed by electromagnetic interactions) [15, 16].

- Formation of structure in the Universe — simulations including dark matter closely match the spectrum of structure observed [17].
- Rotation curves of galaxies — the speed of rotation of stars in galaxies is approximately constant with distance from the centre. However, the visible matter present corresponds to a Newtonian potential where the rotation speed would *fall* with distance. Therefore there must be some non-visible matter present [18].
- Gravitation lensing — independently from the dynamical measurement of rotation curves, general relativity can be used to determine the gravitational mass of clusters through gravitational lensing. This mass is much greater than expected, given the amount of luminous matter present, implying the presence of dark matter.
- CMB spectrum — the height and position of the peaks is fitted well by a model containing cold dark matter (CDM).

Dark matter could be composed of anything that does not interact except through gravitational attraction (or interacts extremely weakly) with particles in the Standard Model. Candidates with zero pressure (CDM) are currently favoured by observations, although do give rise to the substructure problem and the cuspy halo problem, discussed below. CDM can either decouple from thermal equilibrium at some temperature (candidates include the lightest supersymmetric particle or some scalar particle) or be produced via some non-thermal process, such as the homogeneous condensate of scalar particles (candidates here include the axion). Thermal relic CDM is particularly well motivated because particles with masses between a few GeV and a few TeV, with cross sections of electroweak strength (known as WIMPs, or weakly interacting massive particles), naturally produce a relic density of the correct order of magnitude. This is known as the WIMP miracle.

Simulations of CDM show there to be many more small halos or substructures than have been observed [19]. This is the substructure problem. There are two possible solutions to this. It is possible that the small clusters of dark matter are too small to have formed a visible galaxy, so do exist but have not been detected. Another possibility is that these dwarf galaxies did form, but were tidally stripped or accreted by larger galaxies. The second problem is that cosmological simulations show dark matter distributions to be cuspy (sharply increasing in dense parts of the Universe), which is not observed (this is known as the cuspy halo problem) [20, 21]. There is no clear explanation of this at present.

Thermal relic densities using the Lee-Weinberg approximation

If we know the mass of a WIMP and its coupling to the Standard Model, we can calculate the relic density Ω_{DM} that it would produce upon freezing out of thermal equilibrium. Alternatively, we can use a measurement of Ω_{DM} to determine the WIMP mass, given its coupling(s). In this thesis it will be sufficient to use the Lee-Weinberg approximation [22] to calculate the relic density.

The number density of dark matter particles is reduced as the Universe expands and can change through annihilations or pair production (assuming stable dark matter). The rate equation is [23]

$$\frac{dn}{dt} = -3H(t)n - \langle\sigma v\rangle(n^2 - n_0^2) \quad (1.44)$$

where n_0 is the equilibrium number density and σ the annihilation cross section. For $T \ll m$, n_0 is given by the Maxwell-Boltzmann distribution:

$$n_0 = \left(\frac{mT}{2\pi}\right)^{3/2} e^{-\frac{m}{T}}. \quad (1.45)$$

Assuming radiation domination, this can be re-written in terms of $f = \frac{n}{T^3}$ and $f_0 = \frac{n_0}{T^3}$:

$$\frac{df}{dT} = \frac{\langle\sigma v\rangle(f^2 - f_0^2)}{K} \quad (1.46)$$

where

$$K = \left(\frac{\pi^2 g_*(T)}{90M_p^2}\right)^{\frac{1}{2}} \quad (1.47)$$

and $g_*(T)$ is the effective number of relativistic degrees of freedom at temperature T .

In order to solve this, we make several assumptions. The first is that the dark matter particle is the only particle that freezes out of thermal equilibrium near the dark matter freeze-out temperature T_f (this means that $g_*(T)$ is approximately constant). The second is that the Universe is radiation dominated. Then we assume that the dark matter is in exact thermal equilibrium ($f = f_0$) until $T = T_f$. At temperatures lower than T_f , $f_0(T) = 0$. Thus, defining $x_f = \frac{m}{T_f}$, we get

$$x_f^{-1} = \ln \left(\frac{mx_f^2 \langle\sigma v\rangle}{K(2\pi x_f)^{3/2} (1 - \frac{3}{2}x_f)} \right). \quad (1.48)$$

This enables calculation of the current relic density of the dark matter particles [24]:

$$\Omega_S \equiv \frac{\rho_S}{\rho_c} = \frac{g(T_\gamma)}{g(T_f)} \frac{K}{T_\gamma x_f \langle\sigma v\rangle} \left(\frac{T_\gamma^4}{\rho_c}\right) \frac{(1 - 3x_f/2)}{(1 - x_f/2)}, \quad (1.49)$$

once the thermally averaged annihilation cross sections for the particular dark matter candidate

have been computed.

1.6 Minimal extensions to the Standard Model

Although the Standard Model of particle physics (discussed in the next chapter) reproduces experimental results well, it does not provide a mechanism for inflation, dark matter, baryogenesis or neutrino masses. Therefore it cannot be the complete theory of particle physics. Theories which attempt to explain these observations usually involve a new scale between the weak scale and the Planck scale and many additional particles. The Standard Model is then viewed as the low energy remnant of some more complete theory⁹, which is only valid up to some cut off $\Lambda < M_p$.

An alternative philosophy is to add to the Standard Model the minimal number of new fields that are needed to address these issues. One example is the ν MSM [26, 27], which is the Standard Model extended by three singlet fermions to account for neutrino masses. In this case dark matter can be explained by a keV-scale sterile neutrino, while baryogenesis occurs via leptogenesis due to sterile neutrino oscillations [28]. Therefore neutrino masses, dark matter and baryogenesis can all be explained within a very minimal extension of the Standard Model (although this imposes non-trivial conditions on the sterile neutrino masses and couplings [29]). A scale-invariant but very weakly-coupled scalar may also be added to serve as the inflaton [30]. Reheating in this model (with the additional scalar-inflaton) occurs at a low temperature and bounds the inflaton mass to be either $0.1 \text{ GeV} \lesssim m \lesssim 10 \text{ GeV}$ or $300 \text{ GeV} \lesssim m \lesssim 1 \text{ TeV}$ [31].

One motivation for considering weak-scale extensions of the Standard Model is the idea that the hierarchy problems of non-supersymmetric particle theories can be avoided if there is only one mass scale in the effective field theory below the Planck scale [25]. The gauge hierarchy problem is that quantum corrections to the Higgs mass diverge quadratically (due to heavy particles running in loops), and therefore must be cancelled in some way. To achieve this, the theory must be finely tuned either at tree-level (for a SUSY model) or to each order up to ~ 13 loop order (for a non-SUSY model). However, if the effective theory has *no* new mass scale below the Planck scale, then no fine-tuning is necessary (provided the minimal-subtraction scheme for regularisation is used [25]).

In this case (with no new scale), the Landau pole appearing in various couplings (which makes the theory mathematically inconsistent) can be shifted to a value above the Planck scale, where quantum gravity would be expected to provide a UV completion of the theory. Provided

⁹A particular motivation for theories with a new energy scale (such as GUTs) is that they can cause the gauge couplings to unify at some scale. Currently they intersect only in pairs, between 10^{13} and 10^{17} GeV. This apparent unification could either be just a coincidence, or one may wonder if a theory of quantum gravity could cause unification at M_p [25].

this is done, the Standard Model *can* be a mathematically consistent theory, up to the Planck scale. It still cannot be a complete theory, as many observations remain unexplained (neutrino masses, neutrino oscillations, baryogenesis, inflation and many more). However, the additions to the Standard Model do not necessarily need to introduce a new scale.

1.7 Inflation with the Standard Model

Recently it has been suggested that inflation might be explained purely within the framework of the Standard Model, with the Higgs field itself serving as the inflaton [32]. This is possible if the Higgs has a large non-minimal coupling to gravity and has been extensively investigated in a number of papers [32, 33, 34, 35, 36, 37, 38, 39, 40]. However, in order to account for dark matter, baryogenesis and neutrino masses, it is still necessary to extend the Standard Model. This might be achieved by combining Higgs inflation with the ν MSM — but other extensions which are consistent with entirely weak scale particle physics could also be considered. As discussed in Section 1.5, stable particles with weak scale masses and electroweak strength interactions (WIMPs) produce a thermal relic dark matter density which is naturally of the correct order of magnitude. Therefore there is a strong motivation to extend the Standard Model by the addition of a particle with these properties.

The main aim of this thesis is to propose a minimally-extended version of the Standard Model (as an alternative to the ν MSM plus Higgs inflation) which is able to explain both the mechanism for inflation and the presence of thermal relic dark matter. We call the model ‘ S -inflation’ and it is the addition of a stable gauge singlet scalar S to the Standard Model. This is the simplest extension of the Standard Model which obeys gauge symmetry and can account for dark matter [24, 41, 42, 43, 44]. A discrete Z_2 or a global symmetry $U(1)$ must be imposed to ensure stability of the scalars; in the former case it is natural to consider real scalars, in the latter case complex scalars.

After discussing in Chapter 2 aspects of field theory necessary for the remainder of the thesis, we discuss various aspects of the model. In Chapter 3 we show that S can serve simultaneously as a thermal relic dark matter particle and as the inflaton, producing the correct density of dark matter while at the same time obeying the observational constraints on the spectral index n and other inflation observables. Effectively we are replacing the Higgs scalar of Higgs inflation by the dark matter scalar S . As we will show, the model has the potential to relate particle physics, dark matter detection experiments and inflation observables — a connection that will be brought into focus in the near future by the LHC, the Planck satellite and future dark matter detectors.

Next, in Chapter 4, we show that reheating is possible in the model, in spite of the symmetry

which prevents S from decaying. In Chapter 5, we compare the experimental predictions of S -inflation to those of Higgs inflation. We first clarify the confusion in the literature regarding the predictions of Higgs inflation by comparing the two methods of calculating the effective potential, before comparing the predictions of the two models. Chapter 6 includes a discussion of the issue of naturalness and unitarity violation in this class of models. We conclude that it is not possible at present to conclusively determine whether or not the model is safe. We also present a new model of Higgs inflation which, under certain assumptions, we believe conserves unitarity and thus secures the future of non-minimally coupled models, should unitarity prove to be violated in the original version. In Chapter 7, we present our conclusions.

Chapter 2

Effective potential, renormalization group and bounds on field theories

2.1 Field theory

The aim of this chapter is to explain the concept of, method of obtaining and validity of the effective potential (which is necessary to calculate inflation observables). First, we introduce the idea of a field theory — the action, Lagrangian and symmetries of the theory. As an aside we explain the Higgs mechanism and discuss the calculation of scattering amplitudes. We will make use of the Higgs potential in this thesis, and it is important to understand its motivation as a mechanism for giving mass to particles.

In the second part of the chapter, we introduce radiative corrections, divergences and renormalization. We discuss the concept of the effective potential, present the Callan-Symanzik equation, and use it to derive two forms for the effective potential. We introduce the renormalization group (RG) equations for couplings. Finally, we discuss some general bounds on the validity of theories: the concept of a stable vacuum, perturbativity and unitarity (conservation of probability). A comprehensive review of the field theory contained in this chapter can be found in [45, 46], for example.

2.1.1 The concept of a field theory

We are able to make a relatively simple mathematical model of the interactions of all known elementary particles, using quantum field theory. Each particle corresponds to a field (which is an operator in the field theory). We start with the action S , which gives the laws of physics through the action principle:

$$\delta S = 0. \tag{2.1}$$

The action for a field theory with one scalar field ϕ in flat space can be written

$$S \equiv \int_{-\infty}^{+\infty} \mathcal{L}(\phi, \partial_\mu \phi) d^4x \quad (2.2)$$

where \mathcal{L} is the Lagrangian density. For curved space, a factor $\sqrt{-g}$, where g is the determinant of the metric tensor $g_{\mu\nu}$, is inserted so that the action is invariant under coordinate transformations.

Applying the action principle gives the Euler-Lagrange equations of motion (one equation for each field ϕ):

$$\partial_\mu \left(\frac{\partial \mathcal{L}}{\partial(\partial_\mu \phi)} \right) - \frac{\partial \mathcal{L}}{\partial \phi} = 0. \quad (2.3)$$

For example, the simple scalar Lagrangian $\mathcal{L} = \frac{1}{2}g^{\mu\nu}\partial_\mu\phi\partial_\nu\phi - V(\phi)$ with a Robertson-Walker metric (Eq. (1.1)) gives the equation of motion, Eq. (1.16), once we assume a homogeneous field.

To derive \mathcal{L} for the Standard Model, we need two ingredients: (i) the fields and (ii) a procedure for choosing which terms to include. There are two main types of particles — fermion (spin $\frac{1}{2}$) and boson (spin 0 or 1). They transform differently under Lorentz transformations and therefore are represented by different types of field (fermions by spinors, spin-1 bosons by vectors and spin-0 bosons by scalars). Cosmology often deals with spin 0 scalars (particularly for inflation), which have simple transformation properties. The main principle for writing down the terms in the Lagrangian is that the Lagrangian must be invariant under certain symmetry transformations. These include both external transformations (such as Lorentz transformations and coordinate transformations) and internal transformations. The Standard Model is invariant under internal $SU(3)_c \times SU(2)_L \times U(1)$ transformations. After imposing all these restrictions, we write down the terms which remain¹.

Gravity and the Planck scale

The gravitational part of the Lagrangian is

$$\mathcal{L}_{grav} = \frac{1}{2}M_p^2 R + \frac{1}{2} \sum_i \xi_i \phi_i^2 R \quad (2.4)$$

where R is the Ricci scalar and ϕ_i are scalar fields. The second term is usually omitted but is in fact required by the renormalizability of the theory in curved space [47]. Whichever field theory we choose, Einstein gravity (Eq. (2.4)) gives a *maximum* UV cut-off, which is the Planck scale. Above M_p , there is a conflict between general relativity and (standard) quantum field theory². Some new theory, such as string theory or loop quantum gravity, must therefore become

¹There are some exceptions to this rule, such as that terms with more than two derivatives are usually excluded.

²This can be illustrated by comparing the vacuum fluctuations of a massless scalar field within a region of size R to the corresponding Schwarzschild radius. The Schwarzschild radius is $r_s \sim \frac{1}{RM_p^2}$ for the vacuum fluctuation

important at (or before) this point. All quantum field theories are effective theories, which are valid (well) below some UV cut-off (which could be M_p) — but we do not need to know the high energy theory in order to make low energy calculations.

2.1.2 The Standard Model

The Standard Model can be described by the group of transformations it is invariant under: $SU(3)_c \times SU(2)_L \times U(1)$. The Lagrangian contains all terms permitted by the symmetries and is described fully in [48], for example. Once the symmetry is spontaneously broken (by the Higgs mechanism, described below), the theory contains the following particles and their antiparticles:

- three families of leptons, each with one massive charged lepton and one massless neutrino,
- three families of quarks, each with two massive quarks with three colours,
- three massive vector gauge bosons (W^+ , W^- and Z),
- one massless gauge boson (the photon) and
- one real scalar Higgs boson.

We have direct experimental evidence for all spin 1 (boson) and spin $\frac{1}{2}$ (fermion) particles. The Higgs boson has yet to be discovered — but is essential in order to give mass to the gauge bosons. Masses of the fermions are generated through gauge invariant couplings to the Higgs. A measurement of the Fermi constant gives the Higgs vev $v = 246.22$ GeV but provide no information on m_h .

The Higgs mechanism

We explain the Higgs mechanism by considering a local $U(1)_Y \times SU(2)$ transformation (Y is hypercharge). In the theory there is a complex scalar doublet Φ (containing four real fields). Invariance with respect to a local $U(1)_Y$ transformation requires a vector gauge field, B_μ , to be introduced. Invariance with respect to a local $SU(2)$ transformation requires three vector gauge fields W_μ^a to be introduced. The gauge invariant Lagrangian density is

$$\mathcal{L} = -|D_\mu \Phi|^2 + V(|\Phi|^2) - \frac{1}{4}W_{\mu\nu}^a W^{a\mu\nu} - \frac{1}{4}B^{\mu\nu} B_{\mu\nu} \quad (2.5)$$

where the covariant derivative is defined as

$$D_\mu \equiv \partial_\mu + \frac{ig}{2}B_\mu + \frac{ig'}{2}W_\mu^a \sigma^a, \quad (2.6)$$

with energy $E \sim \frac{1}{R}$. If the theory is valid above the Planck scale, i.e. $R \lesssim M_p^{-1}$ then $r_s > R$ and spacetime has strong curvature seemingly corresponding to the production of black holes [8].

where σ^a are the Pauli matrices. The field strength tensors are defined by

$$B_{\mu\nu} \equiv \partial_\mu B_\nu - \partial_\nu B_\mu \quad (2.7)$$

and

$$W_{\mu\nu}^a \equiv \partial_\mu W_\nu^a - \partial_\nu W_\mu^a + g' \epsilon^{abc} W_\mu^b W_\nu^c. \quad (2.8)$$

The mass term

$$\Delta\mathcal{L} = \frac{1}{2} m_W^2 W_\mu W^\mu$$

is forbidden because it explicitly breaks the $SU(2)$ symmetry. Hence, the symmetry $U(1)_Y \times SU(2)$ must be *spontaneously* broken in order for the gauge bosons to acquire a mass.

Considering the Higgs doublet $\Phi = (\phi^+, \phi_0)^T$ with the $SU(2)$ invariant potential

$$V(\Phi^\dagger \Phi) = \lambda \left(\Phi^\dagger \Phi - \frac{v^2}{2} \right)^2,$$

the state of lowest energy (vacuum state) is a degenerate state: any value of Φ where $|\Phi| = \frac{v}{\sqrt{2}}$ is a vacuum state. The symmetry is spontaneously broken once Φ leaves the unstable (but symmetric) maximum at the origin and falls in an arbitrary direction to the minimum. It is this which breaks the symmetry, leaving the $U(1)_{EM}$ symmetry of electromagnetism: $SU(2) \times U(1)_Y \rightarrow U(1)_{EM}$.

In the unitary gauge, $\Phi = \frac{1}{\sqrt{2}} (0, v + h)^T$. The four physical gauge fields (W_μ^+, W_μ^-, Z_μ and A_μ) are formed from linear combinations of W_μ^a and B_μ . They have masses $M_W^2 = \frac{g^2 v^2}{4}$, $M_Z^2 = \frac{(g^2 + g'^2) v^2}{4}$ and $M_A^2 = 0$. Three degrees of freedom of Φ have become the longitudinal degrees of freedom of the massive gauge bosons. A physical Higgs scalar, h , remains. A full description of the Higgs mechanism can be found in [45, 48, 49], for example.

2.1.3 The effective action

The effective action gives the field equations for the classical field ϕ_c , including quantum corrections. It is defined by first adding a source $J(x)$ to the Lagrangian, so $\mathcal{L}(\phi, \partial_\mu \phi) \rightarrow \mathcal{L} + J(x)\phi(x)$. A generating functional $W(J)$ is defined using the classical action $S = \int d^4x [\mathcal{L} + J(x)\phi(x)]$ by

$$e^{iW(J)} = \int [d\phi] e^{iS(\phi)} = \langle 0^+ | 0^- \rangle_J, \quad (2.9)$$

which is the transition (in the presence of the source) from the vacuum to the vacuum. The classical field is

$$\phi_c(x) = \frac{\delta W}{\delta J(x)} = \left[\frac{\langle 0^+ | \phi(x) | 0^- \rangle}{\langle 0^+ | 0^- \rangle} \right]_J. \quad (2.10)$$

The effective action is then defined by a functional Legendre transformation:

$$\Gamma(\phi_c) = W(J) - \int d^4x J(x)\phi_c(x). \quad (2.11)$$

With $J = 0$, the field equations are given by

$$\frac{\delta\Gamma}{\delta\phi_c} = 0. \quad (2.12)$$

The effective action, Γ , can be expanded in position space as

$$\Gamma = \int d^4x \left(-V(\phi_c) + \frac{1}{2}(\partial_\mu\phi_c)^2 Z(\phi_c) + \dots \right) \quad (2.13)$$

where the effective potential, $V(\phi_c)$, is the quantum corrected scalar potential. Its minimum corresponds to the vacuum expectation value (vev) of the field ϕ_c . The n^{th} derivative of V is given by the sum of all 1PI graphs with n external legs. In this thesis we look at the effective potential including the leading order radiative corrections. $Z(\phi_c)$ is the wavefunction renormalization.

2.1.4 Scattering amplitudes

It seems a daunting task to take a field theory and calculate the rate for a scattering process. Fortunately, the use of Feynman diagrams and the associated rules greatly simplify the process. The cross-section for a particular process is given (approximately) by integrating the amplitude over the available phase space. The amplitude is given by Feynman diagrams, provided that perturbation theory can be applied.

A Green's function $G^{(n)}$ is an n -point correlation function. With $|\Omega\rangle$ representing the ground state of the (interacting) theory, the renormalized Green's functions are

$$G^{(n)}(x_1 \dots x_n) = \langle \Omega | T \phi(x_1) \dots \phi(x_n) | \Omega \rangle_{\text{connected}}. \quad (2.14)$$

where T is a time-ordering operator. For example, $G^{(2)}$ is the amplitude for a particle to propagate between y and x .

Calculating the amplitude or correlation function can be done using an elegant formalism of Feynman diagrams. Connected Feynman graphs are drawn, to a particular order in a loop expansion. For a scalar field, each vertex contributes a factor $-i\lambda$, each propagator $\frac{i}{p^2 - m^2 + i\epsilon}$ (where ϵ is a tiny constant to facilitate integration). At each vertex, energy momentum conservation is then imposed, and any 4-momenta not fixed must be integrated over. A factor counting combinations is also included. Similar rules apply to fermions and gauge bosons and can be

found for example in [45, 46].

2.1.5 Radiative corrections, regularisation and renormalization

The leading order scattering process in perturbative theory is known as the tree level process. However, there are also many other higher order ways for a process to occur, usually involving loops. First order processes contain one loop, second order contain two loops, and so on. To make an exact calculation, we would need to sum over *all* terms in this loop expansion. Fortunately we often work with perturbative field theories where contributions from successive orders are less important, and the tree level effect dominates.

In this thesis, we will need to consider the radiative corrections to an inflationary potential. To allow for slow roll inflation, the potential must be reasonably flat, which we arrange at tree level by our choice of model. Thus it will be particularly important to consider if radiative corrections spoil the flat tree-level potential.

Radiative corrections

Calculating radiative corrections involves integrating over momenta in closed loops. This gives divergent results. However, when we make measurements of these quantities in experiments, they are found to be finite. Thus we need to reformulate our theory in order to make reasonable predictions. This is done by first *regularising* the divergence — that is writing it as a finite part plus a divergent part (there are many ways to do this), then *renormalizing* the divergence, leaving only the finite part as a physical observable. We explain this further below.

We will demonstrate the method using the simple example (following [50]) of a single massless field ϕ with self interactions. The tree-level Lagrangian is

$$\mathcal{L} = \frac{1}{2}(\partial_\mu\phi)^2 - \frac{\lambda}{4!}\phi^4. \quad (2.15)$$

The one-loop contributions include an infinite series of n -sided polygons, which give a contribution

$$\Delta V = i \int \frac{d^4k}{(2\pi)^4} \sum_{n=1}^{\infty} \frac{1}{2n} \left(\frac{1}{2} \frac{\lambda\phi_c^2}{k^2 + i\epsilon} \right)^n, \quad (2.16)$$

clearly divergent as $k \rightarrow 0$ (ϕ_c is the classical field).

Regularisation

Regularisation is the process of adding a new scale Λ to the Lagrangian with the aim of writing the previously divergent quantities as finite terms plus divergent terms. The divergence will then

be parameterised, as it will only appear in terms containing Λ when Λ is taken to some particular value (often 0 or ∞).

Examples of methods of regularisation are:

- integrating only up to a sharp momentum cut-off Λ — this suppresses terms at $E \gtrsim \Lambda$ while leaving processes with $E \ll \Lambda$ unaffected
- treating space-time as a lattice, rather than as continuous (lattice regularisation)
- adding terms directly to the Lagrangian, as in Pauli-Villars regularisation and
- using a non-integer number of dimensions (dimensional regularisation).

We now apply a momentum cut-off to our example theory. It gives

$$\Delta V = \frac{\lambda^2 \phi_c^4}{256\pi^2} \left(\ln \left(\frac{\lambda \phi_c^2}{2\Lambda^2} \right) - \frac{1}{2} \right) \quad (2.17)$$

by first doing the sum over n , then doing a Wick rotation ($t \rightarrow it$) and the integration, and finally dropping terms which disappear as $\Lambda \rightarrow \infty$.

Renormalization

The process of renormalization will absorb the divergent terms, order by order, into the bare couplings and masses of the Lagrangian. It is the process of taking the momentum cut-off Λ to infinity (or otherwise taking the limit of the regularisation procedure). To do this, we add counter-terms to the original Lagrangian that exactly cancel the divergent terms. We impose renormalization conditions which define the mass and couplings of the theory at some arbitrary scale μ . These conditions fix the counter terms.

For our example, we first add counter terms to the Lagrangian Eq. (2.15) which becomes

$$\mathcal{L} = \frac{1}{2}(\partial_\mu \phi)^2 - \frac{\lambda}{4!}\phi^4 - \Delta V + \frac{1}{2}A(\partial_\mu \phi)^2 - \frac{1}{2}B\phi^2 - \frac{1}{4!}C\phi^4 \quad (2.18)$$

where A , B and C are the renormalization counterterm coefficients. As an example, we determine B and C order-by-order in the loop expansion by imposing the renormalization conditions

$$\left. \frac{d^2 V}{d\phi_c^2} \right|_{\phi_c=\mu} = m^2 = 0 \quad (2.19)$$

and

$$\left. \frac{d^4 V}{d\phi_c^4} \right|_{\phi_c=\mu} = \lambda. \quad (2.20)$$

Applying these gives

$$B = -\frac{\lambda\Lambda^2}{32\pi^2} \quad \text{and} \quad C = -\frac{3\lambda^2}{32\pi^2} \left(\ln \left(\frac{\lambda\mu^2}{2\Lambda^2} \right) + \frac{11}{3} \right). \quad (2.21)$$

So, we can write the renormalized one-loop effective potential as

$$V = \frac{\lambda}{4!}\phi_c^4 + \frac{\lambda^2\phi_c^4}{256\pi^2} \left(\ln \frac{\phi_c^2}{\mu^2} - \frac{25}{6} \right). \quad (2.22)$$

We note that there is no dependence on the cut-off scale Λ . The scale μ is completely arbitrary, and can be changed without altering the effective action of the theory. This is a core concept in renormalization and is the basis of the Callan-Symanzik equation, discussed below. If μ is changed to μ' , then the masses and couplings also change, as they must now be defined at μ' . The way they change as μ changes is described by RG equations. If we were to work to all orders in perturbation theory, then the invariance with respect to μ would be exact. However, we usually only consider one-loop or two-loop calculations. For this reason, μ is often chosen to be equal to ϕ , to minimise the corrections to the theory.

2.1.6 The Callan-Symanzik equation

We consider a general, renormalized Green's function $G_R^{(n)}(p_i; g_R, \mu)$ for a single field with coupling g . $G_R^{(n)}$ is independent of the cut-off Λ . The corresponding bare Green's function is $G_0^{(n)}(p_i; g_0, \Lambda)$, which is independent of the renormalization point, μ . The functions are related by [45]

$$G_0^{(n)} = Z^{n/2} G_R^{(n)} \quad (2.23)$$

where n is the number of fields and Z is the wavefunction renormalization. Considering

$$\mu \frac{dG_0^{(n)}}{d\mu} = 0. \quad (2.24)$$

gives the Callan-Symanzik equation:

$$\left[\mu \frac{\partial}{\partial \mu} + \beta(g_R) \frac{\partial}{\partial g_R} - n\gamma(g_R) \right] G_R^{(n)}(p_i; g_R, \mu) = 0 \quad (2.25)$$

where

$$\beta(g_R) \equiv \mu \frac{dg_R}{d\mu} \quad (2.26)$$

and

$$\gamma \equiv -\frac{\mu}{2} \frac{d \log(Z)}{d\mu}. \quad (2.27)$$

In a more general theory, there is a β for each coupling and a γ for each field. They can be calculated from the renormalization counter terms of the theory. The beta-function $\beta(g_R)$ gives the rate of change of the renormalized coupling g_R as the renormalization scale is increased. Therefore it can be used to calculate couplings at any scale (in the case of multiple couplings, the beta-functions usually need to be integrated numerically). The change of the wavefunction renormalization (actually $\ln Z$) is given by γ .

We consider two methods for calculating the effective action of a theory. The first was originally due to Coleman and Weinberg [50] and the second computes the corrections to the whole action using the Callan-Symanzik equation. Both are discussed below.

2.1.7 The Standard Model Coleman-Weinberg effective potential

This is derived in the same way that the example calculation was done — so for a massless ϕ^4 potential, the Coleman-Weinberg potential is given by Eq. (2.22). For the Standard Model calculation, we assume all fields other than the physical Higgs field to be at their vevs.

General expressions for the one-loop correction can be used. For a tree-level polynomial scalar potential $U(\phi_c)$ the expression is [51]

$$V_{scalar}^{(1)}(\phi_c) = \frac{\Lambda^2 U''}{32\pi^2} + \frac{(U'')^2}{64\pi^2} \left(\ln \left(\frac{U''}{\Lambda^2} \right) - \frac{1}{2} \right) \quad (2.28)$$

where $U'' = \frac{d^2 U}{d\phi_c^2}$. Equivalent expressions for fermions and vector bosons can be found in [51].

So, for the Standard Model, including only one fermion (the top quark), following the procedure of calculating the counter terms and summing over colours, the one-loop order effective potential is [52]

$$\begin{aligned} 16\pi^2 V^{(1)}(\phi_c) &= \frac{1}{4} H^2 \left(\ln \frac{H}{\mu^2} - \frac{3}{2} \right) + \frac{3}{4} G^2 \left(\ln \frac{G}{\mu^2} - \frac{3}{2} \right) + \frac{3}{2} W^2 \left(\ln \frac{W}{\mu^2} - \frac{5}{6} \right) \\ &+ \frac{3}{4} Z^2 \left(\ln \frac{Z}{\mu^2} - \frac{5}{6} \right) - 3T^2 \left(\ln \frac{T}{\mu^2} - \frac{3}{2} \right), \end{aligned} \quad (2.29)$$

where

$$W = \frac{g^2 \phi_c^2}{4}, \quad Z = \frac{(g^2 + g'^2) \phi_c^2}{4}, \quad T = \frac{y_t^2 \phi_c^2}{2}, \quad H = m_\phi^2 + 3\lambda_h \phi_c^2 \quad \text{and} \quad G = m_\phi^2 + \lambda_h \phi_c^2. \quad (2.30)$$

In order for this to be independent of μ , all couplings must vary with μ . The resulting RG

equations for our model (including the effect of the non-minimal coupling to gravity) can be found in Chapter 3. The Coleman-Weinberg potential is valid over the range of field values ϕ_a to ϕ_b provided

$$\left| \lambda \ln \left(\frac{\phi_a}{\phi_b} \right) \right| \ll 1, \quad (2.31)$$

where λ is the largest coupling in the theory.

The RG equations in this thesis are defined in the $\overline{\text{MS}}$ (modified minimal subtraction) renormalization scheme [45, 53, 54]. The theory is written in terms of $d = 4 - \epsilon$ dimensions (this is dimensional regularisation). When the resulting divergences are renormalized the poles ($\frac{1}{\epsilon}$) are removed, along with extra terms involving $\log(4\pi)$ and γ . These arbitrary constants usually occur alongside the poles and are removed purely to simplify the equations.

2.1.8 The RG improved effective action

An alternative method for computing the effective potential uses the Callan-Symanzik equation (Eq. (2.25)) directly. It will yield a form for the effective potential which is valid provided that the couplings are perturbative — a wider range of ϕ than the Coleman-Weinberg potential.

Considering a ϕ^4 theory as an example, the Callan-Symanzik equation for the effective action Γ is [45]

$$\left[\mu \frac{\partial}{\partial \mu} + \beta(g_R) \frac{\partial}{\partial g_R} - \gamma(g_R) \int dx \phi_c(x) \frac{\delta}{\delta \phi_c(x)} \right] \Gamma(\phi_c; g_R, \mu) = 0. \quad (2.32)$$

Using the expansion (Eq. (2.13)), we see that

$$\left(\mu \frac{\partial}{\partial \mu} + \beta \frac{\partial}{\partial \lambda} - \gamma \phi_c \frac{\partial}{\partial \phi_c} \right) V(t, \lambda) = 0 \quad (2.33)$$

and

$$\left(\mu \frac{\partial}{\partial \mu} + \beta \frac{\partial}{\partial \lambda} - \gamma \phi_c \frac{\partial}{\partial \phi_c} - 2\gamma \right) Z(t, \lambda) = 0. \quad (2.34)$$

Dimensionally, the effective potential must have the form

$$V = \frac{y(\lambda, t) \phi_c^4}{4}. \quad (2.35)$$

Using the definitions

$$t = \ln \frac{\phi_c}{\mu}, \quad \bar{\beta} = \frac{\beta}{1 + \gamma}, \quad \text{and} \quad \bar{\gamma} = \frac{\gamma}{1 + \gamma}, \quad (2.36)$$

the equations become [51]

$$\left(-\frac{\partial}{\partial t} + \bar{\beta} \frac{\partial}{\partial \lambda} - 4\bar{\gamma} \right) y(t, \lambda) = 0 \quad (2.37)$$

and

$$\left(-\frac{\partial}{\partial t} + \bar{\beta} \frac{\partial}{\partial \lambda} - 2\bar{\gamma}\right) Z(t, \lambda) = 0. \quad (2.38)$$

Renormalization conditions are necessary in order to properly define the theory. This can be done at any scale, and here we use $\phi_c = \mu$ (so $t = 0$):

$$y(0, \lambda) = \lambda \quad \text{and} \quad Z(0, \lambda) = 1. \quad (2.39)$$

Applied to Eq. (2.37) and Eq. (2.38), they give

$$\bar{\gamma} = -\frac{1}{2} \frac{\partial}{\partial t} Z(0, \lambda) \quad \text{and} \quad \bar{\beta} = \frac{\partial}{\partial t} y(0, \lambda) - 4\bar{\gamma}\lambda. \quad (2.40)$$

These can be calculated in perturbation theory, using a loop expansion and the associated Feynman rules. Defining λ' through

$$\frac{d\lambda'}{dt} = \bar{\beta}(\lambda'), \quad (2.41)$$

with $\lambda'(0, \lambda) = \lambda$, the solutions of Eq. (2.37) and Eq. (2.38) are therefore

$$Z(t, \lambda) = \exp\left(-2 \int_0^t dt \bar{\gamma}(\lambda'(t, \lambda))\right) \quad (2.42)$$

and

$$y(t, \lambda) = \lambda'(t, \lambda) Z(t, \lambda)^2. \quad (2.43)$$

The RG improved effective potential for a ϕ^4 theory is therefore given by

$$V(t, \lambda) = \frac{\lambda'(t, \lambda) Z(t, \lambda)^2}{4} \phi_c^4. \quad (2.44)$$

In the notation of Chapter 5, $Z \equiv G^2$, so $V = \frac{\lambda'}{4} G^4 \phi_c^4$.

2.2 Bounds on the theory

2.2.1 Vacuum stability

The scalar potential for the Standard Model,

$$V(H^\dagger H) = \lambda_h \left(H^\dagger H - \frac{v^2}{2}\right)^2 \quad (2.45)$$

has a minimum at $H^\dagger H = \frac{v^2}{2}$. The direction is arbitrary but is usually taken to be along the real part of H . An important question for the stability of the Standard Model is to consider whether this is the global minimum of the theory. Other minima can only be tolerated if either (i) the minima appears above the scale Λ where we expect new physics to enter or (ii) the transition from our Standard Model vacuum to the other vacuum has a lifetime of at least the age of the Universe, and the transition could not have been induced by cosmic rays [55]. In practice we will exclude the second possibility as it only changes the allowed range for the Higgs mass slightly (see Fig. (23) of [51]). So, our requirement is that $V(H^\dagger H) > 0$ for large $H^\dagger H$, which implies $\lambda_h > 0$ for all $|H| < \Lambda$. Vacuum stability gives the lower bound for the Higgs mass to be $m_h \gtrsim 130$ GeV [56], if $\Lambda = M_p$ for the Standard Model.

Additional scalar fields

The constraints are more complicated when we include additional scalar fields. In the direction of any field ϕ_i we will find that the self-coupling λ_i must be positive:

$$\lambda_i > 0. \tag{2.46}$$

There are also constraints on interaction terms, from considering an arbitrary direction $\phi_j = \alpha\phi_i$ for large field values. The potential is

$$V = \lambda_i \phi_i^4 + \lambda_j \phi_j^4 + \lambda_{ij} \phi_i^2 \phi_j^2 \tag{2.47}$$

and becomes

$$V = \phi_i^4 (\lambda_i + \alpha^4 \lambda_j + \alpha^2 \lambda_{ij}). \tag{2.48}$$

Requiring $V > 0$ for all α gives

$$\alpha^2 \lambda_{ij} > -(\lambda_i + \alpha^4 \lambda_j). \tag{2.49}$$

The minimum with respect to α is at $\alpha^2 = -\frac{\lambda_{ij}}{2\lambda_j}$. Substituting into Eq. (2.49) gives the conditions on λ_{ij} for vacuum stability:

$$\lambda_{ij} > -2\sqrt{\lambda_i \lambda_j}. \tag{2.50}$$

This can be expanded to theories with more fields by considering directions where only two fields are non-zero.

2.2.2 Perturbativity

The renormalization group equations (β -functions), introduced in Section 2.1.5, describe how the couplings change as the renormalization scale (μ) increases. (Usually μ is chosen to be the energy scale of the process under investigation.) If β_λ ($\sim \frac{d\lambda}{d\mu}$) is positive for a particular coupling λ , then λ will continue to grow as μ is increased, reaching an infinite value at a particular value of μ . This is a Landau pole and its existence means that a theory is mathematically inconsistent. We therefore require there to be no Landau pole below some scale Λ (where new physics is expected to take over and resolve the inconsistency). An alternative view is that new physics may not be necessary if the theory enters a strongly coupled regime for $\lambda \gtrsim 1$. In this regime, loop expansions and other perturbative processes are no longer the correct method to do calculations. Again, we must require that this does not occur below the energy scales we are interested in.

The upper bound $m_h \lesssim 170$ GeV [51] on the Higgs mass in the Standard Model is calculated by requiring the Higgs coupling λ_h to remain perturbative up to the Planck scale.

2.2.3 Unitarity

Unitarity is the requirement that the sum of probabilities equals one. Therefore, if we calculate any quantity and find that it does not obey unitarity, either our theory is not valid at that energy scale, or our method of doing the calculation is not valid (i.e. it may be a non-perturbative process). Within the Standard Model there are occasions (e.g. $e^+e^- \rightarrow W^+W^-$) where unitarity does not appear to be obeyed until several Feynman diagrams are summed over and all problem terms cancel out.

We next outline the origin of the condition for unitarity conservation which can be written as

$$\text{Im}[a_l] \geq |a_l|^2 \tag{2.51}$$

or equivalently

$$|\text{Re}[a_l]| \leq \frac{1}{2}, \tag{2.52}$$

where a_l is a partial wave amplitude. A general scattering amplitude A can be expanded in terms of partial waves³ a_l :

$$A = 16\pi \sum_{l=0}^{\infty} (2l+1) P_l(\cos \theta) a_l, \tag{2.53}$$

where θ is the angle between the outgoing and incoming particle, l is the total angular momentum and $P_l(\cos \theta)$ are Legendre polynomials. Partial waves are radial wavefunctions centred on the

³This is valid for scalar particles with zero spin and zero helicity — a slightly more complex expression applies for particles with spin.

point of interaction.

The Optical Theorem

The Optical Theorem relates the total scattering cross section for $2 \rightarrow$ anything to the $2 \rightarrow 2$ cross-section for *elastic* scattering (with $\theta = 0$):

$$\sigma_{total} = \frac{1}{s} \text{Im} [A(\theta = 0)], \quad (2.54)$$

where $s = E_{CM}^2$ is a Mandelstam variable. This is derived directly as a result of the unitarity of the S matrix as outlined below. The interaction part (T) of the S matrix can be separated out: $S = 1 + iT$. Considering the transition from $|\alpha\rangle$ to $|\alpha\rangle$, we can write this in two different forms. On the left we have inserted a complete set of states and on the right we have used the unitarity of S ($S^\dagger S = I$). The expression therefore is

$$\begin{aligned} \langle \alpha | (1 - S)^\dagger (1 - S) | \alpha \rangle &= \langle \alpha | (1 - S)^\dagger | \alpha \rangle + \langle \alpha | (1 - S) | \alpha \rangle \\ \Rightarrow \int d\gamma \langle \alpha | (1 - S)^\dagger | \gamma \rangle \langle \gamma | (1 - S) | \alpha \rangle &= \langle \alpha | -iT | \alpha \rangle^\dagger + \langle \alpha | -iT | \alpha \rangle \\ &\Rightarrow \int d\gamma |\langle \gamma | T | \alpha \rangle|^2 = 2 \text{Re} (\langle \alpha | -iT | \alpha \rangle) \\ &= 2 \text{Im} (\langle \alpha | T | \alpha \rangle). \end{aligned} \quad (2.55)$$

The right hand side is the imaginary part of the forward scattering amplitude, $|\alpha\rangle \rightarrow |\alpha\rangle$. The left hand side is the total scattering probability from a state $|\alpha\rangle$ to *any* final state $|\gamma\rangle$. Conventional scattering amplitudes are in the form $\langle \beta | T | \alpha \rangle = (2\pi)^4 \delta^4(p_\beta - p_\alpha) A_{\beta\alpha}$. Expressing Eq. (2.55) in terms of A gives the result Eq. (2.54).

Deriving the unitarity constraints

In terms of partial waves, the elastic scattering cross section for $2 \rightarrow 2$ scattering is

$$\begin{aligned} \sigma_{el} &= \frac{1}{64\pi^2} \int \frac{|A|^2}{s} d\Omega \\ &= \frac{16\pi}{s} \sum_{l=0}^{\infty} (2l+1) |a_l|^2. \end{aligned} \quad (2.56)$$

The elastic cross section cannot be larger than the total cross section:

$$\sigma_{total} \geq \sigma_{el}. \quad (2.57)$$

Writing this in terms of partial waves, using Eq. (2.54) and Eq. (2.56), gives

$$\frac{16\pi}{s} \sum_{l=0}^{\infty} (2l+1) \text{Im}[a_l] \geq \frac{16\pi}{s} \sum_{l=0}^{\infty} (2l+1) |a_l|^2 . \quad (2.58)$$

As this is a sum of independent cross sections, it must be true for any l . Therefore, if unitarity is conserved, this gives Eq. (2.51). We can write this in terms of $\text{Re}[a_l]$ by substituting $|a_l|^2 = \text{Re}[a_l]^2 + \text{Im}[a_l]^2$ into Eq. (2.51), giving

$$\text{Re}[a_l]^2 \leq \text{Im}[a_l] - \text{Im}[a_l]^2 . \quad (2.59)$$

Maximising the right hand side gives Eq. (2.52). We will use both of these inequalities in Chapter 6.

Chapter 3

Connecting inflation and dark matter

In this chapter we present our model, S -inflation, where the inflaton S is a gauge singlet scalar — a stable particle which can also account for the currently observed density of dark matter, Ω_{DM} .

The chapter is organised as follows. In Section 3.1 we introduce our model and make a conformal transformation to the Einstein frame. In Section 3.2 we set out the calculation of the radiative corrections and derive the RG (renormalization group) equations. In Section 3.3 we discuss constraints coming from stability and perturbativity of the potential and constraints from slow-roll inflation observables. In Section 3.4 we discuss S as dark matter, relating the Higgs- S coupling λ_{hs} and the S -mass m_s . Then, in Section 3.5 we present the allowed parameter space in terms of λ_{hs} versus m_h and in terms of m_s versus m_h . We also discuss how the spectral index varies with the parameters of the model.

3.1 The S -Inflation Model

3.1.1 Non-minimally Coupled Gauge Singlet Scalar Extension of the Standard Model

The Jordan frame is a frame where the matter part of the action is a simple function of the metric and matter fields only, i.e. $S_m(g_{\mu\nu}, \phi_m)$ [57]. We define the action for our theory (in the Jordan frame) to be

$$S_J = \int \sqrt{-g} d^4x \left(\mathcal{L}_{SM} + (\partial_\mu S)^\dagger (\partial^\mu S) + (D_\mu H)^\dagger (D^\mu H) - \frac{M^2 R}{2} - \xi_s S^\dagger S R - \xi_h H^\dagger H R - V(S^\dagger S, H^\dagger H) \right) \quad (3.1)$$

where $V(S^\dagger S, H^\dagger H) = V^{(0)} + V^{(1)} + \dots$. The tree-level potential is

$$V^{(0)}(S^\dagger S, H^\dagger H) = \lambda_s (S^\dagger S)^2 + m_{s_o}^2 S^\dagger S + \lambda_{hs} S^\dagger S H^\dagger H + \lambda_h \left(H^\dagger H - \frac{v^2}{2} \right)^2 \quad (3.2)$$

and $V^{(1)}, V^{(2)}, \dots$ are the 1-loop and higher-order quantum corrections. $\mathcal{L}_{\overline{SM}}$ is the Standard Model Lagrangian density minus the purely Higgs doublet terms. The parameter $m_{s_o}^2$ is the constant contribution to the total S mass squared, m_s^2 . This also gains a contribution from the coupling to the Higgs. For now we consider only the physical Higgs field h , where $H = \frac{1}{\sqrt{2}} \begin{pmatrix} 0 \\ h + v \end{pmatrix}$ and h is real. We consider the cases of both real S and complex S and choose the direction of inflation such that $S = \frac{s}{\sqrt{2}}$ where s is real. Although it is not strictly correct to ignore the unphysical components of H or the imaginary part of the complex S , the discussion of this will be postponed to Chapter 6. A discrete Z_2 (real S) or a global symmetry $U(1)$ (complex S) must be imposed to ensure stability of the scalars.

Our aim is to make predictions that can be tested by observation and experiment. We will calculate the observables of inflation: the spectral index n , the tensor to scalar ratio r and the running of the spectral index α . This is best done using the slow-roll approximation, which cannot easily be formulated in the Jordan frame due to the non-minimal gravitational sector. We will therefore make a transformation of the whole action, including radiative corrections, to the Einstein frame, and redefine the fields ($s \rightarrow \chi_s$, $h \rightarrow \chi_h$) to ensure canonical normalisation. The Einstein frame is a frame where the couplings to gravity are minimal. From here on we set $M = M_p$, since the correction to M due to the Higgs expectation value is tiny compared with M_p .

3.1.2 Conformal transformation

The Jordan frame and the Einstein frame are related by a conformal transformation which transforms the metric (and hence all other quantities) in a field dependent way. These two frames are mathematically equivalent. The action of S -inflation was defined in terms of the Jordan frame metric in Eq. (3.1). The Jordan frame is usually used for particle physics; its metric is obtained when we define a unit of time in terms of the inverse of an atomic frequency and take the speed of light $c = 1$ to define a unit of distance [57]. In this sense, the Jordan frame is the ‘real world’ frame, where we make measurements in a standard manner. The usefulness of transforming to the Einstein frame is that it transforms away the non-minimal coupling to gravity, leaving the Lagrangian in a familiar form, where methods for calculating physical quantities are well known. In contrast, units of time and distance in the Einstein frame are field dependent — certainly not units in which we are used to making measurements.

For general h and s , the conformal transformation to the Einstein frame is defined by

$$\tilde{g}_{\mu\nu} = \Omega^2 g_{\mu\nu} \quad (3.3)$$

with

$$\Omega^2 = 1 + \frac{\xi_s s^2}{M_P^2} + \frac{\xi_h h^2}{M_P^2}. \quad (3.4)$$

We can use

$$R = \Omega^2 \tilde{R} + 6\Omega \tilde{\nabla}^\mu \tilde{\nabla}_\mu \Omega - 12\tilde{g}^{\mu\nu} \partial_\mu \Omega \partial_\nu \Omega \quad (3.5)$$

and

$$\partial_\mu \Omega = \frac{\xi_\phi \phi}{M_P^2 \Omega} \partial_\mu \phi + \frac{\xi_\sigma \sigma}{M_P^2 \Omega} \partial_\mu \sigma \quad (3.6)$$

to write (disregarding the total derivative which comes from $\Omega^{-1} \tilde{\nabla}^\mu \tilde{\nabla}_\mu \Omega$)

$$S = \int d^4x \sqrt{-\tilde{g}} \left[\tilde{\mathcal{L}}_{SM} + \frac{1}{2} \left(\frac{1}{\Omega^2} + \frac{6\xi_s^2 s^2}{M_P^2 \Omega^4} \right) \tilde{g}^{\mu\nu} \partial_\mu s \partial_\nu s + \frac{1}{2} \left(\frac{1}{\Omega^2} + \frac{6\xi_h^2 h^2}{M_P^2 \Omega^4} \right) \tilde{g}^{\mu\nu} \partial_\mu h \partial_\nu h \right. \\ \left. + \frac{6\xi_s \xi_h s h \tilde{g}^{\mu\nu} \partial_\mu s \partial_\nu h}{M_P^2 \Omega^4} - \frac{M_P^2 \tilde{R}}{2} - \frac{V(s, h)}{\Omega^4} \right]. \quad (3.7)$$

We can then redefine the fields using¹

$$\frac{d\chi_s}{ds} = \sqrt{\frac{\Omega^2 + 6\xi_s^2 s^2/M_P^2}{\Omega^4}} \quad \text{and} \quad \frac{d\chi_h}{dh} = \sqrt{\frac{\Omega^2 + 6\xi_h^2 h^2/M_P^2}{\Omega^4}}, \quad (3.8)$$

resulting in the Einstein frame action

$$S_E = \int d^4x \sqrt{-\tilde{g}} \left(\tilde{\mathcal{L}}_{SM} - \frac{M_P^2 \tilde{R}}{2} + \frac{1}{2} \tilde{g}^{\mu\nu} \partial_\mu \chi_h \partial_\nu \chi_h + \frac{1}{2} \tilde{g}^{\mu\nu} \partial_\mu \chi_s \partial_\nu \chi_s \right. \\ \left. + A(\chi_s, \chi_h) \tilde{g}^{\mu\nu} \partial_\mu \chi_h \partial_\nu \chi_s - U(\chi_s, \chi_h) \right) \quad (3.9)$$

where

$$A(\chi_s, \chi_h) = \frac{6\xi_s \xi_h}{M_P^2 \Omega^4} \frac{ds}{d\chi_s} \frac{dh}{d\chi_h} h s, \quad (3.10)$$

$$U(\chi_s, \chi_h) = \frac{1}{\Omega^4} V(s, h)$$

and

$$U^{(0)}(\chi_s, \chi_h) = \frac{1}{\Omega^4} \left(\frac{\lambda_h}{4} (h^2 - v^2)^2 + \frac{\lambda_s}{4} s^4 + \frac{1}{2} m_{s_o}^2 s^2 + \frac{\lambda_{hs}}{4} s^2 h^2 \right). \quad (3.11)$$

¹These are only total derivatives in the limits $h \rightarrow 0$ and $s \rightarrow 0$ respectively.

3.1.3 Jordan and Einstein Frames

All observables must be conformal-frame invariant — which means that at a classical level the frames are physically equivalent [57]. However, the situation may change when quantum effects are included, although this depends on the approximations used. For example, quantising a full quantum gravity theory in different conformal frames is likely to give differing results. This has been shown explicitly for a certain example in [58]. If instead a semiclassical approximation is used, where both the scalar fields and the metric are treated classically, then frames are physically equivalent [57]. However, if only the metric is treated classically, then the conformal frames are not generally equivalent [59], although this is probably due to the approximations used [57].

The scenario applicable in this thesis is that of an effective field theory: this means that the equivalence theorem [60, 61] of non-linear field re-definitions applies. This states that “the scattering matrix is invariant under non-linear local field redefinitions” [57]. In the context of this thesis, it means that tree-level particle scattering computations will be the same in any conformal frame. In Chapter 6 we use this theorem to compute scalar scattering cross sections.

As well as scattering amplitudes, we wish to compute the curvature perturbation in the Einstein frame. After inflation, the frames will be identical (as $\frac{S^\dagger S}{\xi_s} \ll M_p$ and $\frac{H^\dagger H}{\xi_h} \ll M_p$). Therefore the curvature perturbation spectrum as calculated in the Einstein frame will be suitable to be compared to measurements made in the Jordan frame. It has been shown explicitly in [62] that the spectral index for induced gravity inflation is identical in the Jordan and Einstein frames, provided that a different slow roll expansion is used in the Jordan frame. The Jordan frame spectral index for a non-minimally coupled theory was calculated (although not explicitly compared to the Einstein frame result). In the context of extended inflation [63], “well after extended inflation the Jordan and Einstein frames coincide so that the curvature fluctuations in both frames are the same”. This applies equally as well to our model. As the Einstein frame Lagrangian is minimally coupled to gravity, with a canonical kinetic term, the Einstein frame is the correct frame to calculate the curvature perturbation.

Our procedure is to define the theory, including all radiative corrections, in the Jordan frame. In the Jordan frame, we use the RG equations to run the couplings to an appropriate scale. We then transform to the Einstein frame in order to calculate the spectral index n , tensor-to-scalar ratio r and running of the spectral index α . Quantities in the Einstein frame will be denoted by a tilde (e.g. $\tilde{g}_{\mu\nu}$). As the two frames are equivalent at low values of the fields and all inflation observables are calculated when perturbations re-enter the horizon (i.e. at late times when the fields are small), the results calculated in the Einstein frame are the same as if we had calculated them with the non-minimally coupled scalar field in the Jordan frame.

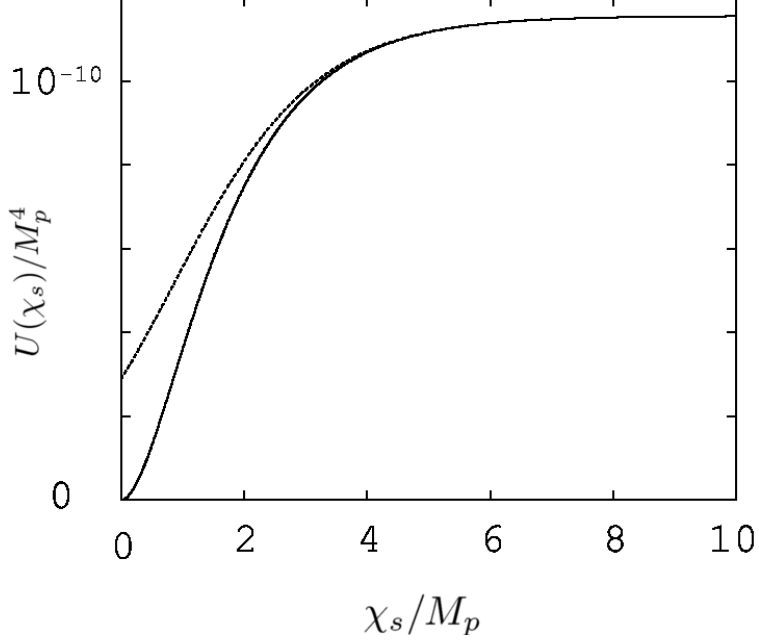


Figure 3.1: Einstein frame potential, in limit $s \gg M_P/\sqrt{\xi}$ (dashed) and exact (solid). This figure is plotted for real S with $m_h = 160$ GeV, $\lambda_s(m_t) = 0.01$ and $\lambda_{h,s}(m_t) = 0$.

3.1.4 Slow Roll Inflation

We will be interested in inflation purely along the s direction². In this case (during inflation) $h = 0$, $A(\chi_s, \chi_h) = 0$ and $\Omega^2 = 1 + \frac{\xi_s s^2}{M_P^2}$. When considering the potential, there are three approximate regimes (for $\xi_s \gg \xi_h$):

- (i) $\frac{\sqrt{\xi_s s}}{M_P} \ll 1$ giving $\Omega^2 \simeq 1$, $s \simeq \chi_s$ and

$$U(\chi_s) \simeq \frac{\lambda_s \chi_s^4}{4}; \quad (3.12)$$

- (ii) $\frac{\sqrt{\xi_s s}}{M_P} \ll 1 \ll \frac{\xi_s s}{M_P}$ giving $\Omega^2 \simeq 1$, $\chi_s \simeq \sqrt{\frac{3}{2}} \frac{\xi_s s^2}{M_P}$ and

$$U(\chi_s) \simeq \frac{\lambda_s M_P^2}{6\xi_s^2} \chi_s^2; \quad (3.13)$$

- (iii) $\frac{\sqrt{\xi_s s}}{M_P} \gg 1$ giving $\Omega^2 \simeq \frac{\xi_s s^2}{M_P^2}$ and $\chi_s \simeq \sqrt{6} M_P \ln\left(\frac{\sqrt{\xi_s s}}{M_P}\right)$ with [32] (for $\xi_s \gg 1$)

$$U^{(0)}(\chi_s, 0) \approx \frac{\lambda_s M_P^4}{4\xi_s^2} \left(1 + \exp\left(-\frac{2\chi_s}{\sqrt{6}M_P}\right)\right)^{-2}. \quad (3.14)$$

The third regime, $s \gg M_P/\sqrt{\xi_s}$, is relevant for inflation and the Einstein frame potential Eq. (3.14) is shown in Fig. (3.1) along with the full tree-level potential. It should be noted that for $\lambda_s \sim \mathcal{O}(1)$, we require a large value of $\xi_s \sim 10^4$ in order to reproduce the observed

²Inflation in the h direction for real S was considered in [64].

curvature perturbation spectrum. This large value of ξ_s seems unnatural.

Thus, $U(\chi_s, 0) \propto 1/\xi_s^2$. Similarly, along the h direction (with $s = 0$), $U(0, \chi_h) \propto 1/\xi_h^2$ for $h \gg M_p/\sqrt{\xi_h}$. Therefore, if $\xi_s \gg \xi_h$ then the minimum of the potential at large s and h will be very close the $h = 0$ direction and so inflation will naturally occur along the s direction. In the remainder of this chapter we will consider the limit where the Higgs boson is minimally coupled to the Ricci scalar at the weak scale, $\xi_h(m_t) = 0$, but we allow for its running by including the RG equation for ξ_h . Although inflation can easily occur with $A \simeq 0$, this term cannot be ignored when considering particle scattering (where $h \neq 0$). This issue is explored in Chapter 6. However for now we will proceed under the assumption that this term does not cause any problems.

3.2 Radiative corrections

It is important to calculate quantum corrections to the tree level potential and we do this in the Jordan frame using the RG equations to run the couplings from the Standard Model scale (m_t) to the inflation scale. We then use those values of the coupling constants to calculate the Coleman-Weinberg correction to the potential, $V = V^{(0)} + V^{(1)}$ [50, 52], where $V^{(0)}$ is given by Eq. (3.2). The potential is then transformed to the Einstein frame to study slow-roll inflation.

In Chapter 5, we will compare different methods for calculating the radiative corrections to this type of model and show how the Coleman-Weinberg potential is not adequate for inflation along the h direction, due to the variation of the non-minimal coupling (ξ_h) during inflation, which is not accounted for by the Coleman-Weinberg potential. This effect is, however, much less important for S -inflation and we will find that our results do not change much, therefore justifying the use of the Coleman-Weinberg potential.

3.2.1 Coleman-Weinberg Potential

Constraints on the scalar couplings will come from the stability of the electroweak vacuum and the requirement that the potential remains perturbative for field values less than M_p . This is important for inflation and for particle scattering, so we will impose the conditions for vacuum stability and perturbativity along both the $h = 0$ and $s = 0$ directions. We assume this is an adequate check on the potential (the constraints should in fact be applied to arbitrary directions of the full potential³). We use the $\overline{\text{MS}}$ renormalization scheme throughout. The one-loop potential

³However, as the $h = 0$ and $s = 0$ directions are limiting cases, this assumption seems reasonable.

for the s direction is

$$16\pi^2 V^{(1)}(s) = \frac{1}{4}H_s^2 \left(\ln \frac{H_s}{\mu^2} - \frac{3}{2} \right) + \frac{3}{4}G_s^2 \left(\ln \frac{G_s}{\mu^2} - \frac{3}{2} \right) + \frac{1}{4}P_s^2 \left(\ln \frac{P_s}{\mu^2} - \frac{3}{2} \right) + \frac{1}{4}Q_s^2 \left(\ln \frac{Q_s}{\mu^2} - \frac{3}{2} \right), \quad (3.15)$$

where

$$H_s = m_h^2 + \frac{1}{2}c_h\lambda_{hs}s^2, \quad G_s = m_h^2 + \frac{1}{2}\lambda_{hs}s^2, \\ P_s = m_{s_o}^2 + 3c_s\lambda_s s^2 \quad \text{and} \quad Q_s = \begin{cases} 0 & (\text{real } S) \\ m_{s_o}^2 + \lambda_s s^2 & (\text{complex } S). \end{cases} \quad (3.16)$$

The one-loop correction for the h direction is

$$16\pi^2 V^{(1)}(h) = \frac{1}{4}H_h^2 \left(\ln \frac{H_h}{\mu^2} - \frac{3}{2} \right) + \frac{3}{4}G_h^2 \left(\ln \frac{G_h}{\mu^2} - \frac{3}{2} \right) + \frac{1}{4}P_h^2 \left(\ln \frac{P_h}{\mu^2} - \frac{3}{2} \right) + \frac{1}{4}Q_h^2 \left(\ln \frac{Q_h}{\mu^2} - \frac{3}{2} \right) + \frac{3}{2}W^2 \left(\ln \frac{W}{\mu^2} - \frac{5}{6} \right) + \frac{3}{4}Z^2 \left(\ln \frac{Z}{\mu^2} - \frac{5}{6} \right) - 3T^2 \left(\ln \frac{T}{\mu^2} - \frac{3}{2} \right), \quad (3.17)$$

where

$$W = \frac{g^2 h^2}{4}, \quad Z = \frac{(g^2 + g'^2) h^2}{4}, \quad T = \frac{y_t^2 h^2}{2}, \quad H_h = m_h^2 + 3c_h\lambda_h h^2, \quad G_h = m_h^2 + \lambda_h h^2, \\ P_h = m_{s_o}^2 + \frac{1}{2}c_s\lambda_{hs}h^2 \quad \text{and} \quad Q_h = \begin{cases} 0 & (\text{real } S) \\ m_{s_o}^2 + \frac{1}{2}\lambda_{hs}h^2 & (\text{complex } S). \end{cases} \quad (3.18)$$

In these equations c_s and c_h are suppression factors to be discussed in the following section.

3.2.2 Suppression of Scalar Propagators

The non-minimal coupling to gravity in the Jordan frame means that the scalar field propagator (proportional to the commutator $[\phi(\vec{x}), \dot{\phi}(\vec{y})]$) is modified. The technique for calculating this modification was introduced by [65] and first applied to the case of Higgs inflation by [38].

The modified commutator

The scalar fields are quantised in flat space, in the Jordan frame. Thus we will need the commutator $[\phi(\vec{x}), \dot{\phi}(\vec{y})]$. The standard commutator

$$[\phi(\vec{x}), \pi(\vec{y})] = i\hbar\delta^3(\vec{x} - \vec{y}). \quad (3.19)$$

applies in the Einstein frame where the gravitational term is minimal and the canonical momentum π can be calculated. It is

$$\begin{aligned}\pi &= \frac{\partial \mathcal{L}}{\partial(\partial_0 \phi)} = \sqrt{-\tilde{g}} \left(\tilde{g}^{0\nu} \left(\frac{d\chi}{d\phi} \right)^2 \partial_\nu \phi \right) \\ &= \Omega^2 \left(\frac{d\chi}{d\phi} \right)^2 \sqrt{-g} (g^{0\nu} \partial_\nu \phi).\end{aligned}\tag{3.20}$$

Using the commutator Eq. (3.19) and rearranging, the result (for flat space) is

$$\begin{aligned}[\phi(\vec{x}), \dot{\phi}(\vec{y})] &= \frac{1}{\Omega^2} \left(\frac{d\chi}{d\phi} \right)^{-2} i\hbar \delta^{(3)}(\vec{x} - \vec{y}) \\ &= i\hbar c_\phi \delta^{(3)}(\vec{x} - \vec{y}).\end{aligned}\tag{3.21}$$

Thus, the commutator in the Jordan frame is suppressed by a factor c_ϕ where [65, 66]

$$c_\phi = \frac{1 + \frac{\xi_\phi \phi^2}{M_p^2}}{1 + (6\xi_\phi + 1) \frac{\xi_\phi \phi^2}{M_p^2}}.\tag{3.22}$$

The commutator and the RG equations

The commutator $[\phi(\vec{x}), \dot{\phi}(\vec{y})]$ enters into calculations through the scalar propagator — which will be suppressed by a factor c_ϕ compared to its minimally coupled value. In our case, all scalars ϕ_i are *in principle* suppressed by differing factors c_{ϕ_i} . However, only the field which has a large value (i.e. the inflaton) is actually suppressed. This can be seen by considering the suppression factor for a field σ with zero expectation value, which is given by Eq. (3.21):

$$c_\sigma = \frac{1}{\Omega^2} \left(\frac{d\chi}{d\sigma} \right)^{-2} = \frac{\Omega^2}{\Omega^2} = 1.\tag{3.23}$$

Note that Ω^2 can be arbitrarily large without affecting c_σ . In practice, when calculating the RG equations or the Coleman-Weinberg potential, one suppression factor is inserted for each h or s propagator in a loop but *not* for the scalars corresponding to imaginary part of S or the unphysical degrees of freedom of H . The suppression factor for the field which is *not* the inflaton is then set to 1. The suppression factors will have a significant effect on the running of the scalar couplings.

We include some factors of c_h in the two loop equations, following [38]. There is a minor difference between our work and [64] relating to a factor of c_ϕ (s in [64]) in the ξ_h RG equation. The term in β_ξ proportional to λ_h is suppressed by a factor $(1 + c_\phi^2)$ in Eq. (A2) of [64], but $(1 + c_\phi)$ in our work [1]. We believe that the latter is correct because only one physical Higgs h runs in the corresponding loop.

3.2.3 Initial conditions

We take the initial values of the coupling constants to be defined at the renormalization scale $\mu = m_t$, with $m_t = 171.0$ GeV and $v = 246.22$ GeV. The gauge couplings are given by

$$\frac{g^2(m_t)}{4\pi} = 0.03344, \quad \frac{g'^2(m_t)}{4\pi} = 0.01027 \quad \text{and} \quad \frac{g_3^2(m_t)}{4\pi} = 0.1071. \quad (3.24)$$

The couplings g and g' are obtained by an RG flow from their values at $\mu = M_Z$, which are given in [67], while g_3 is calculated numerically. (See [37] and references within for details.)

We use the pole mass matching scheme to set the initial conditions $\lambda_h(m_t)$ and $y_t(m_t)$. This relates the physical pole masses to the couplings in the $\overline{\text{MS}}$ renormalization scheme through the following expressions:

$$\begin{aligned} \lambda_h(m_t) &= \frac{m_h^2}{2v^2}(1 + 2\Delta_h) \\ y_t(m_t) &= \frac{\sqrt{2}}{v}m_t(1 + \Delta_t) \end{aligned} \quad (3.25)$$

where Δ_h and Δ_t account for radiative corrections and are given in the appendix of [56].

The remaining coupling constants are not fixed by observation and we are free to choose them. We take $\xi_h(m_t) = 0$ (as discussed earlier) and choose $\xi_s(m_t)$ such that the model is correctly normalised to the COBE results at the inflation scale [68, 69]:

$$\frac{U}{\bar{\epsilon}} = (0.0271M_p)^4. \quad (3.26)$$

As $\lambda_s(m_t)$ is not directly measurable, we take two reasonable values: 0.2 and 0.025. The higher of these corresponds to $\lambda_s(m_t)$ close to its perturbativity limit. $\lambda_{hs}(m_t)$ is treated as a free parameter, although it is in principle measurable through the thermal relic S dark matter density and scattering rate in dark matter detectors, as well as through the Higgs decay width to S pairs (if it is kinematically possible).

If $\xi_h(m_t)$ were not zero then we would expect greater running of ξ_s . In this case, a lower $\xi_s(m_t)$ would be required to obtain the same value of ξ_s at the scale of inflation. We would also expect differences in the spectral index due to the running of ξ_s — see the next chapter. However, as we require $\xi_s \gg \xi_h$ for inflation to occur solely in the s direction, we do not consider these possibilities.

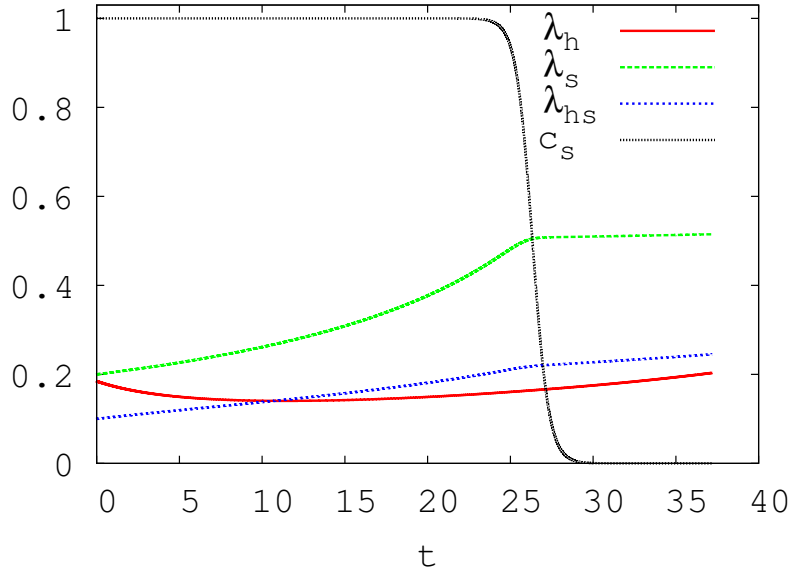


Figure 3.2: Showing the running of the scalar couplings λ_h (solid red), λ_s (green dashed) and λ_{hs} (blue dashed) and the suppression factor c_s (black dotted). The figure is plotted for real S with $m_h = 150$ GeV, $\lambda_s(m_t) = 0.2$, $\lambda_{hs}(m_t) = 0.1$ and $x_{is}(m_t) \approx 16500$ (chosen to match COBE normalisation of curvature perturbation). The figure is plotted in terms of $t = \ln(\mu/m_t)$, from $\mu = m_t$ to $\mu = M_p$. The suppression factor becomes important at the scale $\Lambda \sim \frac{M_p}{\xi_s}$.

3.2.4 RG equations for scalar couplings

In our analysis we use the two-loop RG equations for the Standard Model and modify these to include the leading order contributions of S . We also include the propagator suppression factors for the s and h directions which are given by Eq. (3.22) with $\phi = s, h$. The Standard Model one and two loop equations can be found in [38] and [56]. Using the technique detailed in [70, 71, 72] and applied to the case of S -inflation in the Appendix (page 113) we find that the one-loop β -functions for the scalar couplings are

$$\begin{aligned}
16\pi^2\beta_{\lambda_h}^{(1)} &= -6y_t^4 + \frac{3}{8} \left(2g^4 + (g^2 + g'^2)^2 \right) + (-9g^2 - 3g'^2 + 12y_t^2) \lambda_h \\
&\quad + (18c_h^2 + 6) \lambda_h^2 + \frac{1}{2} \begin{cases} c_s^2 \lambda_{hs}^2 & (\text{real } S) \\ (1 + c_s^2) \lambda_{hs}^2 & (\text{complex } S), \end{cases} \quad (3.27)
\end{aligned}$$

$$\begin{aligned}
16\pi^2\beta_{\lambda_{hs}}^{(1)} &= 4c_h c_s \lambda_{hs}^2 + 6(c_h^2 + 1) \lambda_h \lambda_{hs} - \frac{3}{2} (3g^2 + g'^2) \lambda_{hs} + 6y_t^2 \lambda_{hs} \\
&\quad + \begin{cases} 6c_s^2 \lambda_s \lambda_{hs} & (\text{real } S) \\ (6c_s^2 + 2) \lambda_s \lambda_{hs} & (\text{complex } S) \end{cases} \quad (3.28)
\end{aligned}$$

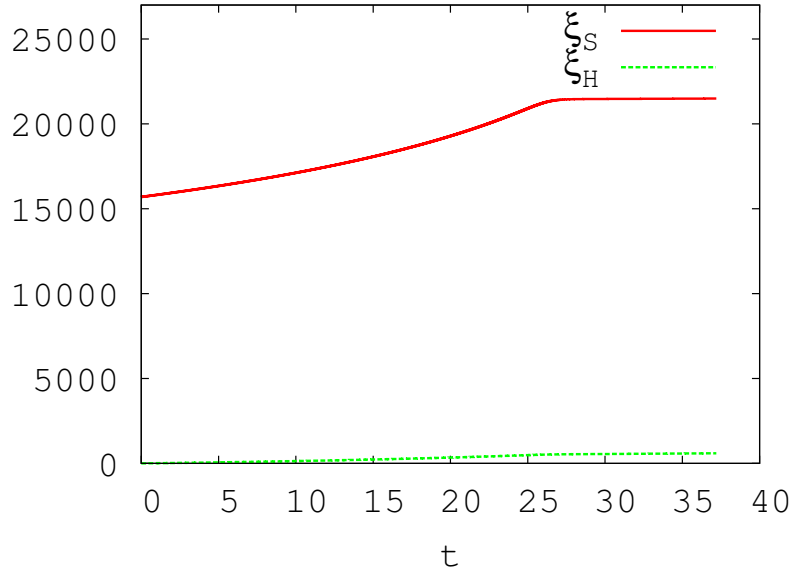


Figure 3.3: Showing the running of the non-minimal couplings ξ_h (solid red) and ξ_s (green dashed). The figure is plotted for real S with $m_h = 150$ GeV, $\lambda_s(m_t) = 0.2$, $\lambda_{h_s}(m_t) = 0.1$, $\xi_h(m_t) = 0$ and $x_{i_s}(m_t) \approx 16500$ (chosen to match COBE normalisation of curvature perturbation). The figure is plotted in terms of $t = \ln(\mu/m_t)$, from $\mu = m_t$ to $\mu = M_p$.

and

$$16\pi^2\beta_{\lambda_s}^{(1)} = \frac{1}{2}(c_h^2 + 3)\lambda_{h_s}^2 + \begin{cases} 18c_s^2\lambda_s^2 & (\text{real } S) \\ (18c_s^2 + 2)\lambda_s^2 & (\text{complex } S), \end{cases} \quad (3.29)$$

where $t = \ln \frac{\mu}{m_t}$, y_t is the top quark Yukawa coupling and $\beta_\lambda = \frac{d\lambda}{dt}$. We choose the value of μ in order to keep the log terms in the Coleman-Weinberg potential small, setting $\mu = s_{\tilde{N}}$, where $s_{\tilde{N}}$ is the field value \tilde{N} e-foldings before the end of inflation. An example showing the running of the scalar couplings, in the s -direction is in Fig. (3.2).

3.2.5 RG equations for ξ_s and ξ_h

We also obtained the RG equations for the non-minimal couplings to one-loop order. The resulting equations are

$$16\pi^2\frac{d\xi_s}{dt} = (3 + c_h)\lambda_{h_s}\left(\xi_h + \frac{1}{6}\right) + \left(\xi_s + \frac{1}{6}\right) \begin{cases} 6c_s\lambda_s & (\text{real } S) \\ (6c_s + 2)\lambda_s & (\text{complex } S) \end{cases} \quad (3.30)$$

and

$$16\pi^2 \frac{d\xi_h}{dt} = \left((6 + 6c_h) \lambda_h + 6y_t^2 - \frac{3}{2}(3g^2 + g'^2) \right) \left(\xi_h + \frac{1}{6} \right) + \left(\xi_s + \frac{1}{6} \right) \begin{cases} c_s \lambda_{hs} & (\text{real } S) \\ (1 + c_s) \lambda_{hs} & (\text{complex } S). \end{cases} \quad (3.31)$$

Fig. (3.3) shows the running of the non-minimal couplings in the s -direction. We observe ξ_h increasing from its initial value of zero, but always remaining much smaller than ξ_s . This is important for the consistency of our model since inflation will occur along the s direction only if $\xi_s \gg \xi_h$. Otherwise we would expect inflation to occur along a more general flat direction in the (s, h) plane. The initial value of ξ_s is approximately 10^4 — necessary for the curvature perturbation to match the COBE value. This seems to be an unnaturally large value and is a major downside to the model⁴.

Deriving the RG equations for ξ

The equations were obtained considering a general theory of scalars⁵ ϕ_i with mass terms and non-minimal couplings in the Lagrangian:

$$\mathcal{L} \supset -\frac{1}{2} m_{ij}^2 \phi_i \phi_j - \frac{1}{2} \xi_{ij} \phi_i \phi_j R. \quad (3.32)$$

Following the procedure of regularisation and renormalization (discussed in Chapter 2) the renormalization group equations can be calculated. Parameters that exist in the flat space theory have the same form in the curved space theory [47]. The bare and renormalized parameters of the theory Eq. (3.32) are related as follows [47]:

$$m_{ij}^2 = Z_{ij}^{kl} m_{kl}^2; \quad (3.33)$$

$$\xi_{ij} = Z_{ij}^{kl} \xi_{kl} - Z_{3ij}. \quad (3.34)$$

At one-loop level, Z_2 and Z_3 are related by the fixed point of the theory: $\xi_{ij} = -\frac{1}{6} \delta_{ij}$ (this was first shown in [73] and proved in [74]). Evaluating Eq. (3.34) at the fixed point gives

$$Z_{3ij}^{(1)} = -\frac{1}{6} \left(Z_{2ij}^{(1)kl} \delta_{kl} - \delta_{ij} \right), \quad (3.35)$$

⁴We might hope that a better understanding of quantum gravity provides an explanation for the large value of ξ_s .

⁵See pages 105–127 of [47] for a full discussion.

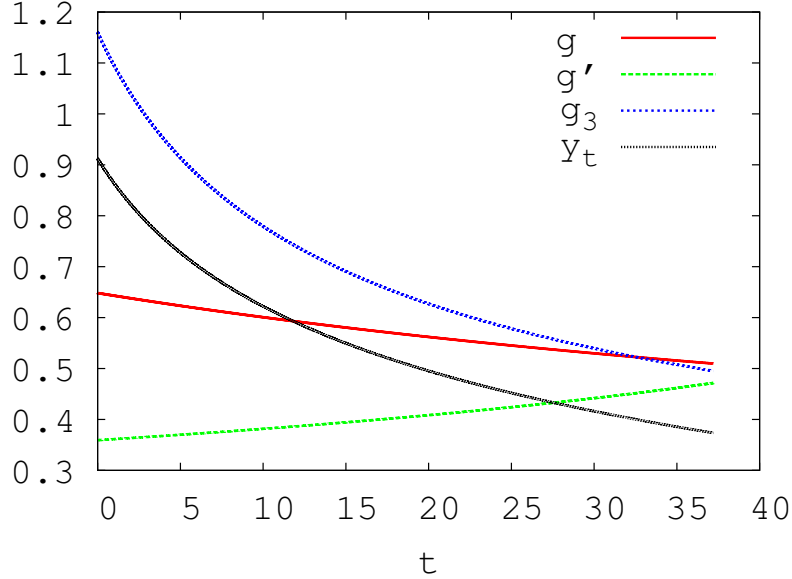


Figure 3.4: Showing the running of the gauge and Yukawa couplings: g (solid red), g' (green dashed), g_3 (blue dashed) and y_t (black dotted). The suppression factor c_s does not directly affect these couplings. The figure is plotted with $m_h = 150$ GeV, with $t = \ln \mu/m_t$ (from $\mu = m_t$ to $\mu = M_p$).

so, at one-loop,

$$\xi_{0ij} = Z_{2ij}^{kl} \left(\xi_{kl} + \frac{1}{6} \delta_{kl} \right) + \frac{1}{6} \delta_{ij}. \quad (3.36)$$

As Z_2 is known from the flat space mass renormalization, it is relatively easy to calculate β_ξ by applying the scalar potential RG equations to the 1-loop effective potential in order to obtain the β -function of the mass term [52], $\beta_{m_{ij}^2} \equiv \bar{\gamma}_{ij}^{ab} m_{ab}^2$. The RG equations for ξ are then given by

$$\mu \frac{d\xi_{ij}}{d\mu} = \left(\xi_{kl} + \frac{1}{6} \delta_{kl} \right) \bar{\gamma}_{ij}^{kl}. \quad (3.37)$$

Finally, the equations must be modified at large s or h by suppressing the propagator for the corresponding real scalar field as explained in Section 3.2.2.

3.2.6 RG equations for gauge and Yukawa couplings

The two-loop RG equations for g , g' , g_3 and y_t are given below. They are taken from the Appendix of [56] and include suppression factors for all components of H running in a loop. This is in fact an error (only the physical h should be suppressed) which is corrected in our later analysis (Chapter 5). We assume that only the top quark Yukawa coupling is important. The two-loop equations are

$$\beta_g = -\frac{20 - c_h}{6} g^3 + \frac{g^3}{16\pi^2} \left(\frac{3}{2} g'^2 + \frac{35}{6} g^2 + 12g_3^2 - \frac{3}{2} c_h y_t^2 \right), \quad (3.38)$$

$$\beta_{g'} = \frac{40 + c_h}{6} g'^3 + \frac{g'^3}{16\pi^2} \left(\frac{199g'^2}{18} + \frac{9g^2}{2} + \frac{44g_3^2}{3} - \frac{17c_h y_t^2}{6} \right), \quad (3.39)$$

$$\beta_{g_3} = -7g_3^3 + \frac{g_3^3}{16\pi^2} \left(\frac{11}{6} g'^2 + \frac{9}{2} g^2 - 26g_3^2 - 2c_h y_t^2 \right), \quad (3.40)$$

and

$$\begin{aligned} \beta_{y_t} = & y_t \left(-\frac{9}{4} g^2 - \frac{17}{12} g'^2 - 8g_3^2 + \frac{9}{2} c_h y_t^2 \right) + \frac{y_t}{16\pi^2} \left[-\frac{23}{4} g^4 - \frac{3}{4} g^2 g'^2 + \frac{1187}{216} g'^4 + 9g^2 g_3^2 - 108g_3^4 \right. \\ & \left. + \frac{19}{9} g'^2 g_3^2 + \left(\frac{225}{16} g^2 + \frac{131}{16} g'^2 + 36g_3^2 \right) c_h y_t^2 + 6(-2c_h^2 y_t^4 - 2c_h^3 y_t^2 \lambda_h + c_h^2 \lambda_h^2) \right]. \quad (3.41) \end{aligned}$$

An example showing the running of these couplings is given in Fig. (3.4).

3.3 Constraints

We calculate the bounds on m_h and $\lambda_{hs}(m_t)$ by applying three constraints: (i) stability of the electroweak vacuum, (ii) perturbativity of the potential and (iii) consistency with the observed spectral index n and with limits on the tensor-to-scalar ratio r and running spectral index α . A possible fourth constraint, ‘wrong-way-roll’ ($\frac{dU}{d\chi_s} > 0$), which plays a role in Higgs inflation [64], is generally not violated in our model. This is because $\beta_{\lambda_s} > 0$ and β_{ξ_s} is small. In Higgs inflation, β_{λ_h} can become negative, causing $\frac{dU}{d\chi_h}$ to become negative.

3.3.1 Vacuum stability and perturbativity

We require stability of the electroweak vacuum for s and h up to M_p . We do not consider the possibility of a metastable vacuum, which depends on the cosmological evolution of the vacuum state. As discussed in Section 2.2.1, this imposes the constraints

$$\lambda_s > 0, \lambda_h > 0 \quad \text{and either} \quad \lambda_{hs} > 0 \quad \text{or} \quad \lambda_{hs}^2 < 4\lambda_h \lambda_s. \quad (3.42)$$

We will check the stability of the vacuum in both the s direction (with $c_h = 1$) and the h direction (with $c_s = 1$).

We also require the coupling constants to lie within the perturbative regime (see Section 2.2.2) up to the Planck scale, in both the s direction and the h direction. We apply the perturbativity condition $\lambda'_i < 4\pi$ to the coupling constants λ'_i defined through the potential

$$V(s, h) = \frac{1}{4!} \lambda'_h h^4 + \frac{1}{4!} \lambda'_s s^4 + \frac{1}{4} \lambda'_{hs} s^2 h^2. \quad (3.43)$$

The couplings in this potential appear in the Feynman vertices without additional numerical factors. $\lambda'_i < 4\pi$ then ensures that loop corrections are smaller than tree-level processes. This leads to the conditions on the couplings as defined in our potential

$$\lambda_h, \lambda_s < 2\pi/3 \quad \text{and} \quad \lambda_{hs} < 4\pi. \quad (3.44)$$

3.3.2 Constraints from slow-roll inflation

The observational constraints on inflation from WMAP five-year data (combined with baryon acoustic oscillations and supernovae data) are $n = 0.960 \pm 0.013$, $r < 0.22$ and $-0.068 < \alpha < 0.012$ [5]. (The error on n is given to $1\text{-}\sigma$, meaning that $0.947 \leq n \leq 0.973$ to 66% confidence.) Inflation occurs through the standard slow-roll mechanism, which we formulate in the Einstein frame. The potential in the χ_s direction is

$$U(\chi_s) = \frac{1}{\Omega(\chi_s)^4} \left(\frac{\lambda_s}{4} s^4(\chi_s) + V^{(1)}(s(\chi_s)) \right), \quad (3.45)$$

where $V^{(1)}(s)$ is given by Eq. (3.15). The slow roll parameters are similar to those in Section 1.2.4 but defined with respect to χ_s :

$$\tilde{\epsilon} = \frac{M_p^2}{2} \left(\frac{1}{\tilde{U}} \frac{d\tilde{U}}{d\chi_s} \right)^2, \quad \tilde{\eta} = \frac{M_p^2}{\tilde{U}} \frac{d^2\tilde{U}}{d\chi_s^2} \quad \text{and} \quad \tilde{\vartheta}^2 = \frac{M_p^4}{\tilde{U}^2} \frac{d\tilde{U}}{d\chi_s} \frac{d^3\tilde{U}}{d\chi_s^3}. \quad (3.46)$$

From these we can calculate the observable quantities

$$n = 1 - 6\tilde{\epsilon} + 2\tilde{\eta}, \quad r = 16\tilde{\epsilon} \quad \text{and} \quad \alpha = \frac{dn}{d \ln k} = -16\tilde{\eta}\tilde{\epsilon} + 24\tilde{\epsilon}^2 + 2\tilde{\vartheta}^2. \quad (3.47)$$

Using the tree-level potential and the approximation $\frac{\xi_s s^2}{M_p^2} \gg 1$ we estimate the tree-level slow-roll parameters to be $\tilde{\epsilon} \simeq \frac{4}{3} \frac{M_p^4}{\xi_s^2 s^4}$, $\tilde{\eta} \simeq -\frac{4}{3} \frac{M_p^2}{\xi_s s^2}$ and $\tilde{\vartheta}^2 \simeq \frac{16}{9} \frac{M_p^4}{\xi_s^2 s^4}$, where $s_N^2 \approx 4M_p^2 \tilde{N} / 3\xi_s$. A calculation of the classical (i.e. without including radiative corrections) spectral index, tensor-to-scalar ratio and running spectral index then gives

$$n_{cl} \approx 1 - \frac{2}{\tilde{N}} - \frac{3}{2\tilde{N}^2} + \mathcal{O}\left(\frac{1}{\tilde{N}^3}\right) = 0.966; \quad (3.48)$$

$$r \approx \frac{12}{\tilde{N}^2} + \mathcal{O}\left(\frac{1}{\xi_s \tilde{N}^2}\right) = 3.3 \times 10^{-3}; \quad (3.49)$$

$$\alpha \approx \frac{2}{\tilde{N}^2} + \frac{12}{\tilde{N}^3} + \mathcal{O}\left(\frac{1}{\tilde{N}^4}\right) = 6.1 \times 10^{-4}. \quad (3.50)$$

Thus r and α are negligibly small when compared with the observational limits. One may wonder whether the above precision is reliable. This is discussed below.

Radiative Corrections

Radiative corrections have a significant effect on the slow-roll parameters, particularly $\tilde{\epsilon}$. This is not surprising, as the tree level potential is exponentially flat and the radiative corrections add a small but significant slope. Including radiative corrections the slow roll parameters are

$$\tilde{\epsilon} = \frac{M_p^2}{2} \left(\frac{ds}{d\chi_s} \right)^2 \left(\frac{4}{s\Omega^2} + \frac{1}{1+\Theta} \frac{L_s}{s} \right)^2 \quad (3.51)$$

and

$$\begin{aligned} \tilde{\eta} = & M_p^2 \left(\frac{ds}{d\chi_s} \right)^2 \left(\frac{12}{s^2\Omega^4} - \frac{12\xi_s}{\Omega^4 M_p^2} + \frac{8L_s}{s^2\Omega^2(1+\Theta)} - \frac{L_s}{s^2(1+\Theta)} \right) \\ & + M_p^2 \frac{d^2s}{d\chi_s^2} \left(\frac{4}{s\Omega^2} + \frac{L_s}{s(1+\Theta)} \right). \end{aligned} \quad (3.52)$$

In these equations,

$$\Theta = \frac{4\Omega^4}{\lambda_s s^4} U^{(1)}, \quad \frac{d\Theta}{ds} = \frac{L_s}{s}, \quad (3.53)$$

$$L_s = \frac{1}{16\pi^2 \lambda_s} \left(\left(\frac{c_h^2 + 3}{2} \right) \lambda_{hs}^2 + \begin{cases} 18c_s^2 \lambda_s^2 & (\text{real } S) \\ 18c_s^2 \lambda_s^2 + 2\lambda_s^2 & (\text{complex } S) \end{cases} \right), \quad (3.54)$$

where L_s does not depend on s and

$$\frac{d^2s}{d\chi_s^2} = \frac{1}{2\Omega^6} \left(\frac{ds}{d\chi} \right)^4 \left[\frac{12\xi_s^3 s^3}{M_p^4} + \frac{2\xi_s \Omega^2 s}{M_p^2} - \frac{12\xi_s^2 s}{M_p^2} \right]. \quad (3.55)$$

The terms originating from $U^{(1)}$ are subdominant in $\tilde{\eta}$, but for a range of values of λ_{hs} and λ_s they can become more important than the tree-level result in $\tilde{\epsilon}$.

Planck scale corrections

It is important to check that Planck scale corrections of the form

$$\Delta V = \frac{a_n s^n}{2^{\frac{n}{2}} n! M_p^{n-4}}, \quad (3.56)$$

where the couplings a_n are $\mathcal{O}(1)$, do not dominate the spectral index. The corrections to $\tilde{\epsilon}$ and $\tilde{\eta}$ are [33]

$$\delta\tilde{\epsilon} = \frac{4(n-4)^2 a_n^2}{3\lambda_s^2 2^n (n!)^2} \left(\frac{s}{M_p} \right)^{2n-8} \quad (3.57)$$

and

$$\delta\tilde{\eta} = \frac{2(n-4)^2 a_n^2}{3\lambda_s 2^{n/2} n!} \left(\frac{s}{M_p} \right)^{n-4}. \quad (3.58)$$

For $n = 6$, this gives $\Delta n = 8.5 \times 10^{-6}$ (higher n corrections will be even smaller). Thus it is safe to say that Planck scale corrections are negligible.

Number of e-foldings

The number of e-foldings of inflation in the Einstein frame is given by the standard expression [68]

$$\tilde{N} = \int_{\chi_{end}}^{\chi_{\tilde{N}}} \frac{1}{M_p^2} \frac{\tilde{U}}{d\chi_S} d\chi_S = \int_{s_{end}}^{s_{\tilde{N}}} \frac{1}{M_p^2} \frac{\tilde{U}}{ds} \left(\frac{d\chi_S}{ds} \right)^2 ds, \quad (3.59)$$

where the end of inflation is defined by $\tilde{\eta} = 1$.

We have defined the end of inflation (and therefore $\tilde{N} = 0$) by $\eta = 1$, as this is where the slow roll parameters break down. The actual end of inflation is where $\ddot{a} = 0$ (equivalent to $\tilde{\epsilon}_H \equiv -\frac{\dot{H}}{H^2} = 1$). (Note that when $\ddot{a} = 0$ the slow roll approximation may not be valid, making computations difficult.) Defining the end of inflation by $\eta = 1$ introduces some error in the value of \tilde{N} . We will therefore take a conservative viewpoint that the total theoretical error in \tilde{N} is ± 1 . An error of $\Delta \tilde{N}$ corresponds to an error on the spectral index of approximately

$$\Delta n_{cl} \approx -\frac{2}{\tilde{N} + \Delta \tilde{N}} + \frac{2}{\tilde{N}} \approx -\frac{2\Delta \tilde{N}}{\tilde{N}^2}. \quad (3.60)$$

For $\Delta \tilde{N} = 1.5$ this gives $\Delta n_{cl} \sim 0.001$.

We will use \tilde{N} to determine the field value $s_{\tilde{N}}$ at the beginning of inflation, which we will need to calculate $\tilde{\eta}$ and $\tilde{\epsilon}$. The number of e-foldings in the Einstein frame \tilde{N} differs from the number of e-foldings N in the Jordan frame. This is because the definition of the scale factor in the Einstein frame and in the Jordan frame are different. They are related via

$$\tilde{N} = \ln \left(\frac{\tilde{a}_{end}}{\tilde{a}} \right) = \ln \left(\frac{a_{end}}{a} \frac{\Omega(t_{end})}{\Omega(t)} \right) = N + \ln \left(\frac{\Omega(t_{end})}{\Omega(t)} \right) \simeq N - \frac{1}{2} \ln \tilde{N}, \quad (3.61)$$

where a_{end} and t_{end} are the scale factor and time at the end of inflation. We use $\tilde{N} = 60$ corresponding to $N \simeq 62.0$ in this chapter. This is a reasonable assumption given that the reheating temperature in this model is high (see Chapter 4).

We calculate the field value at 60 e-foldings before the end of inflation as follows. At tree-level,

$$s_{end}^2 \simeq \frac{4}{3} \frac{M_p^2}{\xi_s}. \quad (3.62)$$

Then Eq. (3.59) is integrated using Eq. (3.51) and the approximation $\Theta = \text{constant}$ to give

$$\tilde{N} = \kappa \ln \left(\frac{4 + L_S \Omega_{\tilde{N}}^2 / (1 + \Theta_{\tilde{N}})}{4 + L_S \Omega_{end}^2 / (1 + \Theta_{end})} \right) - \frac{3}{4} \ln \left(\frac{\Omega_{\tilde{N}}^2}{\Omega_{end}^2} \right), \quad (3.63)$$

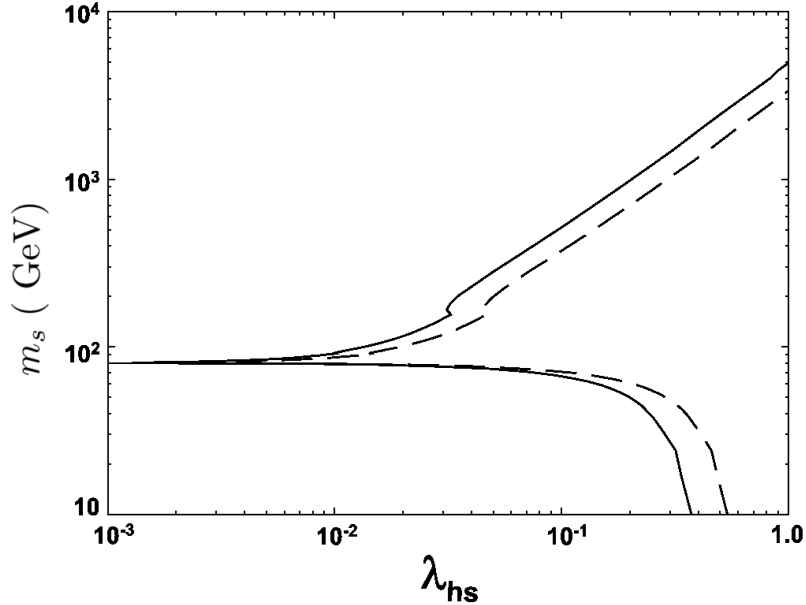


Figure 3.5: The value of m_s as a function of $\lambda_{hs}(m_t)$ necessary to produce the correct density of thermal relic dark matter. In this example $m_h = 150.0$ GeV. The solid line indicates real S and the dashed line complex S .

where

$$\kappa = \frac{1 + \Theta}{2L_S\xi_s} + \frac{6(1 + \Theta)}{2L_S} + \frac{3}{4}. \quad (3.64)$$

3.4 Thermal relic dark matter

We assume that dark matter is due to thermal relic gauge singlet scalars. The non-minimal coupling to gravity will not affect the S dark matter density as the field is at very low values compared to M_p . If we assume that the gauge singlet scalar is responsible for the observed dark matter density, $\Omega_{DM} = 0.228 \pm 0.013$ [5], then we obtain a relationship between m_s and $\lambda_{hs}(m_t)$. We use the Lee-Weinberg approximation [22] to calculate the relic density of S (see Section 1.5 for full details).

Here, we give the S annihilation cross-section times relative velocity, $\langle\sigma v_{rel}\rangle$, and the resulting dark matter density. We will approximate $\langle\sigma v_{rel}\rangle$ by the centre-of-mass cross-section for non-relativistic S annihilation. The tree-level processes contributing to S annihilation are (i) $SS \rightarrow hh$, (ii) $SS \rightarrow WW$, (iii) $SS \rightarrow ZZ$ and (iv) $SS \rightarrow \bar{f}f$ (where f is a Standard Model fermion). (i) proceeds via a 4-point contact interaction, an s-channel Higgs exchange interaction and a t- and u-channel S exchange interaction. The resulting $\langle\sigma v_{rel}\rangle$ is [1, 24]

$$\langle\sigma v_{rel}\rangle_{hh} = \frac{\lambda_{hs}^2}{64\pi m_s^2} \left[1 + \frac{3m_h^2}{(4m_s^2 - m_h^2)} + \frac{2\lambda_{hs}v^2}{(m_h^2 - 2m_s^2)} \right]^2 \left(1 - \frac{m_h^2}{m_s^2} \right)^{\frac{1}{2}}. \quad (3.65)$$

$SS \rightarrow WW, ZZ, \bar{f}f$ all proceed via s-channel Higgs exchange. The corresponding $\langle\sigma v_{rel}\rangle$ are:

$$\langle\sigma v_{rel}\rangle_{WW} = 2 \left[1 + \frac{1}{2} \left(1 - \frac{2m_s^2}{m_W^2} \right)^2 \right] \frac{\lambda_{hs}^2 m_W^4 \left(1 - \frac{m_W^2}{m_s^2} \right)^{\frac{1}{2}}}{8\pi m_s^2 \left((4m_s^2 - m_h^2)^2 + m_h^2 \Gamma_h^2 \right)}, \quad (3.66)$$

$$\langle\sigma v_{rel}\rangle_{ZZ} = 2 \left[1 + \frac{1}{2} \left(1 - \frac{2m_s^2}{m_Z^2} \right)^2 \right] \frac{\lambda_{hs}^2 m_Z^4 \left(1 - \frac{m_Z^2}{m_s^2} \right)^{\frac{1}{2}}}{16\pi m_s^2 \left((4m_s^2 - m_h^2)^2 + m_h^2 \Gamma_h^2 \right)} \quad (3.67)$$

and

$$\langle\sigma v_{rel}\rangle_{\bar{f}f} = \frac{m_W^2}{\pi g^2} \frac{\lambda_f^2 \lambda_{hs}^2 \left(1 - \frac{m_f^2}{m_s^2} \right)^{\frac{3}{2}}}{\left((4m_s^2 - m_h^2)^2 + m_h^2 \Gamma_h^2 \right)}. \quad (3.68)$$

Here the fermion Yukawa coupling is $\lambda_f = m_f/v$ where $v = 246.22$ GeV and m_f is the fermion mass. Γ_h is the Higgs decay width. (Fermions should be summed over colours.)

The cross-sections $\langle\sigma v_{rel}\rangle$ are the same whether the process involves SS or $S^\dagger S$. For real S , the present total mass density in S scalars is given by Eq. (1.49). The density for complex S is twice that for real S , due to the additional degree of freedom. For a given λ_{hs} and m_h there are up to four corresponding values of m_s which give the correct relic density. An example is shown in Fig. (3.5) for the case where $m_h = 160$ GeV. The cusp-like feature is due to S annihilations to WW and ZZ pairs close to the Higgs pole. In this region the S mass is relatively insensitive to λ_{hs} . Note also that large values of λ_{hs} are possible for m_s slightly below the Higgs pole.

3.5 Parameter space for S -inflation

We now present the results, giving the available parameter space for our model to give 60 Einstein frame e-foldings of inflation, while all couplings remain stable and perturbative up to the Planck scale. First, we discuss the parameter space in terms of m_h and λ_{hs} , as shown in Fig. (3.6) and Fig. (3.7).

Small λ_s

In Fig. (3.6a) we show the case of real S with ‘small’ $\lambda_s(m_t) = 0.025$. The range of allowed Higgs mass is $145 \text{ GeV} \lesssim m_h \lesssim 170 \text{ GeV}$, where the lower bound is from vacuum stability in the h direction combined with 5-year WMAP $1\text{-}\sigma$ upper bound $n < 0.973$. The upper bound is from perturbativity of λ_h in the s direction. The corresponding range of $\lambda_{hs}(m_t)$ is $|\lambda_{hs}(m_t)| \lesssim 0.15$. If we were to use the two- σ WMAP bound, we find that larger values of n allow larger $|\lambda_{hs}(m_t)|$, up to an upper bound $|\lambda_{hs}(m_t)| \approx 0.55$ (at $n \gtrsim 0.980$), which comes from the perturbativity bound on λ_s in the h direction. In this case the lower bound on the allowed Higgs masses is

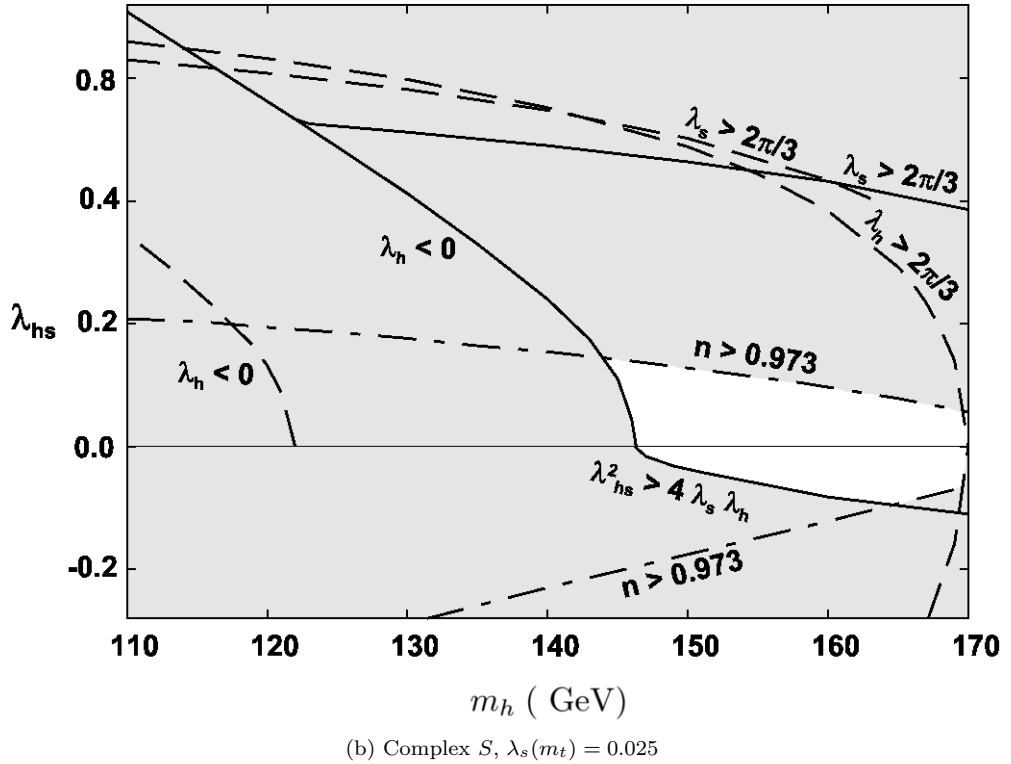
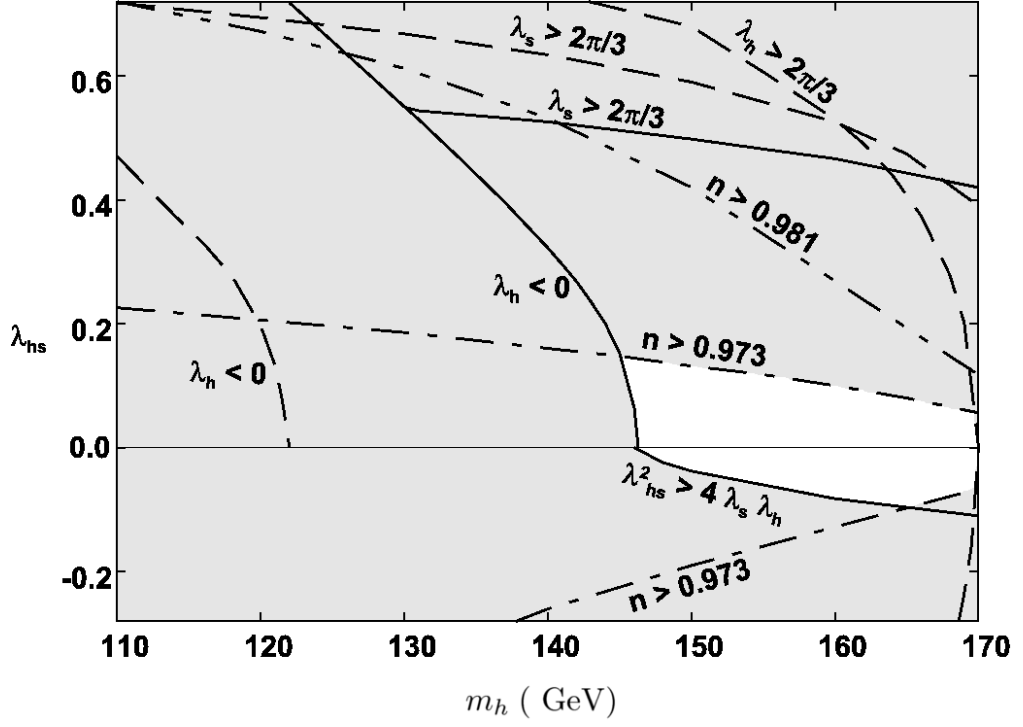


Figure 3.6: Allowed region for inflation in the s -direction for $\lambda_s = 0.025$. Excluded regions are shown in grey. Limits from couplings in the s -direction are shown with dashed lines, those from the couplings running in the h -direction have solid lines and the $1\text{-}\sigma$ upper limit on n is dot-dashed. In (a) we also show the line $n = 0.981$ (dot-dot-dash) demonstrating the variation of n .

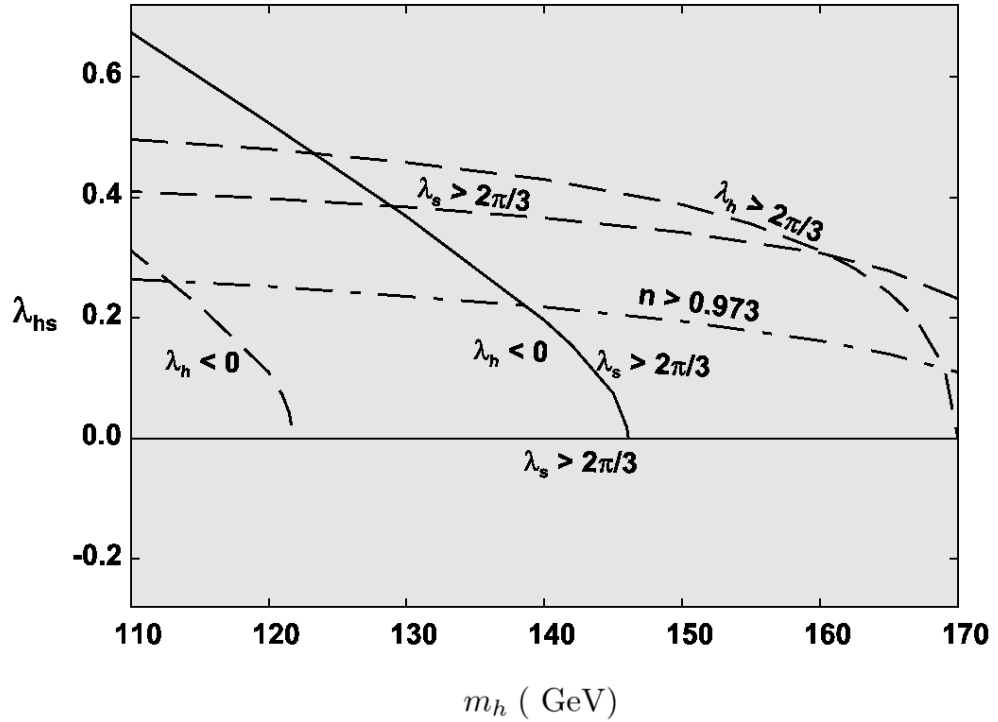
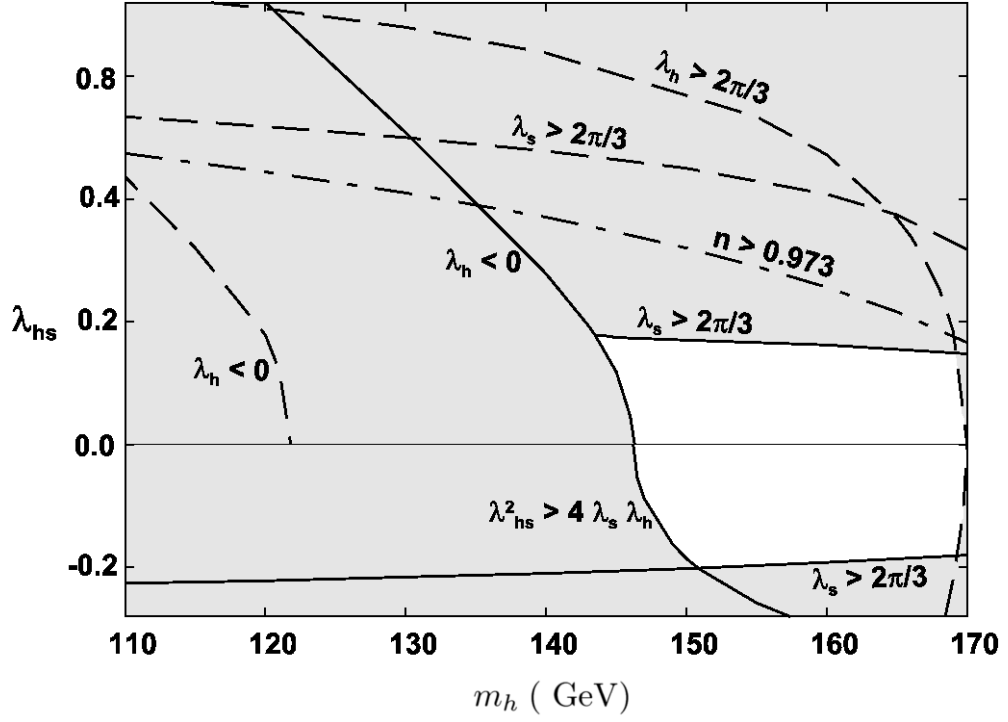


Figure 3.7: Allowed region for inflation in the s -direction for $\lambda_s = 0.2$. Excluded regions are shown in grey. Limits from couplings in the s -direction are shown with dashed lines, those from the couplings running in the h -direction have solid lines and the $1\text{-}\sigma$ upper limit on n is dot-dashed.

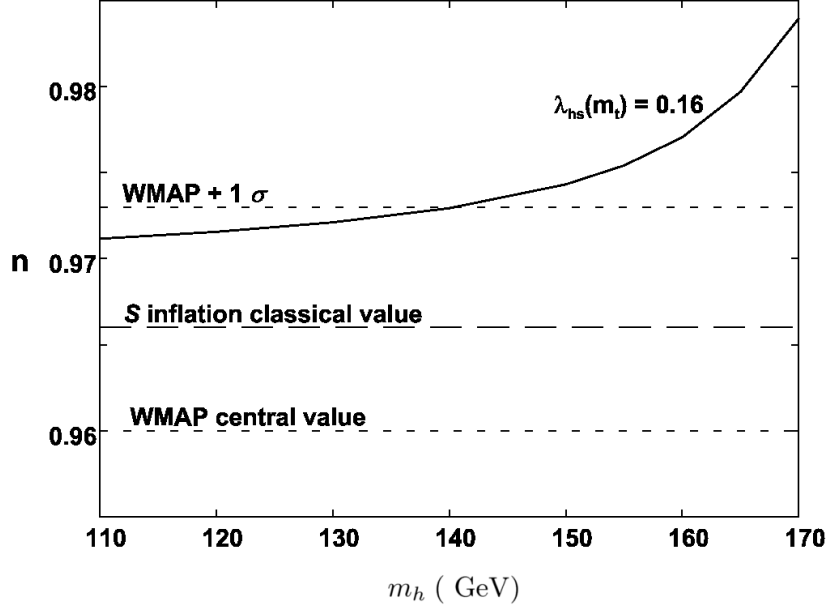


Figure 3.8: Showing the variation of n with m_h for $\lambda_s(m_t) = 0.025$ and $\lambda_{h_s}(m_t) = 0.16$. The WMAP central value and $1\text{-}\sigma$ upper bound are shown with short dashed lines; classical n for S -inflation is shown with a dashed line.

shifted downwards to $130 \text{ GeV} \lesssim m_h \lesssim 170 \text{ GeV}$. In Fig. (3.6b) we show the corresponding results for complex S . The allowed parameter space is very similar to the case of real S .

Large λ_s

In Fig. (3.7a) we show the results for the case of ‘large’ $\lambda_s(m_t) = 0.2$. In this case the range of Higgs mass is similar to the small λ_s case, but now the origin of the bound is perturbativity of λ_s in the h direction rather than the WMAP upper bound on n . As $\lambda_s(m_t)$ increases from 0.2, the allowed parameter space will rapidly diminish due to the decrease of the λ_s perturbativity upper bound on $\lambda_{h_s}(m_t)$. As seen in Fig. (3.7b), the allowed parameter space vanishes for the corresponding case with complex S .

Very small λ_s

As will be discussed in Chapter 6, if unitarity violation is a problem in this class of models, then it *may* be possible to avoid the problem in S -inflation with a very small value of λ_s [1]. This was recently considered in [75]. If this were the case we would expect λ_{h_s} to be low — comparing Fig. (3.6a) and Fig. (3.7a) we see that decreasing λ_s tends to increase n therefore we would expect the allowed values to decrease further with even smaller λ_s . Smaller values of λ_{h_s} will tend to drive m_s closer to the Higgs pole (Fig. (3.5)), increasing the chances that it could be detected in the near future.

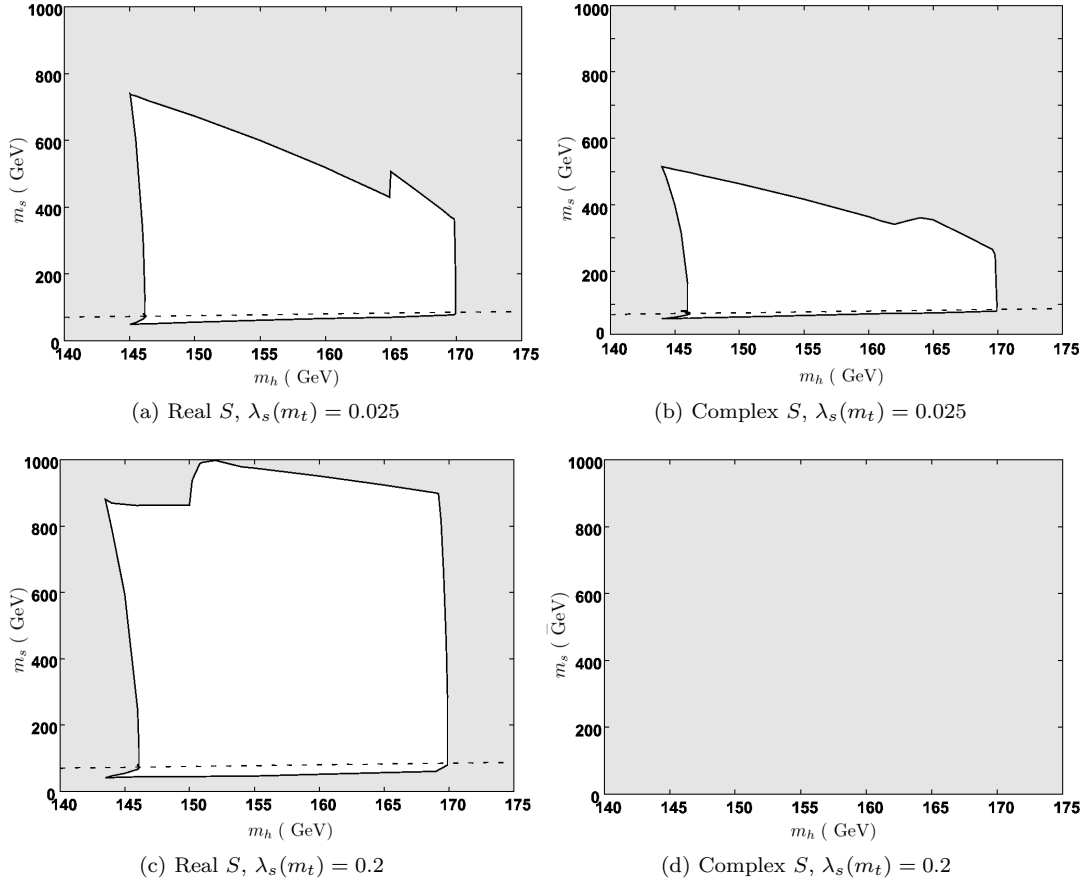


Figure 3.9: Allowed region for inflation in the s -direction, with a $1\text{-}\sigma$ upper limit on n . Excluded regions are shown in grey and all masses are in GeV. The dashed line shows $m_h = 2m_s$. Below this line, production of S -particles at the LHC (via $h \rightarrow S^\dagger S$ decay) is possible. There is no allowed region in (d).

Comparison with Higgs inflation

An important point is that the value of n can be significantly larger than the classical value $n = 0.966$ over the whole range of allowed Higgs mass. In Fig. (3.8) we show an example of the variation of n with m_h for fixed λ_{hs} and λ_s (this is explored in more detail in Chapter 5, Fig. (5.8)). This appears to contrast with the case of Higgs inflation (without additional scalars). Although the predictions in the literature are conflicting, n is either at or below the classical value at large m_h . Thus, the predictions of S -inflation appear to be unique. In [38] a significant increase of n from the classical value is obtained only for $m_h \lesssim 132$ GeV. Contradicting this, [37, 64] find that n is significantly *below* the classical value for both large and small m_h . These results are reviewed and discussed in Chapter 5, where we also re-compute the prediction for Higgs inflation.

Parameter space in terms of m_s

We now convert the range of λ_{hs} to a range of m_s . Fig. (3.9) shows the range of m_s and m_h consistent with S -inflation and thermal relic S dark matter, with $n \leq 0.973$ and all vacuum

stability and perturbativity constraints satisfied. We also show $m_s = m_h/2$, which is the limit at which it is possible to pair produce S scalars via Higgs decay at the LHC [76]. For the case of real S and ‘small’ $\lambda_s(m_t) = 0.025$, Fig. (3.9a), we see that m_s is mostly in the range $50 \text{ GeV} \lesssim m_s \lesssim 500 \text{ GeV}$, reaching 750 GeV close to its lower bound. For complex S , m_s is more constrained, with values in the range 50–500 GeV. This can be easily understood since the dark matter density for a complex S is twice that for a real S of the same mass, therefore a smaller mass is required to produce the same density. From Fig. (3.9c) we see that $\lambda_s(m_t) = 0.2$, permits a wider range of S mass, with m_s in the range 45 GeV to 1 TeV. If instead we were to consider the $2\text{-}\sigma$ WMAP bound, the parameter space in Fig. (3.9a) and Fig. (3.9b) would increase, while Fig. (3.9c) would be unchanged.

We note that while a large region of the allowed parameter space is at values of the S mass which are large compared with the weak scale, there is no reason to expect the S mass to be so large. The S mass squared is $m_s^2 = m_{s_o}^2 + \lambda_{hs}v^2/2$. Therefore if m_{s_o} is of the order of the weak scale (which is the most natural possibility in a theory based on a single mass scale), we would expect m_s to be no larger than a few hundred GeV. A partial cancellation due to either $\lambda_{hs} < 0$ or $m_{s_o}^2 < 0$ would also tend to give a weak scale m_s .

There is a small region of the allowed parameter space which satisfies $m_s < m_h/2$. This means that it is possible for the S inflaton to be produced at the LHC via Higgs decay [76]. Thermal relic S dark matter would then originate from freeze-out of near resonant S annihilation to WW and ZZ close to the Higgs pole. If m_s is slightly below the Higgs pole, this implies that $\lambda_{hs}(m_t)$ can be large, as can be seen from Fig. (3.5). Therefore if $m_s < m_h/2$ then the S -nucleon scattering cross-section due to Higgs exchange is likely to be large, enhancing the possibility of observing S dark matter in direct detection experiments. In this case, the available phase space for producing S particles at the LHC is small [77].

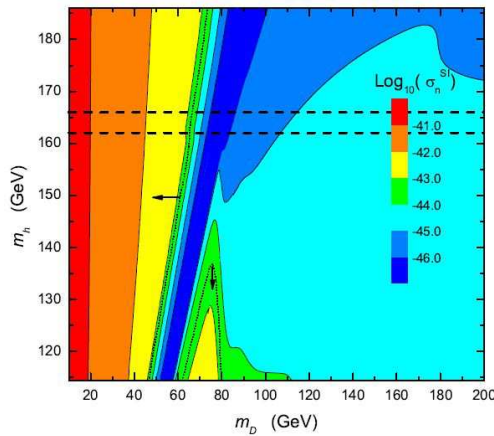
Particle physics constraints

Collider and direct dark matter detection experiments should be able to constrain the allowed parameter space⁶. Combined data from the D0 and CDF collaborations show that a Higgs boson mass in the range $162 \text{ GeV} < m_h < 166 \text{ GeV}$ is excluded at 95% confidence level [79, 80]. This exclusion reduces the available parameter space of the model by a small amount, however it does not make a large difference to the range of m_s , as this is largest at low values of m_h . Present bounds on direct detection of S dark matter from XENON10 and CDMSII rule out S mass in the range 10 GeV to (50,70,75) GeV for Higgs masses (120,200,350) GeV [76, 81]. Comparing with Fig. (3.9), we see that the upper bound from direct detection is already close to the lower bound

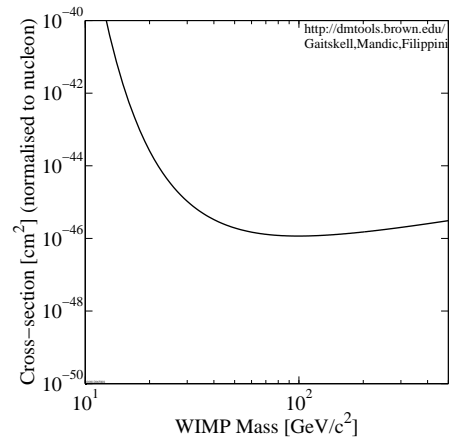
⁶ γ -ray and antimatter signals can also constrain the model [78].

on the range of m_s allowed by the S -inflation model. Thus, although most of the parameter space is allowed at present, a substantial part of the (m_s, m_h) parameter space will be accessible to future dark matter detectors.

In [77], the S -nucleon scattering cross section was plotted for $114.4 \text{ GeV} < m_h < 186 \text{ GeV}$ and $m_s < 200 \text{ GeV}$. The figure is reproduced in Fig. (3.10a). The excluded regions from XENON10 and CDMSII, as discussed above, are clearly seen (shown by arrows). Most of this parameter space will be covered by future experiments, including XENON100, XENON1T and CDMS 100kg. For example, the projected cross section for the XENON1T detector is shown in Fig. (3.10b). As can be seen in this figure, the XENON1T detector would detect S dark matter if the cross section is greater than 10^{-46}cm^2 — this covers all of the parameter space in Fig. (3.10a), except perhaps the dark blue stripe corresponding to the pole at $m_h = 2m_s$. However, if m_s was larger than a few hundred GeV (or very close to the pole at $m_h = 2m_s$), it is more difficult to detect. (We have assumed that the local density of dark matter is 0.3 GeVcm^{-3} [82].)



(a) Figure from [77], showing the S -nucleon scattering cross section (via Higgs exchange) for m_h and $m_D \equiv m_s$ up to 200 GeV. The Tevatron CDF and D0 95% confidence level exclusion is shown between dashed lines. The arrows show the exclusion from dark matter direct searches at CDMSII and XENON10.



(b) Showing the WIMP-nucleon cross section projected for the XENON1T detector, plotted using [83].

Figure 3.10: Figure showing dark matter cross sections (a) predicted for this model and (b) projected for the XENON1T detector.

Chapter 4

Reheating in S -inflation

In this chapter, we first review the mechanism for reheating in the case of pure Higgs inflation [33, 39]. We then show how reheating is possible in S -inflation despite the requirement that S is stable and cannot decay. Unlike many inflation models, the coupling of the inflaton s to the Standard Model is well constrained and we can calculate the temperature of radiation domination T_R . We define T_R to be the effective temperature¹ when the inflaton energy density is equal to the energy density in relativistic particles, ρ_R . The temperature at which thermal equilibrium occurs (the reheating temperature) will be lower than this and could be calculated by considering $2 \rightarrow 3$ processes [84]. Under reasonable assumptions the temperature of radiation domination is high:

$$3 \times 10^{13} \text{ GeV} \lesssim T_R \lesssim 8 \times 10^{14} \text{ GeV}. \quad (4.1)$$

The small range enables us to reasonably estimate \tilde{N} , which is $58 \lesssim \tilde{N} \lesssim 61$, and thus to give the classical spectral index, $0.965 \lesssim n_{cl} \lesssim 0.967$. A measurement of λ_{hs} (or m_s) through dark matter detection experiments will further increase the predictiveness of this model.

Reheating in Higgs inflation

Reheating in Higgs inflation occurs through a stochastic resonance [33]. After inflation, the Higgs-inflaton oscillates in a quadratic potential; the gauge boson masses are proportional to the modulus of the oscillating inflaton field. When the oscillation modulus is small, non-relativistic gauge bosons are produced non-adiabatically; when the modulus is large, the gauge bosons easily decay to relativistic Standard Model particles² [33]. This prevents the build up of gauge bosons. However, the expansion of the Universe causes the maximum amplitude of the oscillation to

¹This is simply a reparameterisation of the energy density: $T_R = \left(\frac{30}{\pi^2 g_*} \rho_R\right)^{1/4}$ where g_* is the effective number of relativistic degrees of freedom.

²It is shown in [33] that the relativistic particles produced via gauge boson decays would not dominate the energy density while the resonant production takes place.

decrease, which decreases the gauge bosons mass. As the decay rate of the gauge bosons is proportional to this mass, eventually the gauge bosons no longer decay appreciably and their density builds up, enabling the stochastic resonance. At this point, the energy of the inflaton is quickly transferred to the gauge bosons, which in turn quickly annihilate to relativistic fermions. Reheating via the production of Higgs excitations is also possible, but the stochastic resonance is expected to occur first [33]. According to [33], the temperature of radiation domination is $3 \times 10^{13} \text{ GeV} < T_R < 15 \times 10^{13} \text{ GeV}$ (where the lower limit is from reheating via the production of excitations of the Higgs-inflaton).

Reheating in Higgs inflation was also considered by [39]. They find a process of reheating similar to that described above, but emphasise the role of back reaction from the gauge bosons to the Higgs condensate. Significant backreaction would narrow the resonance before eventually shutting it off. The backreaction becomes important approximately 7 zero-crossings before reheating would complete, in the absence of the backreaction. They therefore conclude that a further numerical simulation is necessary to determine whether or not this backreaction spoils reheating. However, their analysis does not include the annihilation of the gauge bosons, which was shown by [33] to be an important process. Therefore we expect that backreaction will not spoil reheating. We do not consider the effect of backreaction in our analysis of reheating for S -inflation.

Reheating in S -inflation

Reheating in S -inflation must occur through H — which can then produce the particles of the Standard Model. In order for S to be dark matter as well as the inflaton, it must be stable and cannot decay. This means that any leftover inflaton density can only be transferred to thermal radiation through scattering with Higgs bosons in the thermal background. This is a potential problem in this model, and we need to be sure that the inflaton is a subdominant component of the Universe at the point when the inflaton potential becomes quartic ($\propto s^4$) [85]. In this case, as we will show, any residual oscillating inflaton density will eventually be thermalised by scattering from the dominant thermal background. If this were not the case, then the model of S -inflation may be fundamentally flawed (although it may be possible to still have reheating when χ is oscillating in this quartic potential). Therefore taking a conservative approach, we require reheating to occur during the (first) quadratic potential stage (Eq. (3.13)). We expect reheating to occur via stochastic resonance to Higgs bosons through the $\lambda_{hs}|S|^2|H|^2$ term, similar to Higgs inflation.

4.1 Evolution of the oscillating inflaton

The evolution of the S field is the background solution for the rest of the calculations. We are in the region of the potential where $\chi \simeq \frac{\sqrt{6}\xi_s s^2}{2M_p}$ and $U \simeq \frac{\lambda_s M_p^2 \chi^2}{6\xi_s^2}$ (see Section 3.1.4). The Friedmann equation is

$$H^2(t) = \frac{\rho}{3M_p^2} = \frac{1}{3M_p^2} \left[\frac{\omega^2}{2} \chi^2(t) + \frac{1}{2} \dot{\chi}^2(t) \right] \quad (4.2)$$

where

$$\omega^2 \equiv \frac{d^2 U}{d\chi^2} = \frac{\lambda_s}{3} \frac{M_p^2}{\xi_s^2} \quad (4.3)$$

is the effective mass squared of the inflaton (this is the same for all combinations of couplings, as $\frac{\lambda_s}{\xi_s^2}$ is fixed by the COBE normalisation). The solution is³

$$\begin{aligned} \chi(t) &= X(t) \cos(\omega(t - t_0)) \\ &= X(t) \sin(-\omega(t - t_j)) \end{aligned} \quad (4.4)$$

provided that

$$H^2(t) = \frac{\omega^2 X^2}{6M_p^2} \quad (4.5)$$

and

$$|\dot{X}(t)| \ll \omega X. \quad (4.6)$$

The zero crossing occurs at t_j , so $\chi(t_j) = 0$. The oscillating inflaton behaves like matter as $\rho \propto \frac{1}{a^3}$ [85], giving $H = \frac{2}{3t}$. Using Eq. (4.5), this gives

$$X(t) = 2\sqrt{\frac{2}{3}} \frac{M_p}{\omega} \frac{1}{t} \quad (4.7)$$

and we can now calculate

$$\frac{|\dot{X}|}{X} = \frac{1}{t}. \quad (4.8)$$

So, provided we consider times much larger than the time for one oscillation ($\frac{2\pi}{\omega}$), the approximation Eq. (4.6) is justified.

³The second line of Eq. (4.4) comes from $\cos(\omega(t_j - t_0)) = 0$.

Inflaton energy density

The energy density of the inflaton field is

$$\rho_{inf} = \frac{\omega^2}{2} X^2. \quad (4.9)$$

We will look for the point at which the energy density of relativistic particles is equal to this. This is what we will call the moment of radiation dominance (it is not important whether or not the particles are in equilibrium at this point). If this point occurs before the inflaton potential becomes quartic, then we have successful reheating. The transition between quadratic ($U \propto \chi^2$) and quartic ($U \propto \chi^4$) behaviour of the oscillating inflaton is defined to be the point where we match the amplitudes of the solutions in the two regimes. The two solutions are $\chi_{CR} = s_{CR}$ (radiation-like) and $\chi_{CR} = \frac{\sqrt{6}}{2} \frac{\xi_s s_{CR}^2}{M_p}$ (matter-like). Equating these gives $s_{CR} = \chi_{CR} \equiv X_{CR}$ where

$$X_{CR} = \sqrt{\frac{2}{3}} \frac{M_p}{\xi_s} = \sqrt{\frac{2}{\lambda_s}} \omega. \quad (4.10)$$

4.2 Reheating via stochastic resonance

4.2.1 Evolution of the Higgs boson modes

We consider the Higgs boson to be four real scalars ϕ_i . We calculate for *one* of these, ϕ , and multiply the final result by four, where necessary. The mode equation is

$$\ddot{\phi}_k + 3H\dot{\phi}_k + \left(\frac{k^2}{a^2} + m_\phi^2 \right) \phi_k = 0 \quad (4.11)$$

where k is the comoving wavenumber, $a(t)$ is the scale factor and

$$m_\phi^2 = \frac{\lambda_{hs} s^2}{2} = \frac{\lambda_{hs} M_p |\chi_s|}{\sqrt{6} \xi_s} \quad (4.12)$$

in the Einstein frame, for a quadratic potential. Eq. (4.11) can be written

$$\begin{aligned} 0 &= \ddot{\psi}_k + \left(\frac{k^2}{a^2} + m_\phi^2 - \frac{3}{4} \left(\frac{\dot{a}}{a} \right)^2 - \frac{3}{2} \frac{\ddot{a}}{a} \right) \psi_k \\ &\simeq \ddot{\psi}_k + k_0^2(t) \psi_k \end{aligned} \quad (4.13)$$

where we have rescaled $\psi_k = a^{3/2} \phi_k$. The terms proportional to \dot{a} and \ddot{a} are assumed to be always negligible and are not included in k_0 .

Adiabatic evolution

When \dot{k}_0 can be ignored ($|\dot{k}_0| \ll k_0^2$) then Eq. (4.13) can be easily solved. This is called the adiabatic approximation. The solution is

$$\psi_k = \frac{\alpha_k^j}{\sqrt{2k_0}} e^{-i\theta_k^j} + \frac{\beta_k^j}{\sqrt{2k_0}} e^{+i\theta_k^j} \quad (4.14)$$

where

$$\theta_k^j = \int_0^{t_j} k_0 dt . \quad (4.15)$$

The parameters α_k^j and β_k^j are constant between zero crossings, but can change when the oscillating inflaton crosses zero, at which point the adiabatic approximation is not valid. For $k = 0$, the adiabatic approximation is valid when

$$|t - t_j| \gg \left(\sqrt{\frac{\lambda_s}{2}} \frac{1}{\lambda_{hs}^2 \omega^2 X} \right)^{1/3} . \quad (4.16)$$

At the zero crossings, in our approximation, there is a sudden change in the coefficients α_k^j and β_k^j which is described by a Bogoliubov transformation [86]:

$$\begin{pmatrix} \alpha_k^{j+1} e^{-i\theta_k^j} \\ \beta_k^{j+1} e^{+i\theta_k^j} \end{pmatrix} = \begin{pmatrix} 1/D_k & R_k^*/D_k^* \\ R_k/D_k & 1/D_k^* \end{pmatrix} \begin{pmatrix} \alpha_k^j e^{-i\theta_k^j} \\ \beta_k^j e^{+i\theta_k^j} \end{pmatrix} . \quad (4.17)$$

R_k is a reflection coefficient and D_k is a transmission coefficient, satisfying $|R_k|^2 + |D_k|^2 = 1$.

Non-adiabatic evolution

At the zero crossings, m_ϕ^2 approaches zero and can be approximated as

$$m_\phi^2 \simeq \frac{\lambda_{hs} M_p \omega X(t)}{\sqrt{6} \xi_s} |t - t_j| . \quad (4.18)$$

This approximation is valid when $\sin(\omega|t - t_j|) \simeq \omega|t - t_j|$, which is true for

$$|t - t_j| \ll \frac{\sqrt{6}}{\omega} . \quad (4.19)$$

Following [86], we can transform the equation Eq. (4.13), in order to make it possible to approximately solve in the non-adiabatic regime. Using $\tau = Q(t - t_j)$ and $\kappa = \frac{|k|}{Qa}$, where

$$Q^3 = \frac{\lambda_{hs} \sqrt{\lambda_s} M_p}{6 \xi_s^2} X(t_j) \quad (4.20)$$

gives

$$\frac{d^2\psi_k}{d\tau^2} + (\kappa^2 + |\tau|)\psi_k = 0. \quad (4.21)$$

By definition, the solution of this is a combination of Airy functions. In our case, the coefficients are different either side of the zero crossings. The solutions are

$$\psi_k(\tau < 0) = A_- \text{Ai}(-|\tau| - \kappa^2) + B_- \text{Bi}(-|\tau| - \kappa^2) \quad (4.22)$$

and

$$\psi_k(\tau > 0) = A_+ \text{Ai}(-|\tau| - \kappa^2) + B_+ \text{Bi}(-|\tau| - \kappa^2). \quad (4.23)$$

At $\tau = 0$ the expressions for ψ_k and their derivatives must be equal.

Matching the two solutions

To complete the calculation, we need to match the adiabatic solution to the non-adiabatic solution. This is possible when Eq. (4.16) and Eq. (4.19) are simultaneously satisfied⁴, i.e.

$$X \gg \frac{\lambda_s}{12\sqrt{6}\lambda_{hs}^2} X_{CR}. \quad (4.24)$$

When the above inequality is satisfied, we match the solutions before the zero crossing [Eq. (4.22) and Eq. (4.14), evaluated at j] and after the zero crossing [Eq. (4.23) and Eq. (4.14) evaluated at $j+1$]. This gives (A_-, B_-) in terms of $(\alpha^j = \alpha_k^j e^{-\theta_k^j}, \beta^j = \beta_k^j e^{\theta_k^j})$ and similarly for (A_+, B_+) . Imposing the requirement that the solutions and their derivatives are equal at $\tau = 0$ relates $(\alpha^{j+1}, \beta^{j+1})$ to (α^j, β^j) . D_k and R_k are then calculated using the definition Eq. (4.17) and the resulting expressions are given by [33]:

$$R_k = -e^{2i(\frac{2\kappa}{3} + \frac{\pi}{4})} \frac{\text{Ai}'(-\kappa^2)\text{Ai}(-\kappa^2) + \text{Bi}(-\kappa^2)\text{Bi}'(-\kappa^2)}{[\text{Bi}(-\kappa^2) + i\text{Ai}(-\kappa^2)] [\text{Bi}'(-\kappa^2) + i\text{Ai}'(-\kappa^2)]} \quad (4.25)$$

and

$$D_k = ie^{2i(\frac{2\kappa}{3} + \frac{\pi}{4})} \frac{\text{Ai}'(-\kappa^2)\text{Bi}(-\kappa^2) - \text{Ai}(-\kappa^2)\text{Bi}'(-\kappa^2)}{[\text{Bi}(-\kappa^2) + i\text{Ai}(-\kappa^2)] [\text{Bi}'(-\kappa^2) + i\text{Ai}'(-\kappa^2)]}. \quad (4.26)$$

Occupation number n_k

The occupation number is given by $n_k^j \equiv |\beta_k^j|^2$ where [33]

$$n_k^{j+1} = \frac{|R_k|^2}{|D_k|^2} + \frac{1 + |R_k|^2}{|D_k|^2} n_k^j + 2\sqrt{1 + n_k^j} \sqrt{n_k^j} \frac{|R_k|}{|D_k|^2} \cos(\theta_{tot}^j) \quad (4.27)$$

⁴It is satisfied for all $X > X_{CR}$ if $\lambda_s \geq 29\lambda_{hs}^2$.

and $\theta_{tot}^j = -2\theta_k^j - 2\left(\frac{2}{3}\kappa^3 + \frac{\pi}{4}\right) + \arg \alpha_k^j - \arg \beta_k^j$. There are two regimes, depending on the size of n_k .

(i) $n_k \ll 1$: For each time $\Delta t = \frac{\pi}{\omega}$ corresponding to the time between zero crossings, $n_k^j \simeq \frac{|R_k|^2}{|D_k|^2}$ scalars ϕ_i are produced. The majority of these particles decay (to relativistic Standard Model particles) before the next zero crossing and there is no significant transfer of energy to radiation⁵.

(ii) $n_k \gg 1$: it is now the second and third terms of Eq. (4.27) that are important and we can write (for each ϕ_i)

$$n_k^{j+1} = e^{2\pi\mu_k} n_k^j \quad (4.28)$$

where μ_k is an average over the angle θ_{tot}^j , which we assume to be completely randomly distributed. We calculate μ_k using Mathematica, which gives

$$\begin{aligned} \mu_k &= \frac{1}{2\pi} \int_0^{2\pi} \frac{1}{2\pi} \ln \left(\frac{1 + |R_k|^2}{D_k} + 2 \frac{|R_k|}{|D_k|^2} \cos(\theta) \right) d\theta \\ &= \frac{1}{2\pi} \left[\ln \left(\frac{|R_k| + 1}{|R_k|} \right) + i - \ln(|D_k|^2) \right] \\ &\simeq -\frac{1}{2\pi} \ln(|D_k|^2) . \end{aligned} \quad (4.29)$$

In order to have a resonance, we need the reflection coefficient, $|R_k|$, to be reasonably large. This means that $|D_k|$ is small (from the requirement $|R_k|^2 + |D_k|^2 = 1$) and this gives the final line of Eq. (4.29). We are interested in the rate of change of the total number of particles produced, so must integrate over k . Thus, as the change in n_k in a time $\Delta t = \frac{\pi}{\omega}$ is $\Delta n_k \simeq 2\pi\mu_k n_k$, we have

$$\frac{dn}{dt} \simeq \frac{\omega}{\pi} \int_0^\infty (2\pi\mu_k n_k) \frac{d^3k}{(2\pi)^3}. \quad (4.30)$$

We do not calculate this integral exactly (it would be difficult as $|D_k|^2$ involves products of Airy functions), but assume that μ_k is well approximated by $\mu(k=0)$ [33]. We use Eq. (4.26) to calculate $B \equiv \mu(k=0) = 0.045$. This gives for the total number density of Higgs bosons n_T

$$\frac{dn_T}{dt} \sim 4 \times 2\omega B n = 2\omega B n_T. \quad (4.31)$$

In [33], the components of the W^\pm and Z bosons are treated as scalars. This is not strictly true for that case but is correct for our calculation using the scalar Higgs boson.

⁵This was shown in [33] by demonstrating that the relativistic particles produced via boson decays would not dominate the energy density until well after the resonant production has taken place.

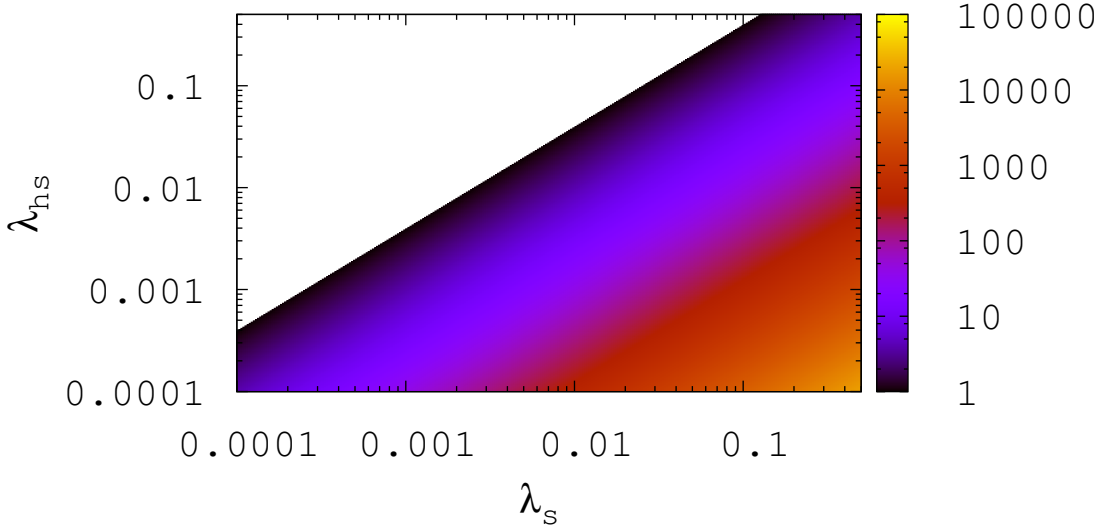


Figure 4.1: Showing the value of $\frac{X_{sto}}{X_{CR}}$ for regions of the parameter space where reheating via stochastic resonance can complete before X_{CR} .

Decay of the H bosons

Higgs bosons which are produced at the zero crossings can decay in the adiabatic regime when their mass is large. The Higgs has a large m_ϕ^2 because the background s field is large. Therefore it has a minimum at zero and decay is via the Yukawa coupling, to fermion pairs (particularly the top quark). The (average) decay width of the variable mass Higgs bosons is given by [87]

$$\Gamma_\phi = \frac{N_c g^2 m_f^2}{32\pi m_W^2} \langle m_\phi \rangle \equiv C \langle m_\phi \rangle \simeq \frac{1}{17.65} \langle m_\phi \rangle \quad (4.32)$$

where $\langle m_\phi \rangle$ is the average of Eq. (4.12). The H -bosons are non-relativistic but the decay products are relativistic.

4.2.2 Stochastic resonance

Once the decay of the produced Higgs bosons becomes subdominant to their production, an exponential regime can begin. Up to this point, no significant energy transfer from χ to the Higgs bosons occurs. Reheating completes fairly rapidly after this, as once the Higgs bosons are produced through this stochastic resonance, they can annihilate and produce a thermal background. The upper limit on reheating is the point at which the decay and the exponential production are equal. Using Eq. (4.32) and Eq. (4.31) we find that the two processes are equal at

$$X_{sto} \simeq \frac{2\pi B^2}{C^2} \frac{\lambda_s}{\lambda_{hs}} X_{CR} \simeq 4.0 \frac{\lambda_s}{\lambda_{hs}} X_{CR} . \quad (4.33)$$

This is the absolute maximum value of X for reheating to occur via production of H bosons at the zero crossings and is shown in Fig. (4.1) for $\lambda_s > 0.25\lambda_{hs}$. After $\chi = X_{sto}$, χ will rapidly decrease to X_{CR} , therefore $\rho_{rad} > \rho_{inf}$ at X_{CR} . The calculation assumes instant annihilation of the H -bosons to relativistic particles and a very efficient stochastic resonance. For this reason all estimates of T_R from stochastic resonance are *upper limits*. It is interesting to note that increasing the Higgs- S coupling, λ_{hs} causes reheating to occur *later*. This is because a large λ_{hs} means that m_ϕ^2 is large, so it can keep decaying for a longer period, preventing the exponential regime from beginning and therefore delaying reheating.

The time of reheating is dependent on the ratio of couplings $\frac{\lambda_s}{\lambda_{hs}}$. Requiring this process of reheating to occur before $\chi = X_{CR}$ gives

$$\lambda_s > 0.25\lambda_{hs} . \quad (4.34)$$

If this condition is not fulfilled, reheating is not ruled out. It could either occur via directly producing excitations of the inflaton, as discussed in the following section, or possibly during the quartic potential regime. We do not consider reheating in a quartic potential here as it is computationally difficult, and because our main aim is to show that reheating is possible in the model of S -inflation. If reheating occurs in the quartic regime, a lower temperature of radiation domination T_R would be expected.

4.3 An alternative mechanism of reheating

An alternative method of draining energy from the background field is the direct production of excitations of the inflaton χ . These excitations have a mass

$$m_\chi^2 = 3\lambda_s\chi^2 \quad (4.35)$$

for $\chi < X_{CR}$, and the mode equation is given by Eq. (4.11) with $m_\phi \rightarrow m_\chi$. As discussed in [33], this can be solved perturbatively, assuming the number of particles produced is small⁶. The particles produced are relativistic, with energy density (valid at late times) [33]

$$\rho_{excitation} = \frac{3}{11} \frac{\omega^5}{2\pi^3} t, \quad (4.36)$$

where t and X are related through Eq. (4.7). We compare this to the inflaton energy density, Eq. (4.9) and find that if the production of excitations is the only process of reheating, radiation

⁶If this were not the case, it could still be solved non-perturbatively in the same way as for the production of Higgs bosons.

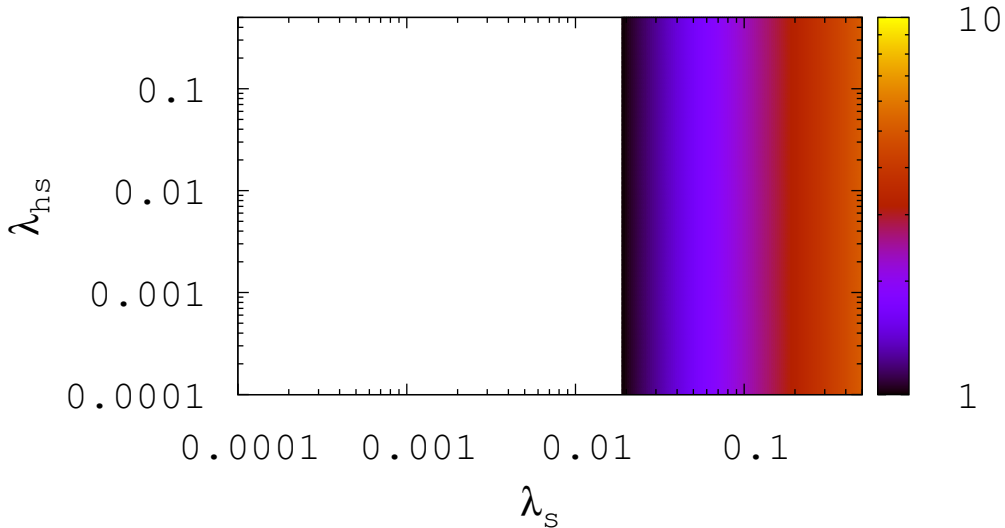


Figure 4.2: Showing the value of $\frac{X_{ex}}{X_{CR}}$ for regions of the parameter space where reheating via production of S excitations can complete before X_{CR} . Note that the scale has a much smaller range than Fig. (4.1).

domination occurs at

$$X_{ex} \simeq 7.3\sqrt{\lambda_s}X_{CR}. \quad (4.37)$$

Fig. (4.2) shows the value of X_{ex} when $\lambda_s > 0.019$. If this mechanism of reheating is to occur before the inflaton potential becomes quartic, we require

$$\lambda_s > 0.019. \quad (4.38)$$

The relativistic χ particles are expected to annihilate to Higgs bosons in order to produce Standard Model particles. This is most efficient for large λ_{hs} . We have assumed a real scalar S — for complex S the process would complete faster.

4.4 Relic density of the inflaton

One should be concerned whether there is any energy density remaining in the inflaton oscillations after reheating. Given the high T_R for this model, in general most of the inflaton oscillation (zero-mode χ particles) will quickly scatter with the Standard Model background (eventually becoming part of the thermal background, although that requires $2 \rightarrow 3$ processes). The condition for sufficient scattering with the background is

$$\Gamma > H, \quad (4.39)$$

where Γ is the scattering rate of the zero-momentum χ particles and H is the Hubble parameter. We will only consider scattering with the Higgs bosons, as it will prove to be sufficient (zero-momentum χ could also scatter with thermal χ). The calculation relies on the radiation density being larger than the inflaton density at X_{CR} . Before calculating Γ and H , we will show that $3T_m > m_{s_o}$ where T_m is the radiation temperature when the potential Eq. (3.11) changes back from quartic to quadratic (at low S).

Transition from quartic to quadratic potential

This transition occurs when

$$\frac{\lambda_s s^4}{4} = \frac{m_{s_o}^2 s^2}{2}, \quad (4.40)$$

giving

$$s = X_m \equiv \sqrt{\frac{2}{\lambda_s}} m_{s_o}. \quad (4.41)$$

Given that $\rho_{rad} > \rho_{inf}$ (this is true under the conditions discussed in Section 4.3 and Section 4.2.2), it follows that at the point where $s = X_m$,

$$\frac{\pi^2}{30} g(T) T_m^4 > \frac{\lambda_s}{4} X_m^4 \quad (4.42)$$

which gives

$$3T_m > \frac{1.2}{\lambda_s^{1/4}} m_{s_o}. \quad (4.43)$$

It is a reasonable assumption that $m_h \lesssim m_s$ — although this does not apply to all the available parameter space (the worst case is that $m_h \sim 3m_s$). So, for any $\lambda_s < 2.3$ (covering all allowed values of λ_s), we find that $3T_m > m_{s_o}$ and expect that $3T_m > m_h$.

Scattering of the inflaton with the thermal background

We now calculate the scattering rate in the quadratic potential:

$$\Gamma = n\sigma v \quad (4.44)$$

where n is the number density of Higgs bosons, given for relativistic particles (assumed to be thermal) by [88]

$$n = \frac{1.2}{\pi^2} g_H(T) T^3, \quad (4.45)$$

$v = 1$ is the velocity of the relativistic Higgs particles, $g_H = 4$ and σ is the cross-section, calculated below, given by

$$\left. \frac{d\sigma}{d\Omega_a} \right|_{CM} = \frac{1}{64\pi^2} \frac{|M|^2}{\varsigma} \frac{|\vec{p}_f|}{|\vec{p}_i|} \quad (4.46)$$

in the centre of mass frame. For elastic scattering, $|\vec{p}_f| = |\vec{p}_i|$ and the Lorentz-invariant Mandelstam variable ς is

$$\varsigma = m_{s_o}^2 + 6m_{s_o}T \simeq 6m_{s_o}T, \quad (4.47)$$

where we have used $3T_m > m_{s_o}$ as shown above. Integrating over the solid angle Ω_a and substituting $|M|^2 = \lambda_{hs}^2$ gives the cross section for Higgs- S scattering:

$$\sigma = \frac{\lambda_{hs}^2}{96\pi m_{s_o}T}. \quad (4.48)$$

Thermalisation of the zero-mode inflaton

In the relativistic limit, assuming $\rho_{total} \simeq \rho_{rad}$, we find

$$H \simeq \frac{3.4T_m^2}{M_p}. \quad (4.49)$$

In order for thermalisation of the background, we require $\Gamma > H$, giving

$$\frac{\lambda_{hs}^2}{24\pi^2} \frac{T_m^2}{m_{s_o}} \gtrsim \frac{3.4T_m^2}{M_p}. \quad (4.50)$$

This is true provided that

$$m_{s_o} < 1.0 \times 10^{-4} \lambda_{hs}^2 M_p. \quad (4.51)$$

This is easily satisfied, as we expect m_{s_o} to be less than a few TeV. Therefore, any inflaton energy density remaining at $s \sim X_m$ will easily be thermalised⁷.

Thermal production of WIMP dark matter

Provided that T_R is greater than the mass of S then relativistic S particles will be produced in thermal equilibrium. As the Universe expands and cools, they will become thermal relic dark matter. We found in Chapter 3 that the S mass is $50 \text{ GeV} \lesssim m_s \lesssim 1 \text{ TeV}$ for $\lambda_s > 0.01$. This is much lower than $T_R \sim 10^{13} \text{ GeV}$.

⁷Thermalisation may also occur earlier, during the quartic regime.

4.5 Determining the temperature of radiation domination

The effective temperature of radiation domination is given by

$$\frac{g_* \pi^2 T_R^4}{30} \simeq \frac{\omega^2}{2} X_R^2 \quad (4.52)$$

where $g_* = 107.75$ and X_R is X_{sto} or X_{ex} , depending on the reheating process. For reheating via excitations, we require $\lambda_s > 0.019$, so

$$T_R \approx 9 \times 10^{13} \lambda_s^{1/4} \text{ GeV}. \quad (4.53)$$

For $0.019 < \lambda_s < 0.3$, this gives $3 \times 10^{13} \text{ GeV} < T_R < 7 \times 10^{13} \text{ GeV}$. For reheating via parametric resonance, we require $\lambda_s > 0.25 \lambda_{hs}$. This gives⁸

$$T_R \approx 3 \times 10^{13} \left(\frac{\lambda_s}{\lambda_{hs}^2} \right)^{1/4} \text{ GeV}. \quad (4.54)$$

Imposing a reasonable but arbitrary⁹ bound, $\frac{\lambda_s}{\lambda_{hs}^2} \lesssim 10^6$, gives

$$3 \times 10^{13} \text{ GeV} < T_R < 8 \times 10^{14} \text{ GeV}. \quad (4.55)$$

The lower bound is similar to that for Higgs inflation [33]. The upper bound for S -inflation is higher because of the freedom in λ_s and λ_{hs} .

A small region of the parameter space is excluded because if $\lambda_s < 0.019$, then we require $\lambda_{hs} < 0.08$. This is shown in Fig. (4.3). However, we were rather conservative in our reheating calculations, requiring it to complete before X_{CR} . Some reheating after this point is likely to occur (but is very difficult to calculate).

4.5.1 Obtaining \tilde{N} from T_R

Under certain assumptions, which we detail below, it is possible to obtain the number of e-foldings of inflation between when a pivot scale k_0 exits the horizon during inflation and the end of inflation. The WMAP spectral index n and power spectrum are calculated at the scale

$$k_0 = \frac{2\pi}{\lambda_0} = 0.002 \text{ Mpc}^{-1} \simeq 8.5 H_0, \quad (4.56)$$

⁸We have used the tree-level slow roll parameter $\bar{\epsilon}$ and potential \bar{U} with the WMAP normalisation (this fixes $\frac{\lambda}{\xi^2}$). We saw in Chapter 3 that radiative corrections are not negligible, particularly for $\bar{\epsilon}$. Therefore we would expect a full calculation to show some variation from these results — although we do not expect the conclusion to change significantly.

⁹We do have some constraints on perturbativity grounds (see Section 3.3). Also, λ_{hs} cannot be too small otherwise we would not achieve the correct relic density of dark matter.

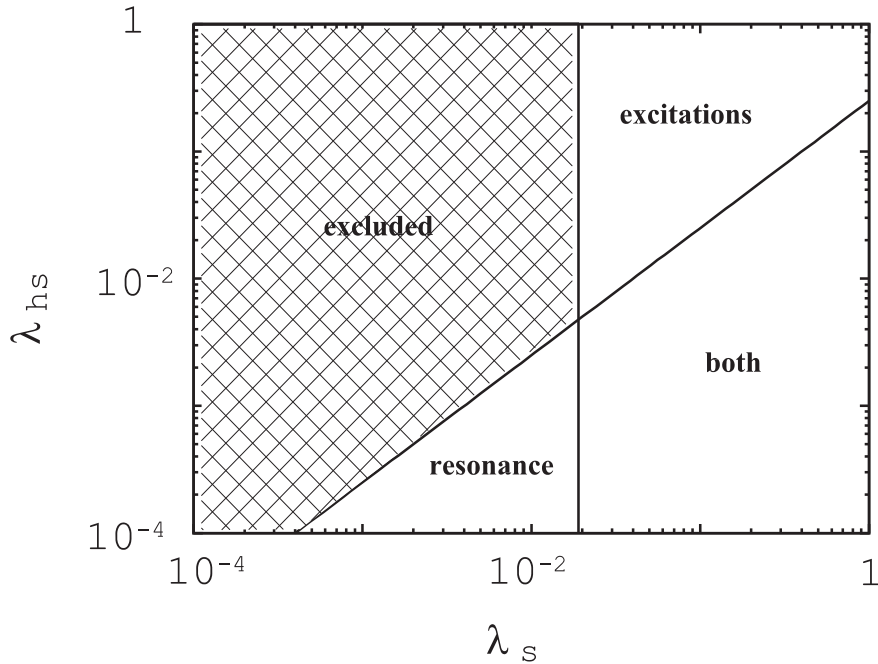


Figure 4.3: Showing the regions of the λ_s and λ_{hs} parameter space allowed by the constraints of reheating. The shaded region is excluded. In most of the region marked ‘both’, $X_{sto} > X_{ex}$ (as can be seen by comparing Fig. (4.1) and Fig. (4.2)), therefore reheating via stochastic resonance is expected to dominate for the majority of this region.

where $H_0 = 70.8 \text{ km s}^{-1} \text{ Mpc}^{-1}$ [89]. We use a method similar to [90] and the estimate for the temperature of radiation domination given in Eq. (4.55). It is important to consider which frame is appropriate for the calculation. Although it ought to be possible in both the Jordan frame and the Einstein frame, in practice it is a lot easier to work in the Einstein frame, as the conventional formalism of inflation and the conventional Friedmann equation applies.

When the conformal factor $\Omega^2 = 1$, the Jordan and Einstein frames are equivalent. This point is reached before the time of reheating. We consider a current physical length λ_0 . At some earlier time during inflation this length is

$$\tilde{\lambda}(t) = \frac{\tilde{a}(t)}{\tilde{a}_0} \lambda_0 = \frac{\tilde{a}_{end}}{\tilde{a}_0} \frac{\tilde{a}(t)}{\tilde{a}_{end}} \lambda_0 = \frac{\tilde{a}_{end}}{\tilde{a}_R} \frac{\tilde{a}_R}{\tilde{a}_0} e^{-\tilde{N}} \lambda_0 \quad (4.57)$$

where $\tilde{a}_0 = a_0$ is the current scale factor, \tilde{a}_{end} is the scale factor at the end of inflation, \tilde{a}_R is the scale factor at the time of reheating and the number of e-foldings \tilde{N} is defined by Eq. (3.61).

At horizon exit, $\tilde{\lambda} = \tilde{H}^{-1}$ and so

$$\tilde{N} = \ln \left(\frac{\tilde{a}_{end}}{\tilde{a}_R} \frac{\tilde{a}_R}{\tilde{a}_0} \tilde{H} \tilde{H}^{-1} \lambda_0 \right). \quad (4.58)$$

Assuming complete matter domination between the end of inflation and the moment of reheating (which we assume to be instant), $\tilde{\rho}_{mat} \propto \tilde{a}^{-\frac{4}{3}}$. We can use entropy conservation for the era

between reheating and the present day,

$$g_* T_R^3 \tilde{a}_R^3 = g_0 T_0^3 \tilde{a}_0^3, \quad (4.59)$$

which allows us to write

$$\tilde{N} = \ln \left(\left(\frac{\tilde{\rho}_R}{\tilde{\rho}_{end}} \right)^{1/3} \left(\frac{g_0 T_0^3}{g_* T_R^3} \right)^{1/3} \tilde{H}_{\tilde{N}} \lambda_0 \right). \quad (4.60)$$

Using the Friedmann equation (Eq. (1.10)) we can write

$$\tilde{H}(t) = \sqrt{\frac{\tilde{\rho}(t)}{3M_p^2}} \quad (4.61)$$

where $\tilde{\rho}$ is the energy density at time t . During inflation, this is given by the potential energy of the inflaton, so

$$\tilde{\rho} = U = \frac{\lambda_s s^4}{4\Omega^4}. \quad (4.62)$$

Using the approximations $s_{end}^2 \simeq \frac{4M_p^2}{3\xi_s}$ and $\frac{\lambda_s}{\xi_s^2} \simeq 3 \frac{(0.0275)^4}{\tilde{N}^2}$ (from Chapter 3), we can estimate

$$\tilde{\rho}_{\tilde{N}}^{1/4} \simeq 8.0 \times 10^{15} \left(\frac{60}{\tilde{N}} \right)^{1/2} \text{ GeV} \quad (4.63)$$

and

$$\tilde{\rho}_{end}^{1/4} \simeq 6.0 \times 10^{15} \text{ GeV}. \quad (4.64)$$

At reheating, when the Universe is dominated by thermal radiation, we have

$$\rho = \frac{\pi^2 g(T) T^4}{30}, \quad (4.65)$$

where $g(T)$ is the effective number of degrees of freedom of the thermal radiation and T is the effective temperature ($\Omega = 1$ at this point). Just after reheating, $g(T_R) \simeq 107.75$ and at the present time, $g(T_0) \simeq 2$ (as only photons are part of the thermal background). Putting this together gives the number of e-foldings of inflation since the scale k_0 left the horizon:

$$\tilde{N} = 58.6 - \frac{1}{3} \ln \left(\frac{\tilde{N}}{60} \right) + \frac{1}{3} \ln \left(\frac{T_R}{10^{13} \text{ GeV}} \right). \quad (4.66)$$

So, with T_R given by Eq. (4.55) we find $59 \lesssim \tilde{N} \lesssim 60$. Due to uncertainties relating to the end of inflation and calculation of the temperature of radiation domination we assume a theoretical

error of ± 1 on \tilde{N} . Finally this gives us

$$58 \lesssim \tilde{N} \lesssim 61 . \tag{4.67}$$

This allows a fairly precise determination of the observable quantities (such as n and r), in contrast to models where T_R is unknown.

Chapter 5

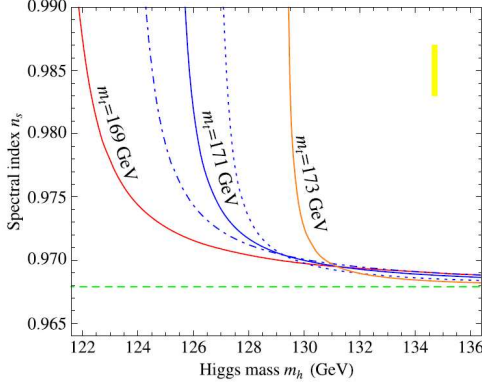
Comparing the predictions of S -inflation and Higgs inflation

In Chapter 3, we discussed the model of S -inflation. It was not possible to make a clear comparison with the predictions of Higgs inflation at that stage, due to the variety of Higgs inflation predictions in the literature. Each collaboration used different methods, and the conclusions reached (particularly spectral index versus Higgs mass) are somewhat different in each case. We wish to determine whether S -inflation has a different observational signature to Higgs inflation. To do so, we calculate the predictions of both models using the same method. Before we make a comparison of the models, it will be necessary to consider the calculation of the effective potential.

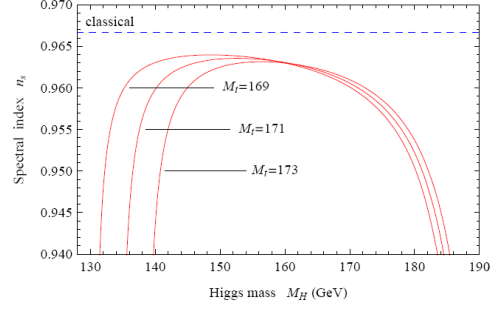
In Section 5.1 we review the methods used in the literature and the corresponding results for n versus m_h . In Section 5.2 we compute n versus m_h for the case of pure Higgs inflation, using two different methods of calculating the effective potential: the standard Coleman-Weinberg potential and the RG improved effective action. We find (Section 5.3) that the results differ, due to the inclusion of β_{ξ_h} in the RG improved method. Then, in Section 5.4, using the RG improved effective action, we re-compute the experimental predictions for all three variants of the model — pure Higgs inflation, Higgs inflation with an additional singlet scalar and S -inflation. In this way we can be sure that any differences in the predictions are due to the fundamental differences of the models and not the initial conditions, method of obtaining the effective potential or specifics of the code used. Finally, we show how the spectral index n is able to distinguish between S -inflation and Higgs inflation in a significant portion of the parameter space.

5.1 Differing approaches to calculating the effective potential

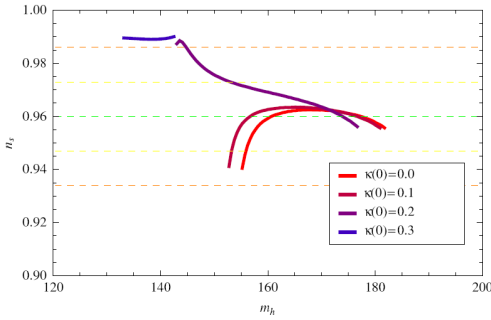
Here, we summarise the different methods each collaboration has used to obtain the spectral index for the Higgs inflation model. Only the most recent paper of each collaboration has been



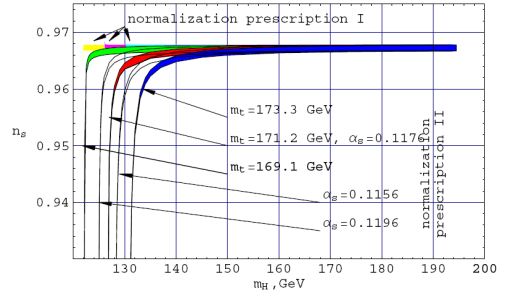
(a) Showing the results of [38] — see (i) in text. The spectral index increases for small m_h and takes its tree level value (dashed green line) above ~ 130 GeV.



(b) Showing the results of [37] — see (ii) in text. The spectral index is always below the classical value (dashed blue line), strongly deviating at $m_h \lesssim 150$ GeV and $m_h \gtrsim 170$ GeV.



(c) Showing the results of [64] — see (iii) in text. The lowest curve is pure Higgs inflation and the horizontal lines show the one and two sigma WMAP values for n_s .



(d) Showing the results of [35] — see (iv) in text. Deviation from the classical result is most significant for prescription II with $m_h \lesssim 130$ GeV.

Figure 5.1: Showing n as a function of m_h for Higgs inflation, taken from papers in the literature — see text for details of each method. Although general features are in agreement between some figures (particularly (b) and (c)), it is not apparent which prediction is to be trusted.

considered and we reproduce the predictions in Fig. (5.1). It is clear from the figure that the results do not agree. Therefore, in order to make a consistent comparison of S -inflation to Higgs inflation we must choose and apply a consistent method.

(i) De Simone et al [38] use the RG improved potential (Eq. (5.15)). The RG equations are given by $\frac{d\lambda}{dt} = \frac{\beta_\lambda}{1+\gamma}$ where β are given to two-loop, λ represents *any* coupling such as g' , λ_h or ξ_h . The Higgs commutator is suppressed by a factor s (c_ϕ in our notation) which is inserted when *any* component of H runs in a loop. This contrasts with our method and with [64] where the suppression factor is only inserted when a *physical* Higgs runs in a loop. Consequently, the RG equations in [38] are different to ours. Corrections to the kinetic and gravitational sectors are considered to be negligible. The analysis uses $\tilde{N} = 60$, inflation ends when $\tilde{\epsilon} = 1$ and an approximate expansion for $\tilde{\epsilon}$ and $\tilde{\eta}$ seems to have been used. The results are shown in Fig. (5.1a). The spectral index only deviates from its classical value at $m_h \lesssim 130$ GeV.

(ii) Barvinsky et al [37]¹ focus on \mathbf{A}_I , the ‘inflationary anomalous scaling’ coefficient. This

¹The first version of this work (v1) presented very different results as it did not include the running of ξ_h

includes the contribution from the running of ξ_h and is given by

$$\mathbf{A_I} = \frac{3}{8\lambda_h} \left(2g^4 + (g^2 + g'^2)^2 - 16y_t^4 \right) - 6\lambda_h. \quad (5.1)$$

The β -functions are equivalent to [38]. Two-loop equations (with suppression of physical Higgs only) are used to run couplings up to the scale corresponding to the end of inflation. Then an analytic expression

$$V_J = M_p^4 \frac{\lambda_{end}}{4\xi_{end}^2} \left(1 + \frac{\mathbf{A_I}(t_{end})}{16\pi^2} \log \phi / \phi_{end} \right) \quad (5.2)$$

is used to compute slow roll parameters, with couplings held constant. Inflation ends when $\tilde{\epsilon} = \frac{3}{4}$. Pole mass matching is used for y_t and λ_h . The results are shown in Fig. (5.1b).

(iii) Clark et al [64] consider Higgs inflation in the presence of an additional gauge-singlet scalar. They use the RG improved effective action, modifying the gravitational, kinetic and potential sectors of the theory, with one-loop running of all couplings. Clark et al neglect two loop effects, however these may have a significant effect at low m_h , especially relating to the top quark (e.g. using $y_t(0) = \frac{\sqrt{2}m_t}{v}$ instead of the pole mass matching scheme). Clark et al use $\tilde{N} = 60$, choose the end of inflation to be at $\tilde{\epsilon} = 1$ and make an accurate calculation of $\tilde{\epsilon}$ and $\tilde{\eta}$ (see their Eq. (22)). Their results for n are shown in Fig. (5.1c), where the lowest curve corresponds to pure Higgs inflation (Fig. (6a) in [64]).

(iv) Bezrukov et al [35] consider the ‘Chiral Standard Model’ which is the Standard Model without the physical Higgs — equivalent to setting $c_h = 0$. They run the usual RG equations (but in the Einstein frame) up to the scale M_p/ξ_h then match onto the equations of the chiral SM. They also consider two different prescriptions for the renormalization scale μ , corresponding to (I) $\mu^2 \propto M_{eff}^2 = M_p^2 + \xi h^2$ and (II) $\mu \propto M_p$ (both in the Jordan frame). We would expect the results to be independent of the choice of μ and so these results, Fig. (5.1d), showing that n depends on the renormalization scale are surprising. Prescription (II) corresponds to our work and the other papers mentioned in this section. They use $\tilde{N} = 59$ and use pole mass matching to obtain the initial conditions.

(v) Our previous work [1] studied inflation along the direction of a singlet scalar, coupled to the Higgs, therefore the results are not directly comparable to any of the papers here, which all consider the Higgs as the inflaton. We summarise the methods used in [1] for completeness. The standard² Coleman-Weinberg potential was used, with the couplings run to two-loop (except β_ξ which was used to one-loop in common with the other papers, and the additional contributions due to the singlet scalar, which were also computed to one-loop). A suppression factor was

within the effective potential and all components of H were suppressed, rather than just the physical h .

²No gravitational loops.

inserted for the inflaton s and for the physical higgs h . Pole mass matching was used to set the initial conditions, inflation ends at $\tilde{\eta} = 1$ and $\tilde{N} = 60$ was used. $\tilde{\epsilon}$ and $\tilde{\eta}$ were calculated accurately and the results can be seen in Chapter 3.

5.2 A Comparison of two approaches to calculating the effective potential in pure Higgs inflation

We now compare two particular methods of calculating the effective potential for the case of pure Higgs inflation. The Jordan and Einstein frame Lagrangians are the same as in Section 3.1 except that $\xi_s = \lambda_s = \lambda_{hs} = 0$ and we use the notation ϕ (rather than h) for the physical Higgs field. We remind the reader that issues relating to unitarity and naturalness are not the subject of this chapter and will be discussed in the next chapter.

The first method uses the Coleman-Weinberg potential, with two-loop running of coupling constants to fixed values — this is similar to our work on S-inflation, and to the work of Shaposhnikov et al [35]. The second method uses the RG improved effective action, again with two-loop running of the coupling constants, but now the couplings depend on the field ϕ . This is the two-loop version of [64], is similar to [38] (however [38] ignores the RG improvement of the kinetic and gravitational sectors) and shares similarities with [36]. We first calculate the slow-roll parameters $\tilde{\epsilon}$ (this is important for normalising the potential and thus determining $\xi(m_t)$) and $\tilde{\eta}$ (this gives the largest contribution to the spectral index n). From these we can calculate the observable quantities n and r , as in Chapter 3.

The gauge and Yukawa RG equations used in this chapter are

$$\beta_g = -\frac{39 - c_h}{12}g^3 + \frac{g^3}{16\pi^2} \left(\frac{3}{2}g'^2 + \frac{35}{6}g^2 + 12g_3^2 - \frac{3}{2}c_h y_t^2 \right), \quad (5.3)$$

$$\beta_{g'} = \frac{81 + c_h}{12}g'^3 + \frac{g'^3}{16\pi^2} \left(\frac{199g'^2}{18} + \frac{9g^2}{2} + \frac{44g_3^2}{3} - \frac{17c_h y_t^2}{6} \right), \quad (5.4)$$

and

$$\begin{aligned} \beta_{y_t} = & y_t \left(-\frac{9}{4}g^2 - \frac{17}{12}g'^2 - 8g_3^2 + \left(\frac{23}{6} + \frac{2}{3}c_h \right) y_t^2 \right) + \frac{y_t}{16\pi^2} \left[-\frac{23}{4}g^4 - \frac{3}{4}g^2g'^2 \right. \\ & + \frac{1187}{216}g'^4 + 9g^2g_3^2 + \frac{19}{9}g'^2g_3^2 - 108g_3^4 + \left(\frac{225}{16}g^2 + \frac{131}{16}g'^2 + 36g_3^2 \right) c_h y_t^2 \\ & \left. + 6 \left(-2c_h^2 y_t^4 - 2c_h^3 y_t^2 \lambda_h + c_h^2 \lambda_h^2 \right) \right]. \quad (5.5) \end{aligned}$$

The initial conditions at m_t for g , g' , g_3 , y_t and λ_h are the same as in the previous chapter, Section 3.2.3. We choose $\xi_h(m_t)$ such that the model is correctly normalised to the WMAP

7-year mean value for $\Delta_{\mathcal{R}}^2$ at the inflation scale [7, 68]:

$$\frac{U}{\epsilon} = (0.00275 M_p)^4. \quad (5.6)$$

For both methods we fix $\tilde{N} = 58$ and use this to determine $\phi_{\tilde{N}}$ by exact integration of Eq. (3.59) with $s \rightarrow \phi$. We use an approximate value of ϕ_{end} , given by $\phi_{end} \simeq \sqrt{4M_p^2/3\xi}$. We outline below the two methods that we will compare.

5.2.1 The standard Coleman-Weinberg potential

The one-loop effective potential of the Standard Model [52] is

$$U(\chi_\phi) = \frac{1}{\Omega^4} \left(\frac{\lambda_\phi}{4} \phi^4(\chi_\phi) + V^{(1)}(\phi(\chi_\phi)) \right) = \frac{\lambda_\phi \phi^4}{4\Omega^4} [1 + \Theta(\phi)] \quad (5.7)$$

where

$$\Omega^2 = 1 + \frac{\xi_\phi \phi^2}{M_p^2}, \quad \Theta = \frac{V^{(1)}}{V^{(0)}}, \quad V^{(0)} = \frac{\lambda_h \phi^4}{4}, \quad (5.8)$$

$$\begin{aligned} 16\pi^2 V^{(1)}(\phi) &= \frac{1}{4} H^2 \left(\ln \frac{H}{\mu^2} - \frac{3}{2} \right) + \frac{3}{4} G_\phi^2 \left(\ln \frac{G_\phi}{\mu^2} - \frac{3}{2} \right) + \frac{3}{2} W^2 \left(\ln \frac{W}{\mu^2} - \frac{5}{6} \right) \\ &\quad + \frac{3}{4} Z^2 \left(\ln \frac{Z}{\mu^2} - \frac{5}{6} \right) - 3T^2 \left(\ln \frac{T}{\mu^2} - \frac{3}{2} \right) \end{aligned} \quad (5.9)$$

and

$$\begin{aligned} W &= \frac{g^2 \phi^2}{4}, \quad Z = \frac{(g^2 + g'^2) \phi^2}{4}, \quad T = \frac{y_t^2 \phi^2}{2}, \\ H &= m_h^2 + 3c_\phi \lambda_h \phi^2 \simeq 3c_\phi \lambda_h \phi^2, \quad G_\phi = m_h^2 + \lambda_h \phi^2 \simeq \lambda_h \phi^2. \end{aligned} \quad (5.10)$$

We refer to this as the standard Coleman Weinberg potential, which sums over contributions from particles with ϕ -dependent mass terms [50]. It does not include the effect of the non-minimal coupling, except through the suppression factor c_ϕ . This is an important point which we will return to.

We use the two-loop RG equations for all the Standard Model couplings, inserting the suppression factor c_ϕ for each physical Higgs ϕ running in a loop, as described in the previous chapter (and g , g' and y_t modified according to Eqs. (5.3) to (5.5)). In this scheme, $\frac{d\lambda}{dt} = \beta_\lambda$ where λ is any coupling. The couplings are run from m_t to a scale μ , where λ_h , ξ_ϕ , c_ϕ , g , g' , g_3 , and y_t are assigned constant values, not varying with ϕ .

The results should be independent of the choice of the normalisation point³, μ , which is

³We find that this is approximately true, although increasing μ results in a small increase in n . The effect is

chosen to minimise the corrections to the Coleman-Weinberg potential Eq. (5.9). In practice, we choose μ such that $|\Theta| = \left| \frac{V^{(1)}}{V^{(0)}} \right|$ is minimised throughout inflation. This means that $\frac{\sqrt{\xi}}{M_p} \mu$ is approximately $(134 - 0.94m_h)$ for $m_h < 140$ GeV and approximately 2 otherwise. By contrast, $\phi_{inf} \sim \frac{9M_p}{\sqrt{\xi}}$.

A full calculation of the slow roll parameters using

$$\frac{d\Theta}{d\phi} = \frac{L}{\phi} \quad \text{and} \quad L = \frac{1}{16\pi^2 \lambda_h} \left((18c_\phi^2 + 6) \lambda_h^2 + \frac{3g^4}{4} + \frac{3(g^2 + g'^2)^2}{8} - 6y_t^4 \right) \quad (5.11)$$

gives

$$\tilde{\epsilon} = \frac{M_p^2}{2} \left(\frac{1}{\tilde{U}} \frac{d\tilde{U}}{d\chi_\phi} \right)^2 = \frac{M_p^2}{2} \left(\frac{d\phi}{d\chi_\phi} \right)^2 \left(\frac{4}{\phi\Omega^2} + \frac{1}{1+\Theta} \frac{L}{\phi} \right)^2 \quad (5.12)$$

and

$$\begin{aligned} \tilde{\eta} = \frac{M_p^2}{\tilde{U}} \frac{d^2 \tilde{U}}{d\chi_\phi^2} &= M_p^2 \left(\frac{d\phi}{d\chi_\phi} \right)^2 \left(\frac{12}{\phi^2 \Omega^4} - \frac{12\xi_\phi}{\Omega^4 M_p^2} + \frac{8L}{\phi^2 \Omega^2 (1+\Theta)} - \frac{L}{\phi^2 (1+\Theta)} \right) \\ &+ M_p^2 \frac{d^2 \phi}{d\chi_\phi^2} \left(\frac{4}{\phi\Omega^2} + \frac{L}{\phi(1+\Theta)} \right). \end{aligned} \quad (5.13)$$

The term $\frac{d^2 \phi}{d\chi_\phi^2}$ is given by

$$\frac{d^2 \phi}{d\chi^2} = \frac{1}{2\Omega^6} \left(\frac{d\phi}{d\chi} \right)^4 \left[\frac{12\xi_\phi^3 \phi^3}{M_p^4} + \frac{2\xi_\phi \Omega^2 \phi}{M_p^2} - \frac{12\xi_\phi^2 \phi}{M_p^2} \right]. \quad (5.14)$$

The terms originating from $U^{(1)}$ give a negative, subdominant contribution to $\tilde{\eta}$ (at most around $0.04 \times \tilde{\eta}_{tree}$). However, terms from $U^{(1)}$ give a substantial positive contribution to $\tilde{\epsilon}$ (becoming dominant for $m_h \lesssim 125$ GeV and $m_h \gtrsim 165$ GeV), up to $7.3 \times \tilde{\epsilon}_{tree}$ for $m_h = 180$ GeV.

5.2.2 The RG improved effective action

The Jordan frame action in the unitary gauge, writing explicitly only the terms directly relevant for inflation, is given by

$$S_J = \int \sqrt{-g} d^4x \left(\frac{1}{2} G^2 \partial_\mu \phi \partial^\mu \phi - \frac{M^2 R}{2} - \frac{1}{2} G^2 \xi_\phi \phi^2 R - V(\phi) \right) \quad (5.15)$$

where

$$V = \frac{1}{4} \lambda_h (t(\phi)) G(t(\phi))^4 \phi^4 \quad (5.16)$$

most significant (a 5% effect) for small m_h , where we believe higher order effects are likely to be important.

and⁴

$$G(t) = \exp\left(-\int_0^t \frac{dt' \gamma(t')}{1 + \gamma(t')}\right). \quad (5.17)$$

The derivation of this was explained in Section 2.1.8. Making the conformal transformation $\tilde{g}_{\mu\nu} = \Omega^2 g_{\mu\nu}$, with

$$\Omega^2 = 1 + \frac{\xi G^2 \phi^2}{M_p^2}, \quad (5.18)$$

gives

$$S = \int \sqrt{-\tilde{g}} d^4x \left[\frac{1}{2} \frac{G^2}{\Omega^2} \tilde{g}^{\mu\nu} \partial_\mu \phi \partial_\nu \phi - \frac{M^2}{2\Omega^2} \left(\Omega^2 \tilde{R} - 6\tilde{g}^{\mu\nu} \partial_\mu \Omega \partial_\nu \Omega \right) - U(\phi(t)) \right] \quad (5.19)$$

where $t = \ln \frac{\phi}{m_t}$ and $U = \frac{V(\phi)}{\Omega(\phi)^4}$. With a canonically normalised kinetic term, this becomes

$$S_E = \int d^4x \sqrt{-\tilde{g}} \left(-\frac{M_P^2 \tilde{R}}{2} + \frac{1}{2} \tilde{\partial}_\mu \chi_\phi \tilde{\partial}^\mu \chi_\phi - U(\chi_\phi) \right), \quad (5.20)$$

where

$$\frac{d\chi_\phi}{d\phi} = \sqrt{\frac{G^2 \Omega^2 + 6M_P^2 \Omega^2 \left(\frac{d\Omega}{d\phi}\right)^2}{\Omega^4}} \quad (5.21)$$

and

$$\frac{d\Omega}{d\phi} = \frac{1}{2\Omega} \frac{\xi \phi G^2}{M_p^2} \left(2 - \frac{2\gamma}{1 + \gamma} + \frac{1}{\xi} \frac{d\xi}{dt} \right). \quad (5.22)$$

G is the wavefunction renormalization⁵ of ϕ and has initial condition $G(t = 0) = 1$. The anomalous dimension of h is given by

$$\begin{aligned} \gamma_\phi = & -\frac{1}{16\pi^2} \left(\frac{9g^2}{4} + \frac{3g'^2}{4} - 3y_t^2 \right) - \frac{1}{(16\pi^2)^2} \left(\frac{271}{32} g^4 - \frac{9}{16} g^2 g'^2 - \frac{431}{96} c_h g'^4 \right. \\ & \left. - \frac{5}{2} \left(\frac{9}{4} g^2 + \frac{17}{12} g'^2 + 8g_3^2 \right) y_t^2 + \frac{27}{4} c_h y_t^4 - 6c_h^3 \lambda_h^2 \right). \end{aligned} \quad (5.23)$$

Our sign convention is the same as [38] but different from some other sources which have $\gamma_h \rightarrow -\gamma_h$ everywhere (consistently). G and the coupling constant λ_h are calculated for each value of ϕ , contrasting with the CW method where the coupling constants are calculated at one value of the renormalization scale, and then held constant with respect to ϕ . Both methods have particular calculational advantages. In this method the β -functions are those in Section 3.2.4

⁴Note that G in this section is related to the field renormalization and is not connected to G_ϕ in the previous section.

⁵We have not included G^2 in the suppression factor c_ϕ .

and Section 5.2, but now (as explained in Chapter 2)

$$\frac{d\lambda}{dt} = \frac{\beta_\lambda}{1 + \gamma_\phi} \quad (5.24)$$

for *all* couplings ($\lambda = g, y_t, \xi_\phi, \lambda_h \dots$).

Slow roll parameters

To calculate ϵ in this framework, we start with the definition

$$\tilde{\epsilon} = \frac{M_p^2}{2} \left(\frac{1}{U} \frac{dU}{d\chi_\phi} \right)^2 = \frac{M_p^2}{2} \left(\frac{d\phi}{d\chi_\phi} \right)^2 \left(\frac{dU}{d\phi} \frac{1}{U} \right)^2. \quad (5.25)$$

We use

$$\frac{dG}{dt} = -\frac{G(t)\gamma_h(t)}{1 + \gamma_h(t)} \quad (5.26)$$

and

$$\frac{1}{U} \frac{dU}{d\phi} = \frac{4}{\phi\Omega^2} + \frac{1}{\phi} \left(\frac{1}{\lambda_h} \frac{d\lambda_h}{dt} - \frac{4\gamma_h}{\Omega^2(1 + \gamma_h)} - \frac{2\phi^2 G^2}{\Omega^2 M_p^2} \frac{d\xi}{dt} \right) \quad (5.27)$$

to give

$$\tilde{\epsilon} = \frac{M_p^2}{2\phi^2} \left(\frac{d\phi}{d\chi_\phi} \right)^2 \left(\frac{4}{\Omega^2} + \frac{1}{\lambda_h} \frac{d\lambda_h}{dt} - \frac{4\gamma_h}{\Omega^2(1 + \gamma_h)} - \frac{2\phi^2 G^2}{\Omega^2 M_p^2} \frac{d\xi}{dt} \right)^2. \quad (5.28)$$

To find $\tilde{\eta}$, we begin with

$$\tilde{\eta} = \frac{M_p^2}{U} \frac{d^2 U}{d\chi_\phi^2} = \frac{M_p^2}{U} \left(\frac{d\phi}{d\chi} \right)^2 \frac{d^2 U}{d\phi^2} + \frac{M_p^2}{U} \frac{d^2 \phi}{d\chi^2} \frac{dU}{d\phi} \quad (5.29)$$

This expression will be more complicated than for $\tilde{\epsilon}$, so we assume $c_\phi = 0$ is a good approximation.

This is very reasonable since we will evaluate n and r during inflation, where $c_\phi \simeq 0$ (see Eq. (3.22)). Then we have

$$\begin{aligned} \frac{1}{U} \frac{d^2 U}{d\phi^2} &= -\frac{1}{\phi} \frac{1}{U} \frac{dU}{d\phi} + \frac{1}{U^2} \left(\frac{dU}{d\phi} \right)^2 - \frac{8\xi_\phi G^2}{\Omega^4 M_p^2} - \frac{8G^2}{(1 + \gamma_h)\Omega^4 M_p^2} \frac{d\xi_\phi}{dt} \\ &\quad + \frac{2\phi^2 G^4}{\Omega^4 M_p^4} \left(\frac{d\xi_\phi}{dt} \right)^2 - \frac{2G^2}{\Omega^2 M_p^2} \frac{d^2 \xi_\phi}{dt^2} + \frac{8\xi G^2(2\gamma_h + \gamma_h^2)}{\Omega^4 M_p^2(1 + \gamma_h)^2} \\ &\quad + \frac{1}{\phi^2} \left(-\frac{1}{\lambda_h^2} \left(\frac{d\lambda_h}{dt} \right)^2 + \frac{1}{\lambda_h} \frac{d^2 \lambda_h}{dt^2} - \frac{4}{\Omega^2(1 + \gamma_h)^2} \frac{d\gamma_h}{dt} \right) \end{aligned} \quad (5.30)$$

where

$$\begin{aligned} \frac{d^2\lambda_h}{dt^2} \simeq & -\frac{1}{1+\gamma_h} \frac{d\gamma_h}{dt} \frac{d\lambda_h}{dt} + \frac{1}{16\pi^2(1+\gamma_h)} \left[12\lambda_h \frac{d\lambda_h}{dt} - 24y_t^3 \frac{dy_t}{dt} + \frac{9}{2}g^3 \frac{dg}{dt} \right. \\ & + \frac{3}{2}g'^3 \frac{dg'}{dt} + \frac{3}{2}gg'^2 \frac{dg}{dt} + \frac{3}{2}g^2g' \frac{dg'}{dt} + (-9g^2 - 3g'^2 + 12y_t^2) \frac{d\lambda_h}{dt} \\ & \left. + \left(-18g \frac{dg}{dt} - 6g' \frac{dg'}{dt} + 24y_t \frac{dy_t}{dt} \right) \lambda_h \right], \end{aligned} \quad (5.31)$$

$$\begin{aligned} \frac{d\gamma_h}{dt} \simeq & -\frac{1}{16\pi^2} \left(\frac{9g}{2} \frac{dg}{dt} + \frac{3g'}{2} \frac{dg'}{dt} - 6y_t \frac{dy_t}{dt} \right) - \frac{1}{(16\pi^2)^2} \left[\frac{271}{8}g^3 \frac{dg}{dt} - \frac{9}{8}gg'^2 \frac{dg}{dt} \right. \\ & - \frac{9}{8}g^2g' \frac{dg'}{dt} - \frac{5}{2} \left(\frac{9}{2}g \frac{dg}{dt} + \frac{17}{6}g' \frac{dg'}{dt} + 16g_3 \frac{dg_3}{dt} \right) y_t^2 \\ & \left. - 5 \left(\frac{9}{4}g^2 + \frac{17}{12}g'^2 + 8g_3^2 \right) y_t \frac{dy_t}{dt} \right] \end{aligned} \quad (5.32)$$

and

$$\frac{d^2\xi_\phi}{dt^2} \simeq \frac{1}{\xi_\phi + 1/6} \left(\frac{d\xi_\phi}{dt} \right)^2 + \left(\frac{\xi_\phi + 1/6}{16\pi^2} \right) \left(6 \frac{d\lambda_h}{dt} + 12y_t \frac{dy_t}{dt} - 9g \frac{dg}{dt} - 3g' \frac{dg'}{dt} \right). \quad (5.33)$$

To tree level, $\tilde{\epsilon}$ and $\tilde{\eta}$ are the same as calculated using the Coleman-Weinberg potential, once expanded out. We also need

$$\frac{d^2\phi}{d\chi^2} = \frac{1}{\Omega^3} \left(\frac{d\phi}{d\chi} \right)^4 \frac{d\Omega}{d\phi} \left[1 + 3M_p^2 \left(4 \left(\frac{d\Omega}{d\phi} \right)^2 - \frac{d^2(\Omega^2)}{d\phi^2} \right) \right] \quad (5.34)$$

where $\frac{d\Omega}{d\phi}$ is given by Eq. (5.22) and

$$\frac{d^2(\Omega^2)}{d\phi^2} = \frac{2\Omega}{\phi} \frac{d(\Omega)}{d\phi} \frac{1+3\gamma_h}{1+\gamma_h} - \frac{\xi G^2}{M_p^2} \left(\frac{2}{(1+\gamma_h)^2} \frac{d\gamma_h}{dt} + \frac{1}{\xi^2} \left(\frac{d\xi}{dt} \right)^2 - \frac{1}{\xi} \frac{d^2\xi}{dt^2} \right). \quad (5.35)$$

Putting these all together gives us $\tilde{\eta}$, remembering that the couplings are functions of $t(\phi)$.

For $130 \text{ GeV} \lesssim m_h \lesssim 170 \text{ GeV}$, radiative corrections to $\tilde{\eta}$ are negligible. At $m_h \sim 180 \text{ GeV}$, radiative corrections cause $\tilde{\eta}$ to be increased by 13% compared to η_{tree} . For $m_h = 122 \text{ GeV}$, $\tilde{\eta}$ is decreased by 20% compared to its tree-level value. Radiative corrections have a larger impact on $\tilde{\epsilon}$. At low $m_h \approx 122 \text{ GeV}$, $\tilde{\epsilon}$ is 3 times the tree level value, at $m_h = 160 \text{ GeV}$ $\tilde{\epsilon} = 0.64\tilde{\epsilon}_{tree}$ and at $m_h = 180 \text{ GeV}$ $\tilde{\epsilon}$ is dramatically reduced to be only $0.14\tilde{\epsilon}_{tree}$.

5.3 RG improved effective action is a more complete method

Fig. (5.2) shows the spectral index n versus Higgs mass m_h for the Coleman-Weinberg potential (solid) and RG improved method (dashed). Below about 122 GeV, the potential becomes

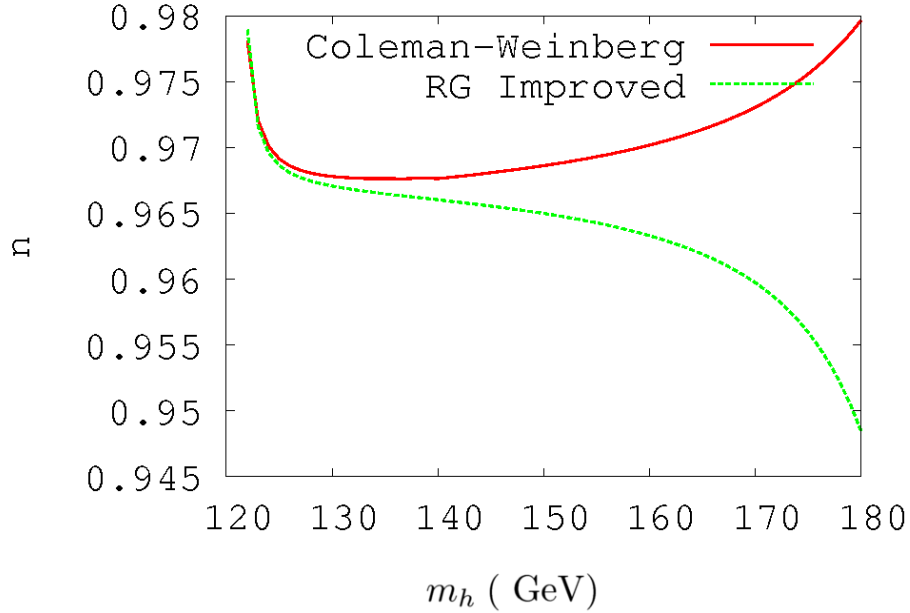


Figure 5.2: Spectral index n versus Higgs mass m_h for Coleman-Weinberg (solid red) and RG improved (green dashed) methods.

negative and above ~ 185 GeV we reach the (arbitrary) limit of perturbativity imposed on the couplings ($\lambda_s < 100$). For $m_h \lesssim 130$ GeV, there is agreement between the two methods and n rises as m_h decreases. However above ~ 130 GeV, the Coleman-Weinberg n increases with m_h while n decreases with m_h for the RG improved method, becoming steep at large m_h . Fig. (5.3) shows the tensor to scalar ratio r for the Coleman-Weinberg potential (solid) and RG improved method (dashed), for $122 \leq m_h \leq 180$ GeV. Interestingly, this follows approximately the same shape as n . This is interesting because it allows us to trace the origin of the variation of n with m_h . In both cases $\tilde{\eta}$ is always the dominant contribution to the spectral index: $n = 1 + 2\tilde{\eta} - 6\tilde{\epsilon} \simeq 1 + 2\tilde{\eta}$. As we noted in the previous section, radiative corrections to $\tilde{\eta}$ are generally very small, so $\tilde{\eta}$ is well approximated by its classical value and

$$n \simeq 1 - \frac{8 M_p}{3 \xi \phi^2}. \quad (5.36)$$

Thus, the shape of n is determined by $\xi \phi^2$. This is determined by $\tilde{\epsilon}$, through the normalization to the COBE data (Eq. (5.6)) and through the integration to get \tilde{N} (Eq. (3.59) with $s \rightarrow \phi$). For a given ξ , at a first approximation, we find $\tilde{N} \sim \int_{\phi_{end}}^{\phi_{\tilde{N}}} \frac{1}{\sqrt{\tilde{\epsilon}}} d\chi \sim \xi \phi^2$. Thus, if radiative corrections cause $\tilde{\epsilon}$ to increase above its classical value, we would expect $\xi \phi^2$ to be larger for a fixed \tilde{N} . This means that the magnitude of $\tilde{\eta}$ is decreased and so n is increased. This explains the similar shape of Fig. (5.3) and Fig. (5.2). We must now explain the origin of the strong deviation of $\tilde{\epsilon}$ from its classical value, and why this is different for the Coleman-Weinberg and RG improved

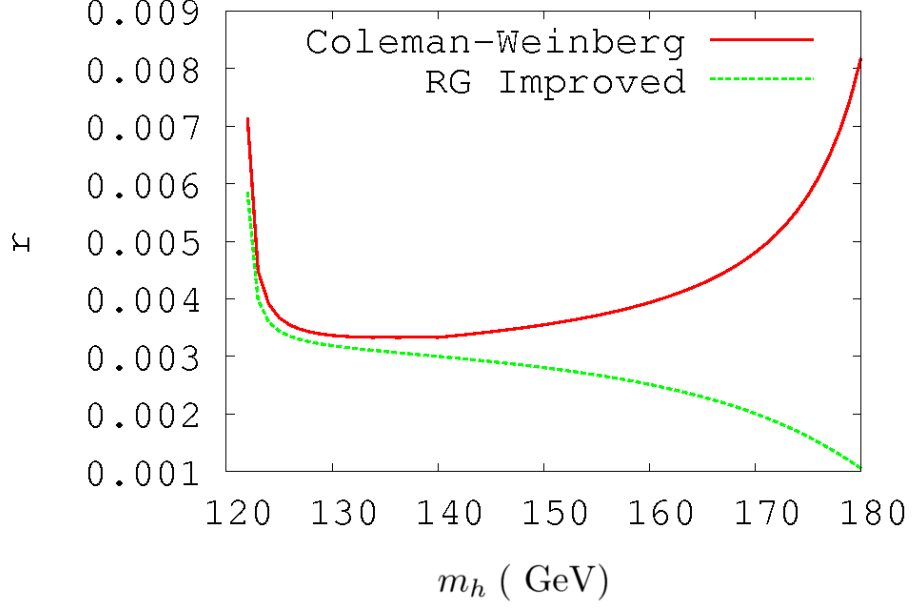


Figure 5.3: Tensor to scalar ratio r versus Higgs mass m_h for Coleman-Weinberg (solid red) and RG improved (green dashed) methods.

methods.

For the Coleman-Weinberg potential, consider

$$16\pi^2 L_{CW} \simeq 6\lambda_h + \frac{1}{\lambda_h} \left(\frac{3g^4}{4} + \frac{3(g^2 + g'^2)^2}{8} - 6y_t^4 \right) \quad (5.37)$$

(given by Eq. (5.11) with $c_\phi = 0$). The first term, $6\lambda_h$, increases with m_h while the second, $\propto \frac{1}{\lambda_h}$, increases when m_h decreases (g , g' and y_t have only a tiny variation with λ_h). Thus, for both large and small m_h , L_ϕ increases. The placement of c_h is crucial⁶: if the whole term $\propto \lambda_h$ had been suppressed (as for example in [38]), then we would expect L_ϕ to increase at small m_h — but *not* at large m_h .

For the RG improved method, we can construct an equivalent to L_{CW} by expanding out the terms in $\tilde{\epsilon}$ (Eq. (5.28)). This gives

$$16\pi^2 L_{RGI} \simeq -6\lambda_h + \frac{1}{\lambda_h} \left(\frac{3g^4}{4} + \frac{3(g^2 + g'^2)^2}{8} - 6y_t^4 \right). \quad (5.38)$$

At small m_h , the second term dominates and the behaviour is identical to the Coleman-Weinberg method. However, at large m_h , the first term (which is now negative) dominates and L_{RGI} becomes negative. This negative term has come from the addition of $-12(1 + c_h)\lambda_h$ from the $\frac{1}{\xi} \frac{d\xi}{dt}$ term in $\tilde{\epsilon}$.

We therefore see that the RG improved effective potential gives a more correct result for

⁶As we evaluate this during inflation, $c_h = 0$ for the inflaton, but not for any other scalars.

the spectral index n . This is because the method takes into account the variation of ξ during inflation. The standard Coleman-Weinberg potential does not include the quantum effects of the non-minimal coupling to gravity (except through the commutator suppression factor c_ϕ). It should be possible to compute a correction⁷ to the standard Coleman-Weinberg one-loop potential which would account for the effect of the non-minimal coupling. We also note that the result at low m_h is strongly dependent on y_t , as only a small increase in y_t will cause the negative term in L to dominate for small m_h . We believe this is a plausible explanation for why some previous results have n below the classical value for small m_h . Future precise measurements of m_t may help to determine the correct behaviour.

Our results mirror those of [38] (Fig. (5.1a)) at low m_h and mirror those of [37] (Fig. (5.1b)) and [64] (Fig. (5.1c)) at larger m_h . We believe the discrepancy at low m_h between our results and the results of [64] are due to the initial value of the top quark coupling.

Application to S -inflation

At first glance this result (that the RG improved effective potential is more correct) would seem also to apply to S -inflation. However, we will see that for real S , $\beta_{\xi_s} \simeq 0$ during inflation, due to the suppression factor $c_s \simeq 0$. Consequently we expect the results from both methods to be similar for S -inflation. This is confirmed by comparing Fig. (3.8) to the results in the following section, Fig. (5.6). If a complex S were used instead, we would expect the methods to give somewhat different results — as in that case β_{ξ_s} is not zero during inflation.

5.4 Distinguishing S -inflation from Higgs-inflation through observations

In this section, we consider the predictions for the spectral index n from three variants of the model: S -inflation [1], Higgs inflation including S [64] and pure Higgs inflation [32, 33, 34, 35, 36, 37, 38]. We focus on the simplest case where S is real.

5.4.1 Defining the models

We use the RG improved effective action, given by

$$S_J = \int \sqrt{-g} d^4x \left(\mathcal{L}_{SM} - \frac{M_p^2 R}{2} - \xi_h G_H^2 H^\dagger H R - \xi_s G_S^2 S^\dagger S R + G_H^2 (D_\mu H)^\dagger (D^\mu H) + G_S^2 (\partial_\mu S)^\dagger (\partial^\mu S) - V(S^\dagger S, H^\dagger H) \right) \quad (5.39)$$

⁷Such corrections have been considered in [91, 92, 93] for example.

where

$$\begin{aligned}
V(S^\dagger S, H^\dagger H) &= \lambda_h \left(G_H^2 (H^\dagger H) - \frac{v^2}{2} \right)^2 + \lambda_{hs} G_H^2 G_S^2 S^\dagger S H^\dagger H \\
&\quad + \lambda_s G_S^4 (S^\dagger S)^2 + m_{s_o}^2 G_S^2 S^\dagger S.
\end{aligned} \tag{5.40}$$

The anomalous dimension γ_h is given by Eq. (5.23), while $\gamma_s = 0$, giving

$$G_H(t) = \exp\left(-\int_0^t \frac{dt' \gamma_h(t')}{1 + \gamma_h(t')}\right); \quad G_S(t) = 1. \tag{5.41}$$

For inflation in the H direction, we set $S = 0$ and for inflation in the S direction, we set $H = 0$.

For pure Higgs inflation, $\lambda_{hs} = \lambda_s = \xi_s = 0$.

As before, we make a conformal transformation (see Eq. (3.3) to Eq. (3.10)) with

$$\Omega^2 = 1 + \frac{2\xi_h G_H^2 H^\dagger H}{M_p^2} + \frac{2\xi_s S^\dagger S}{M_p^2} \tag{5.42}$$

resulting in

$$U(\chi_s, \chi_h) \simeq \frac{1}{\Omega^4} \left(\frac{\lambda_h}{4} G_H^4 h^4 + \frac{\lambda_s}{4} s^4 + \frac{\lambda_{hs}}{4} s^2 h^2 \right). \tag{5.43}$$

Initial conditions are as in Section 5.2, except that we set either $\xi_s(m_t) = 0$ or $\xi_h(m_t) = 0$ as appropriate and normalise the other to the WMAP data. The β -functions are given in Section 3.2.4 and Section 5.2, but (for *all* couplings ($\lambda = g, y_t, \xi_\phi, \lambda_h \dots$)),

$$\frac{d\lambda}{dt} = \frac{\beta_\lambda}{1 + \gamma_H} \tag{5.44}$$

for inflation in the H direction, and

$$\frac{d\lambda}{dt} = \beta_\lambda \tag{5.45}$$

for inflation in the S direction.

Slow roll inflation

As discussed earlier in the chapter, it is the radiative corrections to $\tilde{\epsilon}$ which are of prime importance. We find, where ϕ is either s or h ,

$$\frac{1}{U} \frac{dU}{d\phi} = \frac{4}{\phi \Omega^2} + \frac{1}{\phi} \left(\frac{1}{\lambda_\phi} \frac{d\lambda_\phi}{dt} - \frac{4\gamma_\phi}{\Omega^2(1 + \gamma_\phi)} - \frac{2\phi^2 G_\phi^2}{\Omega^2 M_p^2} \frac{d\xi_\phi}{dt} \right). \tag{5.46}$$

We use the equations of Section 5.2.2 — which also apply to S -inflation — where ϕ is replaced by h or s as appropriate.

5.4.2 Theoretical differences

We have introduced two new parameters λ_s and λ_{hs} compared to pure Higgs inflation. The second can potentially be fixed by experiment, when m_s is known. There will be a minimum value of λ_{hs} below which the S particles cannot account for the observed density of dark matter. In this section, we examine all values of λ_s and λ_{hs} where all couplings (except ξ) remain < 100 up to the scale of inflation, including negative values of λ_{hs} . This limit is less strict than in Chapter 3, where we required $\lambda_h, \lambda_s < 2\pi/3$ and $\lambda_{hs} < 4\pi$ up to the scale M_p (see Eq. (3.44)). Our aim is to look at the variation of the spectral index, rather than limits from perturbativity. We have not imposed limits on the non-inflationary direction. As demonstrated for the S -direction in Fig. (3.6) and Fig. (3.7), this would impose stronger bounds on the permitted combinations of m_h, λ_s and λ_{hs} .

The couplings λ_h and λ_s always increase with RG running when λ_{hs} is non-zero, as β_{λ_h} and β_{λ_s} contain terms $\propto \lambda_{hs}^2$. One term in $\beta_{\lambda_{hs}}$ (Eq. (3.28)) is also $\propto \lambda_{hs}^2$, so is always positive; the others are proportional to λ_{hs} . Thus λ_{hs} will tend to increase in magnitude but retain its original sign (provided that the term $\propto \lambda_{hs}^2$ never dominates for $\lambda_{hs} < 0$). The increase is larger if λ_h or λ_s are large too. The running for negative λ_{hs} will be less strong.

In Section 5.3 we used the quantity L (the part of $\frac{dU}{d\phi}$ due to radiative corrections) to explain how n deviated from its classical value: large L corresponds to large n . We can calculate L for the models, making the same approximations as in the previous section (for pure Higgs inflation, we gave the result in Eq. (5.38)). With $c_\phi = 0$ for the inflaton, and $c_\phi = 1$ for the other scalars, we find

$$16\pi^2 L_S \simeq \frac{2\lambda_{hs}^2}{\lambda_s} - 2\frac{\xi_h}{\xi_s} \left(12\lambda_h + 6y_t^2 - \frac{3}{2}(g^2 + g'^2) \right) \quad (5.47)$$

and

$$16\pi^2 L_H \simeq -6\lambda_h + \frac{1}{\lambda_h} \left(\frac{3g^4}{4} + \frac{3(g^2 + g'^2)^2}{8} - 6y_t^4 + \frac{\lambda_{hs}^2}{2} \right) - 2\lambda_{hs} \frac{\xi_s}{\xi_h}. \quad (5.48)$$

The terms $\propto \frac{\xi_a}{\xi_b}$ are likely to be subdominant. We will use L_S and L_H to help explain the results presented below.

5.4.3 Higgs inflation in the presence of an additional scalar

Firstly, we investigate the effect of λ_{hs} on Higgs inflation and so set $\lambda_s(m_t) = 0$ (but allow for its running). The results are shown in Fig. (5.4) for $\lambda_{hs} = 0$ (red; pure Higgs inflation), $\lambda_{hs} = 0.1$ (green), 0.3 (pink) and 0.5 (blue). The shape of the curves and range of n for all λ_{hs} are quite similar (for $m_h > 122$ GeV), but two main features can be seen: (i) as λ_{hs} increases, the curves shift to the left, also shifting the range of m_h and (ii) there is a turnover at low m_h for $\lambda_{hs} = 0.3$.

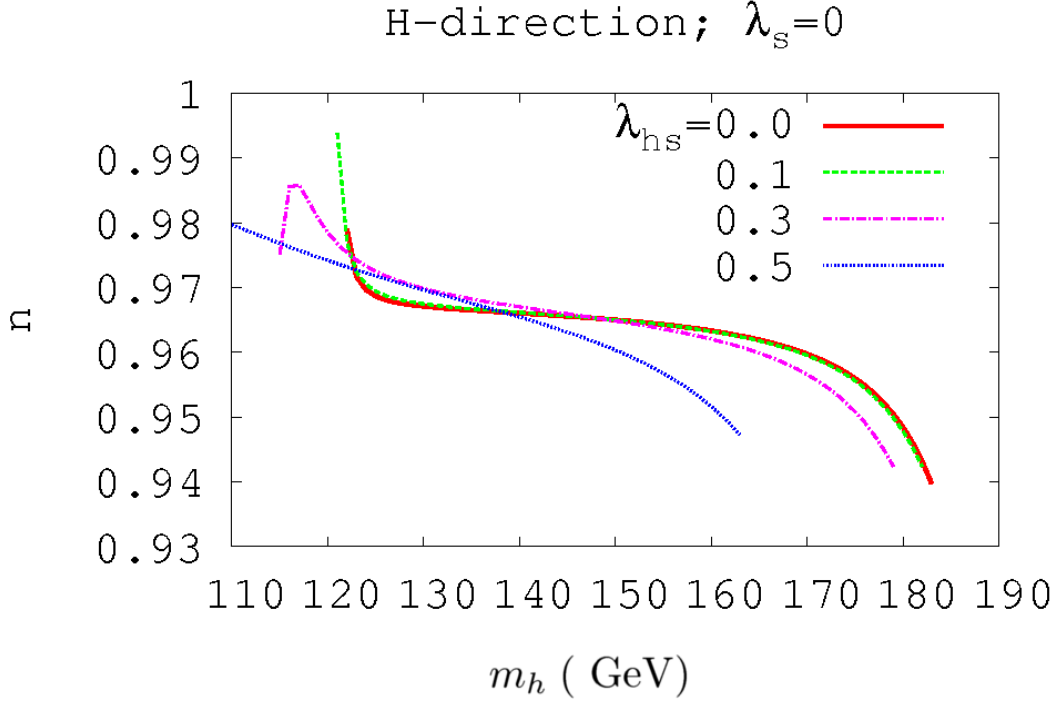


Figure 5.4: Spectral index n versus Higgs mass m_h for inflation in the Higgs direction with $\lambda_s = 0$ and varying λ_{hs} : $\lambda_{hs} = 0$ (pure Higgs inflation; red), $\lambda_{hs} = 0.1$ (green), $\lambda_{hs} = 0.3$ (pink) and $\lambda_{hs} = 0.5$ (blue).

These are explained below.

(i) A larger λ_{hs} increases β_h , giving a larger λ_h for a given m_h . At large m_h , $L_H \propto -6\lambda_h$ (Eq. (5.48)), and so n falls faster with larger λ_{hs} . This explains the shift to the left as λ_{hs} increases. The range of m_h accessible to this model is shifted downwards as λ_{hs} increases. A larger λ_{hs} can prevent λ_h becoming negative at low values of m_h . Large λ_{hs} causes the couplings to grow faster and the perturbativity limit to be reached at a lower m_h . Thus, the range of m_h is shifted.

(ii) The turnover at low m_h (seen for the case $\lambda_{hs} = 0.3$ in Fig. (5.4)) is due to the term in $L_H \propto \frac{\xi_s}{\xi_h}$. Small λ_h means that ξ_h is small (from normalization, Eq. (3.26)). Large λ_{hs} gives a large running of ξ_s (remember that $\xi_s(m_t) = 0$) so the ratio $\frac{\xi_s}{\xi_h}$ is of $\mathcal{O}(1)$ at the scale of inflation⁸. Thus there is a large negative contribution (last term of Eq. (5.48)) almost balancing the positive term $\propto \frac{1}{\lambda_h}$.

As shown in Fig. (5.5), λ_s has a steepening effect on n . However, this is a relatively small effect for $\lambda_{hs}(m_t) = 0.3$. Above about $\lambda_s = 0.15$, we reach the perturbativity limit of λ_s . The steepening is due to λ_s causing λ_{hs} to increase, therefore exaggerating the effects of Fig. (5.4) further. The last term in Eq. (5.48), $-2\lambda_{hs}\frac{\xi_s}{\xi_h}$, may also play a role. Increasing λ_s increases ξ_s ,

⁸However, with ξ_s and ξ_h of similar magnitudes, we can no longer assume that inflation is in the H -direction. Therefore this is perhaps not a valid region of the parameter space — however we do not impose any constraint on $\frac{\xi_s}{\xi_h}$ in this chapter.

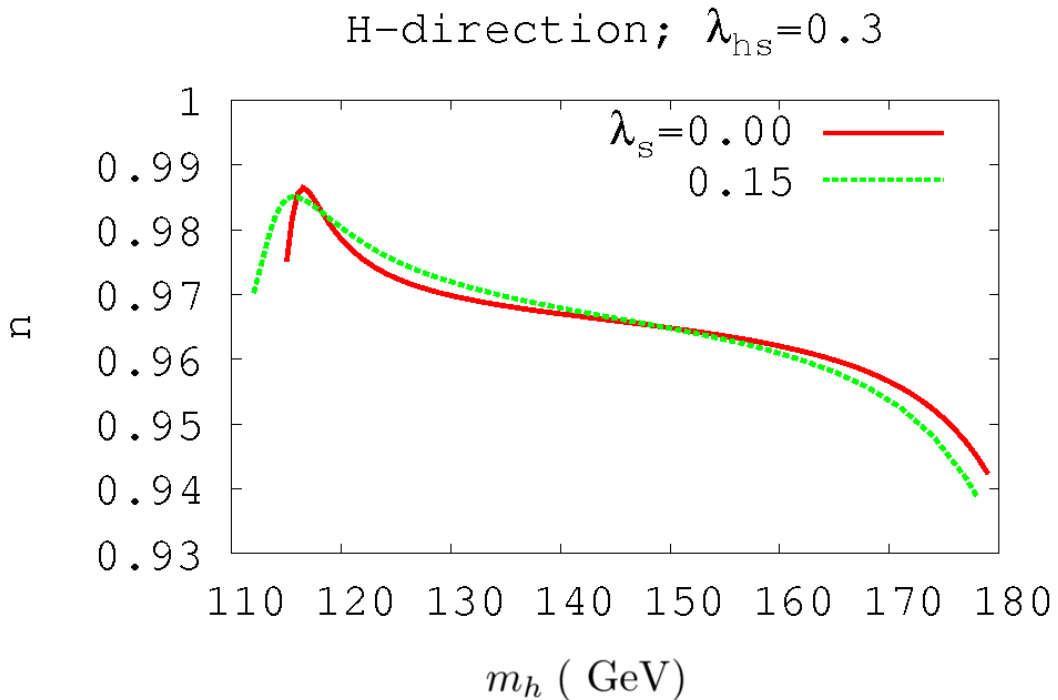


Figure 5.5: Spectral index n versus Higgs mass m_h for inflation in the Higgs direction, with $\lambda_s = 0.0$ (solid red) and $\lambda_s = 0.15$ (green dashed).

which may give some contribution to the decrease in n at larger m_h . For $\lambda_{hs}(m_t) = 0.1$ (not shown) we find that increasing λ_s has a negligible effect on n (λ_s becomes non-perturbative at $\lambda_s(m_t) \sim 0.3 - 0.4$ in this case).

We conclude that introducing a real singlet scalar to the model of Higgs inflation can affect the spectral index prediction, increasing it at low m_h and decreasing it at higher m_h . This effect is controlled mainly by the magnitude of λ_{hs} which is, in principle, measurable. The addition of λ_{hs} also changes the range of m_h , decreasing both upper and lower limits. Negative values of λ_{hs} are allowed and give similar results.

5.4.4 S -inflation

We now consider inflation in the direction of the singlet scalar, S . Firstly, with $\lambda_{hs}(m_t) = 0$, the spectral index does not vary noticeably with m_h — see Fig. (5.6) (where we show the pure Higgs inflation case for comparison). This is reassuring, since with $\lambda_{hs} = 0$, the model is completely decoupled from the Higgs sector. We also see that n does not vary with λ_s (if λ_s is increased much further than shown in the figure, it reaches its perturbativity limit). This is because the deviation of n from its classical value is determined by L_S (Eq. (5.47)) which is $\propto \lambda_{hs}^2 = 0$.

We now investigate the effect of varying λ_{hs} . The results for $\lambda_s(m_t) = 0.1$ (solid) and $\lambda_s(m_t) = 0.01$ (dashed) are shown in Fig. (5.7). We see that increasing λ_{hs} has a dramatic

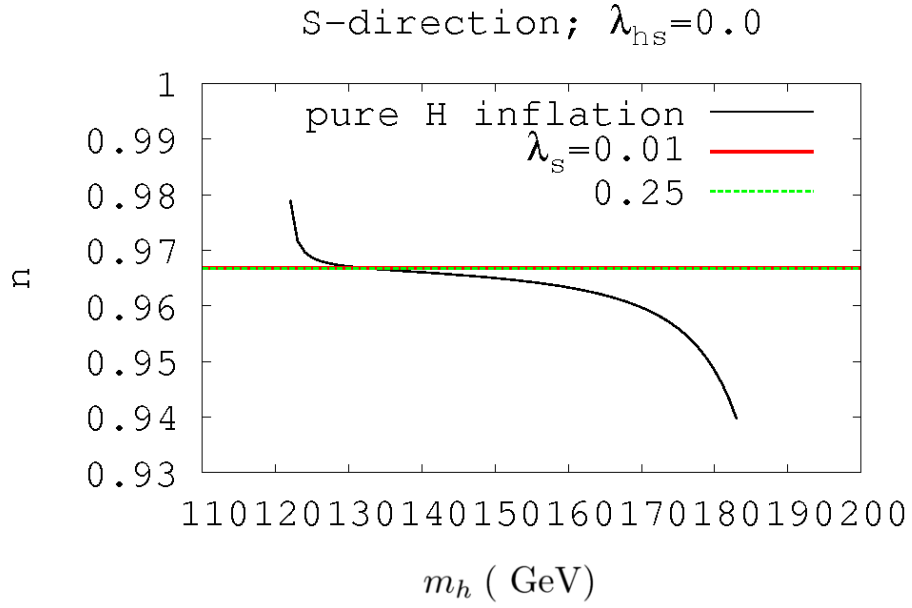


Figure 5.6: Spectral index n versus Higgs mass m_h for inflation in the S -direction with $\lambda_{hs} = 0.0$: $\lambda_s = 0.01$ (solid red) and $\lambda_s = 0.25$ (green dashed). ‘Pure’ Higgs inflation is shown for comparison (solid black)

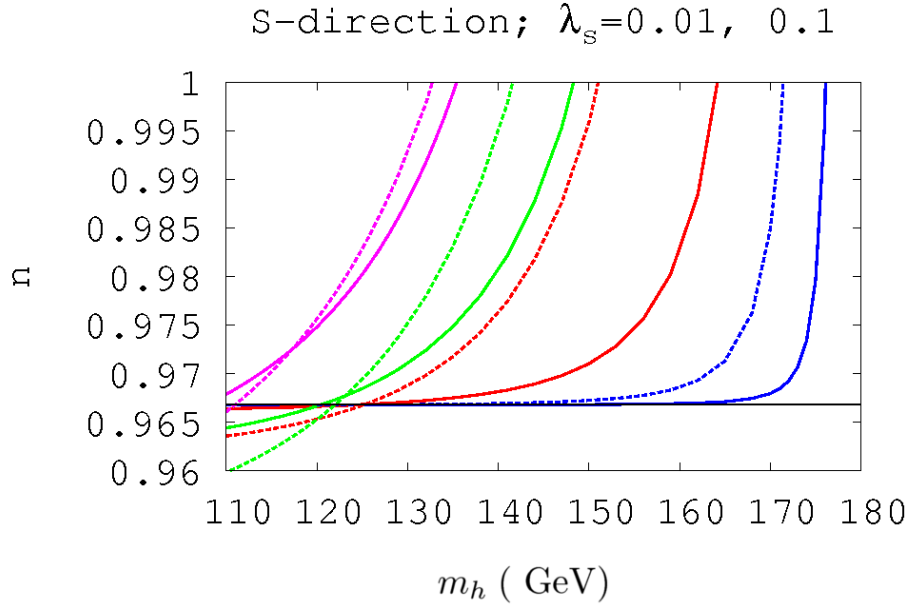


Figure 5.7: Spectral index n versus Higgs mass m_h for inflation in the S -direction, with $\lambda_s = 0.1$ (solid) and $\lambda_s = 0.01$ (dashed). Various values of λ_{hs} are shown: $\lambda_{hs} = 0.0$ (black), $\lambda_{hs} = 0.01$ (blue), $\lambda_{hs} = 0.1$ (red), $\lambda_{hs} = 0.3$ (green) and $\lambda_{hs} = 0.5$ (pink).

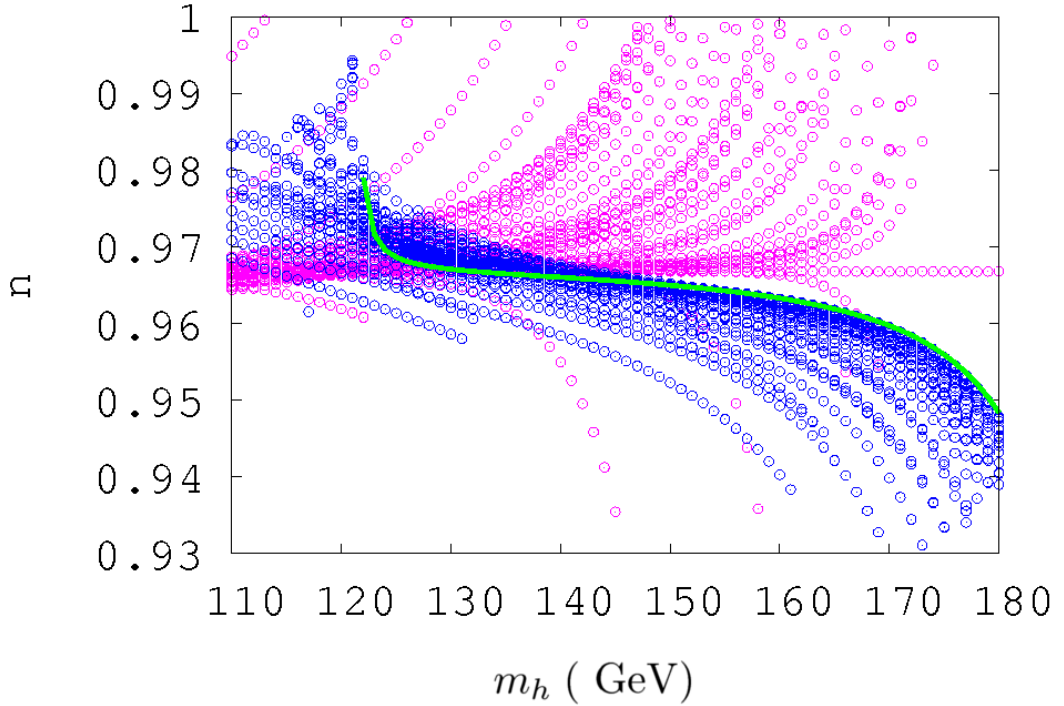


Figure 5.8: Spectral index n versus Higgs mass m_h for inflation in the S-direction (pink circles), for inflation in the H-direction (blue circles) and pure Higgs inflation (solid green line). Couplings have been varied by 0.1 and required to remain less than 100.

effect on n . This is because $L_S \propto \frac{\lambda_{hs}^2}{\lambda_s}$. Large $|\lambda_{hs}|$ (at inflation scale) will therefore cause L_S to increase. As described in the previous chapter, this will cause n to increase. Smaller λ_s gives larger L_S , increasing n further (the effect of λ_{hs} is dominant).

5.4.5 Distinguishing the models observationally

We show in Fig. (5.8) the approximate range of n for each model, when λ_s and λ_{hs} are allowed to take any values that are multiples of 0.1 (we impose the restriction $|\lambda| < 100$ up to the scale of inflation). Introducing other bounds would cause these areas to decrease in size. We see that there is a substantial difference in shape between the two models. At $m_h \gtrsim 150$ GeV the possible values of n are very different⁹. There is more overlap at lower m_h — for $125 \lesssim m_h \lesssim 135$ GeV, it appears unlikely that n could discriminate between the models. Of course, a measurement of λ_{hs} will leave only one free parameter (λ_s), reducing the number of points available.

We show in Fig. (5.9) the equivalent figure for r , with the same restrictions on λ_s and λ_{hs} as above. We see that r is in general low ($r \lesssim 0.02$) — although for large m_h (S -direction) and small m_h (H -direction), it can take values which are only just within the current WMAP limit $r < 0.22$. Thus there is a small chance that r may be detectable by Planck. It should be noted

⁹The small number of S -direction points with $n < n_{cl}$ are likely to be ruled out by perturbativity and stability constraints on the couplings.

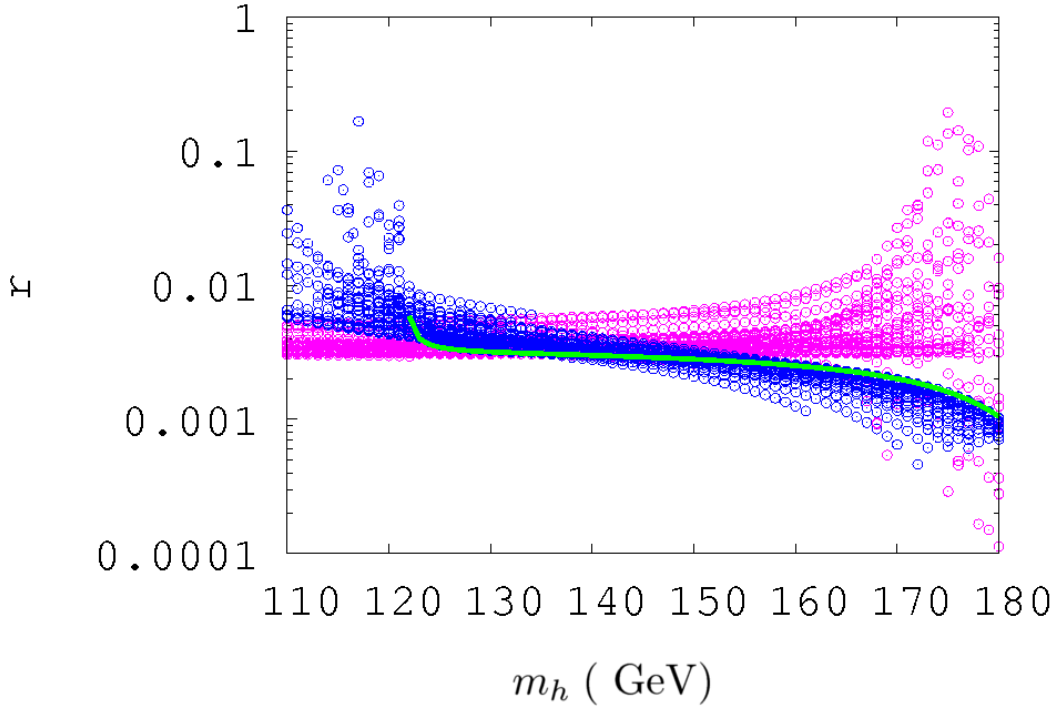


Figure 5.9: Tensor to scalar ratio r (log scale) versus Higgs mass m_h for inflation in the S -direction (pink circles), for inflation in the H -direction (blue circles) and pure Higgs inflation (solid green line). Couplings have been varied by 0.1 and required to remain less than 100.

that these extreme points may be excluded when full stability and perturbativity constraints are applied to the models¹⁰. The points with large r may also be excluded because the corresponding value of n may be outside of the WMAP limits.

It is important to consider the effect of other bounds on the models. In Chapter 3 we required vacuum stability and perturbativity up to $s = M_p$ and $h = M_p$. This dramatically restricted the parameter space (Fig. (3.6)) with the bounds mainly coming from vacuum stability and perturbativity in the h direction (although the upper limit on m_h was from perturbativity of λ_h in the S -direction). To reach $m_h \lesssim 140$ GeV we needed $\lambda_{hs} \gtrsim 0.3$ which in turn requires λ_s to be small in order to remain perturbative. So, S -inflation favours $140 \lesssim m_h \lesssim 170$ GeV. This is the region where predictions for S -inflation are most distinct from those of Higgs inflation.

The bounds on the couplings for Higgs inflation will be slightly different, due to different ξ_s and ξ_h affecting the suppression factors c_s and c_h . For inflation in the Higgs direction, $135 \text{ GeV} \lesssim m_h \lesssim 190 \text{ GeV}$, $\lambda_s(m_t) \lesssim 0.25$ and $-0.2 \lesssim \lambda_{hs}(m_t) \lesssim 0.3$ according to [64] (see their Fig. (10)). Perturbativity and vacuum stability constraints were applied *only* in the h direction up to the scale of inflation. Further regions of this parameter space are ruled out due to ‘wrong way roll’ of the potential (see their Fig. (5)).

¹⁰These constraints should be applied in *both* directions (h and s), regardless of the direction of inflation, and should be applied at least to a scale just above the scale of inflation.

In [94], the range of m_h allowed by vacuum stability and perturbativity in the Standard Model is given as $128.6 \text{ GeV} \lesssim m_h \lesssim 175 \text{ GeV}$, where the lower bound is from vacuum stability and the upper bound is from perturbativity of the Higgs self-coupling up to M_p . We see that the allowed range in both S and Higgs inflation is somewhat narrower. Therefore both models may be ruled out relative to the conventional SM if m_h is observed close to the SM lower or upper bound. The exact range of m_h , λ_s and λ_{hs} permitted for both models remains to be calculated.

5.4.6 Dependence on \tilde{N}

The classical value $n_{cl} = 1 - \frac{2}{\tilde{N}} - \frac{3}{2\tilde{N}^2}$ which acts as the border between the two models is dependent on the number of e-foldings of inflation \tilde{N} . The number of e-foldings \tilde{N} is calculable through the reheating temperature — in Chapter 4 we found $58 \lesssim \tilde{N} \lesssim 61$ for S -inflation (including a theoretical error ± 1). For pure Higgs inflation, the range is given as $58 \lesssim \tilde{N} \lesssim 59$ [33]. The range of \tilde{N} for S -inflation is slightly higher than for Higgs inflation, which means that n_{cl} for S -inflation could be higher. Although the effect is small, it could help the discrimination between the models as it may increase the separation between the S -inflation and Higgs inflation predictions.

For S -inflation, the error on \tilde{N} mainly comes from the error on the reheating temperature and the error in precisely defining the end of inflation and beginning of post-inflation era. As discussed in Chapter 3, an error $\Delta\tilde{N} \sim 1.5$ corresponds to $\Delta n \sim 0.001$. Therefore we conclude that the classical spectral index for S -inflation lies in the range $0.965 \leq n_{cl} \leq 0.967$.

We see therefore that if we restrict \tilde{N} to the range of $58 \leq \tilde{N} \leq 61$ and consider the effect of radiative corrections, then a measurement of n significantly *above* 0.967 would point to S -inflation, while a measurement of n significantly *below* 0.965 would point to Higgs inflation. If $0.965 \leq n \leq 0.967$ then the uncertainty due to \tilde{N} may prevent us from distinguishing between the models by means of the spectral index alone. However, the models may be distinguished once the Higgs mass is known and if the S -particle is detected.

In conclusion, we expect the Planck experiment to measure n to a $2\text{-}\sigma$ accuracy of ± 0.005 . If Planck should find n significantly larger than 0.967 while LHC finds a Higgs with mass larger than 135 GeV, then S -inflation will be compatible with the observations but Higgs inflation will be strongly disfavoured. If the spectral index n is measured to be significantly less than 0.965 then Higgs inflation will be compatible with the observations and S -inflation is disfavoured.

Chapter 6

Naturalness and Unitarity

The naturalness of non-minimally coupled inflation models, such as Higgs inflation and S -inflation, has been questioned. A specific concern is whether or not unitarity is violated in Higgs or S scattering mediated by graviton exchange¹ at a scale $\Lambda \sim M_p/\xi \ll M_p$ where $\xi \sim 10^4$ for pure Higgs inflation. In particular, in [95] it was noted that the effective coupling in tree-level graviton-mediated Higgs scattering becomes strong at $E \sim \Lambda$, while in [96] it was concluded that unitarity would be violated in graviton-mediated Higgs scattering at $E \sim \Lambda$. The modification of the theory suggested by these problems seems to imply that new terms such as $\frac{(H^\dagger H)^3}{\Lambda^2}$ will be added to the effective potential. Given that during inflation $h \sim \frac{\sqrt{N}M_p}{\sqrt{\xi}} \gg \Lambda$, then it may be presumed that these terms either spoil inflation or must be fine-tuned in order to allow for inflation. This fine-tuning would mean that the model is unnatural.

These analyses were based on the original Higgs inflation model, which considered a single real Higgs scalar in the unitary gauge and neglected gauge interactions. In [2] we noted that there are no strong coupling or unitarity-violating interactions in the single scalar model when considered in the Einstein frame, indicating that the apparent strong coupling or unitarity-violating effects in the Jordan frame at $E \sim \Lambda$ do not occur and that the results of [95, 96] are incorrect. It is an important point to emphasise that if unitarity violation is shown to occur in one frame, it *must* occur in the other. Equally, if it is shown not to occur in one frame, it must not occur in the other frame either. This is due to the equivalence theorem, discussed in Chapter 3. It means that we can use whichever frame is most suited to the particular calculation. The absence of unitarity violation in the Jordan frame can be understood in terms of a cancellation of the leading s-, t- and u-channel contributions to the graviton-mediated Higgs amplitude in the Jordan frame [97, 98]. However, once longitudinal gauge fields are included in the unitary gauge (or, equivalently, Goldstone bosons in a covariant gauge), the Jordan frame cancellation

¹This is the process in the Jordan frame. As will be shown, it is equivalent to a four-point non-renormalizable interaction vertex in the Einstein frame.

of the graviton-mediated Higgs scattering amplitude no longer occurs [98, 99]. This manifests itself in the Einstein frame as non-renormalizable interactions which cannot be eliminated by field redefinitions².

In this chapter, our first aim is to clearly explain the origin of the apparent violation of unitarity. Then we will discuss the results of [100] which show that perturbation theory will break down *before* unitarity violation is reached and that *tree-level* unitarity violation does not always mean that unitarity is actually violated. This *may* point towards strong coupling at $E \sim \Lambda$, rather than a violation of unitarity. We conclude that a full calculation is necessary to determine whether or not unitarity is violated. Even if unitarity is violated and new physics is necessary, it is not clear that such new physics will exclude Higgs inflation. To show this, we present a unitarity conserving model of Higgs inflation (this has distinct predictions to the original model). We remind the reader of the conditions for unitarity conservation which were explained in Section 2.2.3. They are

$$\text{Im}[a_l] \geq |a_l|^2 \tag{6.1}$$

or equivalently

$$|\text{Re}[a_l]| \leq \frac{1}{2}. \tag{6.2}$$

6.1 Unitarity violation in Higgs inflation models

In this section, we demonstrate the apparent problem of tree-level unitarity violation in Higgs inflation. The argument applies in general to any non-minimally coupled theory with more than one scalar. This includes our model of S -inflation with complex *or* with real S (the Higgs scalars are coupled to S so the theory still has multiple scalars if S is real).

The Equivalence Theorem for non-linear field redefinitions [57, 60, 61, 101] states that the S-matrix for scattering processes is invariant under non-linear redefinitions, which implies that the scattering rate is the same whether calculated in the Jordan or in the Einstein frame. If the theory violates unitarity, the unitarity violation will be observed in *both* frames — although it is sufficient to clearly demonstrate the (non-) violation in either frame. This must be done carefully — the original claim of Jordan frame unitarity violation for the singlet case was incorrect — a fact which was obvious when the equivalent process was studied in the Einstein frame [2].

We consider the scattering in the Einstein frame with the conformal factor $\Omega^2 = 1$. This is justified because at scattering energies $E \sim \frac{M_p}{\xi}$, h is given dimensionally by $h \sim \frac{M_p}{\xi}$. We do not

²Although we did not realise the significance at the time, our original S -inflation paper [1] did point out a cross term in h and s that could not be removed by field redefinitions.

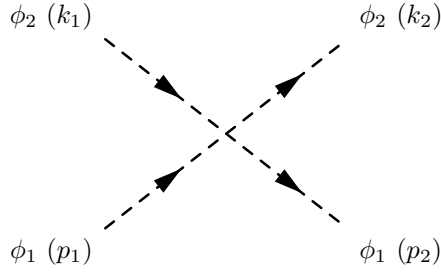


Figure 6.1: Feynman diagram for the scattering of two scalars: $\phi_1\phi_2 \rightarrow \phi_1\phi_2$.

use the unitary gauge, so the Einstein frame action is given by

$$S_E = \int d^4x \sqrt{-\tilde{g}} \left[-\frac{M_p^2}{2} \tilde{R} + \frac{1}{\Omega^2} \tilde{g}^{\mu\nu} (D_\mu H)^\dagger (D_\nu H) - \frac{V(H^\dagger H)}{\Omega^4} - \frac{1}{4} \tilde{F}_{\mu\nu} \tilde{F}^{\mu\nu} + \frac{3}{\Omega^2} \frac{\xi^2}{M_p^2} \tilde{g}^{\mu\nu} \partial_\mu (H^\dagger H) \partial_\nu (H^\dagger H) \right], \quad (6.3)$$

where $\tilde{F}^{\mu\nu} \tilde{F}_{\mu\nu}$ represents the total of all gauge kinetic terms. Considering the last term in the action, \mathcal{L}_{int} and writing H in terms of four real scalars (setting $\Omega = 1$) gives

$$\mathcal{L}_{int} = \frac{3\xi^2}{M_p^2} \sum_{i,j} \phi_i \phi_j \partial_\mu \phi_i \partial^\mu \phi_j. \quad (6.4)$$

We will consider the scattering $\phi_1\phi_2 \rightarrow \phi_1\phi_2$, as shown in Fig. (6.1), giving a tree-level amplitude

$$A = -i \times i \frac{6\xi^2}{M_p^2} (k_1 \cdot k_2 + k_1 \cdot p_2 + k_2 \cdot p_1 + p_1 \cdot p_2). \quad (6.5)$$

Working in the centre of mass frame, where

$$k_1 = (E, \vec{k}), \quad k_2 = (E, -\vec{k}), \quad p_1 = (E, \vec{p}) \quad \text{and} \quad p_2 = (E, -\vec{p}), \quad (6.6)$$

and assuming massless particles ($\vec{k}^2 = \vec{p}^2 = E^2$) we have

$$A = \frac{36\xi^2 E^2}{M_p^2} \left(1 + \frac{1}{3} \cos \theta \right). \quad (6.7)$$

The θ -independent part corresponds to the $l = 0$ partial wave, giving

$$a_0 = \frac{9\xi^2 E^2}{4\pi M_p^2}. \quad (6.8)$$

With the result in this form, we can apply the unitarity constraint Eq. (6.2) and get the constraint on E :

$$E \leq \frac{\sqrt{2\pi} M_p}{3 \xi}. \quad (6.9)$$

Thus it appears at energies above $\sim \frac{M_p}{\xi}$, the scattering $\phi_1\phi_2 \rightarrow \phi_1\phi_2$ violates unitarity at tree-level. It is possible to also calculate this in the Jordan frame, where the unitarity limit is from graviton exchange in $\phi_1\phi_2 \rightarrow \phi_1\phi_2$ scattering, and also in the unitary gauge (Einstein frame) with the process [96] $\chi Z_L \rightarrow \chi Z_L$ (where Z_L is the longitudinal component of the Z -boson and χ is rescaled Higgs).

6.1.1 The singlet scalar case

In a model where the inflaton is a real singlet scalar which is not coupled to any other scalar fields at all (so it cannot be a complex field and it cannot be coupled to the Higgs doublet), there is no unitarity violation when considering Jordan frame scattering by graviton exchange (or the equivalent Einstein frame process). This theory, in the Einstein frame, is a free theory as the redefinition of $s \rightarrow \chi$ using Eq. (3.8) gives a theory with no interactions in the Einstein frame [2]. As we have seen, the unitarity violating effects come from the interaction terms; therefore it is not surprising that the problem disappears for a single field. This occurs because the scattering can occur via three different channels — s , t and u . The sum of these Mandelstam variables is m^2 and the unitarity violation (previously seen in just the s channel) cancels out [98]. If additional scalars are added to the model, then some scattering processes such as $\phi_1\phi_2 \rightarrow \phi_1\phi_2$, can only occur through the s channel, in which case there is no cancellation.

This singlet model has a major problem — with no couplings to the Higgs, reheating will not be possible through the mechanisms discussed in Chapter 4. Unless reheating is possible through another mechanism, such as gravitational reheating [102, 103, 104] or a coupling to leptons, this completely rules out the model. The Fermi exclusion principle means that resonant production of leptons is not possible, although it might be possible for them to be produced as a result of annihilations of excitations of the inflaton.

6.1.2 Non-polynomial potential

A completely separate concern is that the non-polynomial potential

$$\tilde{U} = \frac{\frac{1}{4}\lambda\phi^4}{(1 + \xi\phi^2/M_p^2)^2} \quad (6.10)$$

is difficult to handle as a quantum field theory. However, we believe this is a quite different issue from tree-level unitarity violation associated with the non-minimal coupling to gravity in the Jordan frame. It is a separate issue because tree-level unitarity violation in $2 \rightarrow 2$ Higgs scattering via graviton-exchange is independent of the potential. Therefore the analogous interactions in the Einstein frame should also be independent of the potential.

It has been claimed (for example, see [98]) that the non-polynomial potential causes the theory to fail at $E \sim \Lambda$ due to terms in the expansion of the potential. It is claimed that “the breakdown of this theory would appear in many-particle hard scattering processes” [98]. Expanding the potential in terms of χ gives

$$U(\chi) = \frac{\lambda\chi^4}{4} - \frac{\lambda\xi^2\chi^6}{M_p^2} + \dots \quad (6.11)$$

for $\xi_h h^2 \ll M_p^2$. The second term appears to be suppressed by the scale Λ and would therefore be large at $\chi > \Lambda$. This is a false argument because we know *exactly* the form of the tree-level potential. It is non-polynomial, but known. The potential does not have any strange behaviour at $\chi \gtrsim \Lambda$. The apparent problem with the second term in Eq. (6.11) is due to the fact that it is not appropriate to make this expansion of the potential without including all terms in the expansion. We believe that $V(|H|)/\Omega^4$ will not lead to unitarity violation because in the limit $|H|^2 \gg M_p^2/2\xi$, there is an almost perfect cancellation of the $|H|^4$ factors in $V(|H|)$ and in Ω^4 , completely eliminating interactions³.

To illustrate how the potential term differs from other terms with respect to unitarity violation, we can consider perturbations about a large background Higgs field: $H = \langle H \rangle + \delta H = (0, v)^T + \delta H$ (note that v is the large Higgs field that we are expanding about, not 246.22 GeV). In this case the potential term in Eq. (6.3) tends towards that for massless non-interacting scalars, with unitarity-violating interactions suppressed by powers of $|H|$:

$$\begin{aligned} V(H^\dagger H) &= \frac{\lambda_h M_p^4}{4\xi_h^2} \left(1 - \frac{M_p^2}{\xi_h H^\dagger H} + \dots \right) \\ &= \frac{\lambda_h M_p^4}{4\xi_h^2} \left(1 - \frac{M_p^2}{\xi_h v^2} \left(1 - \frac{\langle H^\dagger \rangle \delta H + h.c.}{v^2} - \frac{|\delta H|^2}{v^2} + \dots \right) + \dots \right). \end{aligned}$$

Changing to canonically normalised fields $\delta\phi = \sqrt{\frac{M_p^2}{2\xi_h v^2}} \delta H$, the first non-renormalizable term is

$$\Delta V = \frac{\lambda_h M_p}{\sqrt{\xi_h v^2}} \left(\frac{\langle H^\dagger \rangle \delta\phi}{v} + h.c. \right)^5. \quad (6.12)$$

Dimensionally, this gives the amplitude for $\delta\phi\delta\phi \rightarrow \delta\phi\delta\phi\delta\phi$ to be $\frac{\lambda_h M_p \tilde{E}}{\sqrt{\xi_h v^2}}$, which violates unitarity at $\tilde{E} \sim \frac{\sqrt{\xi_h v^2}}{\lambda_h M_p}$. Taking v to be large, the energy of unitarity violation for the potential can be arbitrarily large. This contrasts with the second term in Eq. (6.3), for example, which leads to unitarity violation at $E \sim M_p/\sqrt{\xi}$, independent of $|H|$. Expanding the term as we did for the

³More generally, we expect that any non-polynomial potential interpolating between renormalizable potentials at small and large field strength will not lead to unitarity violation.

potential,

$$\begin{aligned}\Delta\mathcal{L} &= \frac{1}{\Omega^2}(\partial_\mu\delta H)^\dagger(\partial^\mu\delta H) \\ &= (\partial_\mu\delta\phi)^\dagger(\partial^\mu\delta\phi) + \frac{2\xi_h}{M_p^2}(\partial_\mu\delta\phi)^\dagger(\partial^\mu\delta\phi)\delta\phi^\dagger\delta\phi + \dots\end{aligned}\tag{6.13}$$

we see that the second term violates unitarity at $\tilde{E} \sim \frac{M_p}{\sqrt{\xi_h}}$ *independently* of the size of $|H|$. This indicates that the derivative term and the non-polynomial potential have quite different behaviour with respect to unitarity violation, with the derivative term generally more dangerous. Therefore in the following, we consider apparent unitarity violation from the non-polynomial potential not to be dangerous.

6.2 Breakdown of perturbation theory and strong coupling

The fact that the unitarity constraint is violated below the energy scale of inflation *at tree-level* in models with multiple scalars is not disputed. However, this may not be the end of the story. In this section we present two results from a paper by Han and Willenbrock [100]. The first result demonstrates that perturbation theory is not valid at the energy scale of unitarity violation. As the unitarity bound in Higgs inflation was calculated using perturbation theory, this is a compelling reason to consider this bound $E \lesssim \Lambda \sim \frac{M_p}{\xi}$ more carefully. The second result is rather remarkable and shows that in the large \mathcal{N} limit⁴ of a theory similar to ours, unitarity is violated at tree level but *not* when summed to all orders in a loop expansion. Thus we argue that to be certain whether or not the theory is unitarity violating, a full, non-perturbative calculation is necessary. We now review and discuss these results.

6.2.1 Breakdown of perturbation theory *before* unitarity violation

Following [100] but generalising⁵ to arbitrary J rather than $J = 2$, we show how unitarity violation based on perturbation theory is not consistent. Specifically, that the imaginary part of the one-loop partial wave is half of the tree-level partial wave, when unitarity is violated. To show this, we will assume that the tree-level partial wave $a_J^{(0)}$ is real⁶. We begin by assuming that perturbation theory is valid, meaning

$$\left|a_J^{(0)}\right|^2 \gg \left|a_J^{(1)}\right|^2 \gg \left|a_J^{(2)}\right|^2 \gg \dots\tag{6.14}$$

⁴ \mathcal{N} is the effective number of particles.

⁵We use J (total angular momentum) rather than l (orbital angular momentum) as this result is also valid for non-scalar particles.

⁶It is real in our case — see Eq. (6.8).

where $a_J^{(n)}$ is the n^{th} order in a loop expansion and $a_J^{(0)}$ is the tree-level amplitude. If unitarity is conserved, the inequality Eq. (6.2) is satisfied, so

$$\begin{aligned} \text{Re}[a_J] &\leq \frac{1}{2} \\ &\equiv \frac{1}{m} \end{aligned} \tag{6.15}$$

where $m \geq 2$. We are assuming that Eq. (6.14) is valid, so $\text{Im}[a_J] \simeq \text{Im}[a_J^{(1)}]$ and $|a_J|^2 \simeq |a_J^{(0)}|^2 = |\text{Re}(a_J^{(0)})|^2$. Thus, the other condition (Eq. (6.1)) becomes

$$\text{Im}[a_J^{(1)}] \geq |\text{Re}[a_J^{(0)}]|^2. \tag{6.16}$$

Upon substitution of Eq. (6.15) this becomes

$$\text{Im}[a_J^{(1)}] \geq \frac{1}{m} \text{Re}[a_J^{(0)}]. \tag{6.17}$$

At the moment of unitarity violation, both inequalities (Eq. (6.17) and Eq. (6.15)) are saturated and

$$\text{Im}[a_J^{(1)}] = \frac{1}{2} \text{Re}[a_J^{(0)}]. \tag{6.18}$$

At this point, the theory is clearly not perturbative as the one-loop (imaginary) amplitude is half of the tree-level amplitude.

6.2.2 Tree level unitarity violation can be misleading

We now consider the large \mathcal{N} limit of the theory, with $G_{\mathcal{N}}\mathcal{N}$ fixed. As $G_{\mathcal{N}} \propto \frac{1}{M_p^2}$, taking $\mathcal{N} \rightarrow \infty$ effectively means we are taking $M_p \rightarrow \infty$. The large \mathcal{N} limit was first applied to gravity theories by [105] and this particular calculation was taken from [100]. At tree level, unitarity violation occurs at the scale $\Lambda \sim \frac{M_p}{\xi}$. In the limit $\mathcal{N} \rightarrow \infty$, it is easy to sum over all orders of loop diagrams. This is because the dominant diagrams for large \mathcal{N} are iterations of the one-loop diagrams [100]. The result is

$$a_J = \frac{a_J^{(0)}}{1 - \frac{\text{Re}(a_J^{(1)})}{a_J^{(0)}} - ia_J^{(0)}}. \tag{6.19}$$

Calculating $\text{Im}[a_J]$ and $|a_J|^2$ we find that they are equal, exactly saturating the unitarity constraint Eq. (6.1). This particular theory is unitarity conserving when summed to all orders in perturbation theory, even though it appears to violate unitarity at tree-level.

The result cannot be directly applied to Higgs inflation (or S -inflation) as these theories have a finite number of scalars. However, combined with the fact that perturbation theory is not valid

at the point of apparently unitarity violation, this result does suggest that further investigation is required before unitarity violation is confirmed. The theory may simply be strongly coupled as $h \rightarrow \Lambda$, meaning that no new physics is necessary.

6.3 The future of non-minimally coupled models of inflation

Logically, the action of the original Higgs inflation model is either consistent or inconsistent as a quantum field theory. If it is an inconsistent theory then we expect unitarity to be violated at some energy, requiring a completion of the theory. However, if the theory is consistent, then we would expect any process which appears to violate unitarity to be modified as the energy approaches that of unitarity violation. Considering the case where unitarity *is* violated at $E \sim \Lambda$, we must add new terms to the action to restore unitarity. We develop this idea in Section 6.4. The model of S -inflation has an unconstrained self coupling, λ_s . If this is very small, the unitarity bound may be evaded, even if the model contains additional scalars. This is because the value of ξ_s is determined by the WMAP normalization (see Eq. (3.26)) which mean that at tree level, $\xi_s \propto \sqrt{\lambda_s}$. The case of small λ_s is discussed below. (It has also been shown that in a pure singlet scalar case, there is no unitarity violation [98].)

A non-perturbative analysis is necessary in order to establish unitarity conservation in Higgs inflation, so it may be difficult to either prove or disprove. In this case the best strategy would be to consider both possibilities and use collider experiments and precision CMB observations to establish whether Higgs inflation is consistent with observations. This strategy is feasible because of the uniquely predictive nature of Higgs inflation. The inflation observables, in particular the spectral index, are entirely determined by Standard Model couplings and ξ_s . Therefore precision measurement of the spectral index and the Higgs mass m_h can, in principle, allow the nature of Higgs inflation to be determined experimentally. We also discuss these possibilities below.

6.3.1 Avoiding the unitarity bound with small λ_s

The coupling λ_h is constrained to be $\mathcal{O}(0.1)$ for Higgs inflation, but the corresponding coupling for S -inflation, λ_s , is unconstrained. As the WMAP normalization fixes $\frac{\lambda}{\xi^2}$, a small λ_s will give a small ξ_s . This may or may not avoid the unitarity bound, depending on whether we require $\phi_{\bar{N}} \simeq \sqrt{\frac{\bar{N}}{\xi}} M_p < \Lambda$, $U^{1/4} \simeq \frac{\lambda^{1/4}}{\sqrt{2\xi}} M_p < \Lambda$ or $H_* \simeq \sqrt{\frac{\lambda_s}{3}} \frac{1}{2\xi_s} < \Lambda$ (H_* is the Hubble parameter during inflation).

The simplest assumption is that the theory is completely modified by new terms in the Lagrangian which become important once $E > \Lambda$. Since the unitarity problem is due to scattering of the scalar particles, in general we would expect the scalar sector, and in particular the scalar

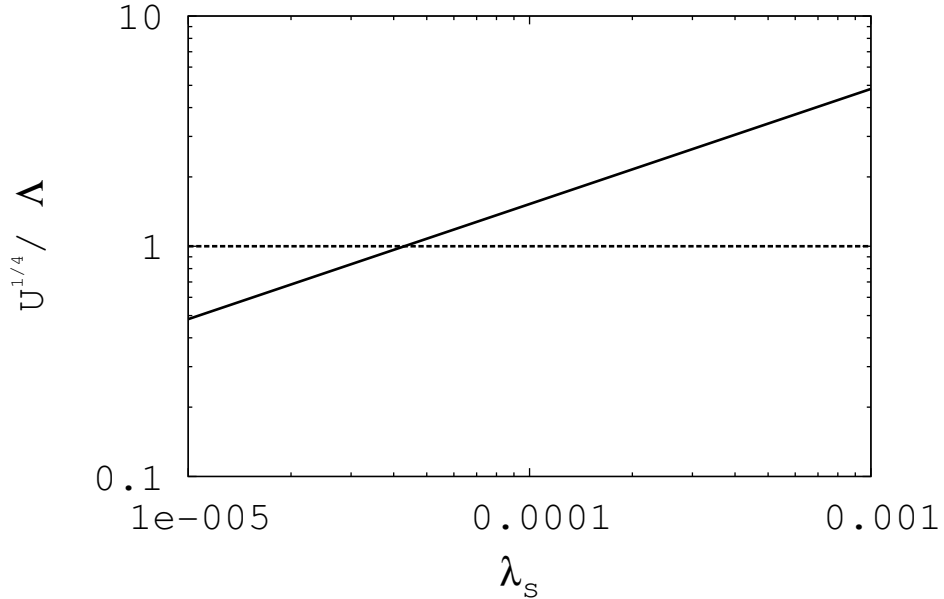


Figure 6.2: Showing the ratio $\frac{U^{1/4}}{\Lambda}$ (solid black line). The ratio becomes less than 1 for $\lambda_s < 4.3 \times 10^{-5}$.

potential, to be modified by terms involving inverse powers of Λ , which completely ruin the inflation potential. Therefore, the conservative conclusion must be that $\phi < \Lambda$ is necessary to avoid the unitarity bound. In this case, small λ_s offers no advantage and the S -inflation model will suffer from the same problems as Higgs inflation.

If instead we were to assume that the new physics involves only terms which do not contribute to the scalar potential (i.e. involving derivatives of the scalar fields only), then the unitarity bound is satisfied if the energy scale during inflation is less than Λ . The energy scale during inflation could be $U^{1/4}$ (as considered for S -inflation by [75]) or H_* (as considered by [2, 96, 106]).

For the case $U^{1/4} < \Lambda$, a back-of-the-envelope calculation shows that we would require $\xi_s \lesssim 3 \times 10^3$ and $\lambda_s \lesssim 5 \times 10^{-5}$ to satisfy the bound. We show in Fig. (6.2) λ_s versus $\frac{U^{1/4}}{\Lambda} \approx \frac{\lambda_s^{1/4} \sqrt{\xi_s}}{\sqrt{2}}$, where λ_s and ξ_s have been obtained using the full radiative corrections and WMAP normalization of the previous chapters with $\lambda_{hs} = 0$. We find $U^{1/4} < \Lambda$ for $\lambda_s < 4.3 \times 10^{-5}$. Reheating (via stochastic resonance) would then require $\lambda_{hs} < 1.7 \times 10^{-4}$. Although this is near the lower bound of λ_{hs} required to produce thermal relic dark matter, the scenario is not ruled out. A different mechanism of reheating, perhaps via couplings to fermions, could loosen the bound on λ_{hs} .

The loosest constraint is to consider the Hubble parameter during inflation, as $\phi_{\tilde{N}} \gg U^{1/4} \gg H_*$. The requirement that the model is unitarity conserving in this case is simply $\lambda_s \ll 1$. This is easily satisfied by the S -inflation model and couplings can easily be within the reheating bounds.

6.3.2 Strong coupling as an alternative to unitarity violation

Higher-order corrections to the scattering amplitude become important in non-minimally coupled models as the energy approaches that at which tree-level unitarity is violated. As noted in [2], this leads to the possibility that strong-coupling itself is the new physics required to maintain unitarity. The possibility that strong coupling could ensure unitarity-conservation was noted earlier in [34]. The essential point is that if strong coupling can deal with the apparent unitarity violation in particle scattering processes, then the action of the theory is complete as is, requiring no new terms. The effective potential and the analysis of inflation can then be carried out by calculating with this action in the conventional way [34, 35, 36, 37]. This would imply that calculations of scattering processes would be near-impossible at large energies. However, this would *not* affect the calculation of the effective potential necessary to investigate slow roll inflation, which remains completely unchanged.

The strongly coupled viewpoint is supported by the observations of [100] which we discussed in Section 6.2. For the case of s-channel scattering mediated by graviton exchange, the imaginary part of the 1-loop contribution to the amplitude is half of the tree-level contribution at the energy of unitarity-violation, so perturbation theory may not be appropriate for scattering calculations at energies $E \sim \Lambda$. Also, in the large- N limit (where N is roughly the number of particles contributing to the loop corrections), the all-order graviton-mediated scattering cross-section (excluding graviton loops) is unitary at all energies, even though the tree-level cross-section violates unitarity.

There are suggestions in the literature that general relativity could be a strongly coupled, non perturbative theory. For example, loop quantum gravity (see [107] for a review) is a non-perturbative theory. Whether non-minimally coupled models can be derived from loop quantum gravity is an interesting question deserving further investigation.

6.4 A Unitarity conserving model of Higgs inflation

If unitarity is not conserved in the original Higgs inflation model, then a modified, unitarity-conserving model can be considered [3]. We aim to construct a new model of Higgs inflation, keeping the core idea that it is the non-minimal coupling to gravity that provides a potential flat enough for inflation. The concern expressed in [95, 96] is that the terms added to the action to conserve unitarity must include Higgs potential terms suppressed by powers of Λ , spoiling the flatness of the potential and ruling out slow-roll inflation. However, this is a false assumption, as we will show. Our goal here is to derive the minimal modification of Higgs inflation necessary to restore unitarity and to show that it can, in principle, support successful inflation.

As discussed earlier, the Einstein frame provides a particularly clear way to understand unitarity violation in graviton-mediated Higgs scattering due to the non-minimal coupling. On transforming to the Einstein frame, where the non-minimal couplings are eliminated, unitarity violation manifests itself via non-renormalizable interactions. Therefore the minimal unitarity-conserving completion of the Higgs inflation Lagrangian in the Jordan frame will correspond to the Einstein frame Lagrangian which removes all the dangerous non-renormalizable terms.

6.4.1 The unitarity-conserving action

It is clear that the only way to eliminate unitarity violation in the Einstein frame is to replace the non-minimal Higgs kinetic term with a canonical kinetic term. We must therefore add terms to the Jordan frame action Eq. (3.1) to achieve this. We consider all terms which are scaled by inverse powers of Ω in the Einstein frame to lead to unitarity violation, with the exception of $V(|H|)/\Omega^4$ (see Section 6.1.2). The final action in the Einstein frame therefore has the form

$$S_E = \int d^4x \sqrt{-\tilde{g}} \left(-\frac{M_p^2}{2} \tilde{R} + \tilde{g}^{\mu\nu} (D_\mu H)^\dagger (D_\nu H) - \frac{1}{4} \tilde{F}_{\mu\nu} \tilde{F}^{\mu\nu} - \frac{V(|H|)}{\Omega^4} \right). \quad (6.20)$$

On transforming back to the Jordan frame, additional terms in S_J which are required to conserve unitarity up to the Planck scale are generated. The resulting unitarity-conserving action in the Jordan frame is given by

$$S_J = \int d^4x \sqrt{-g} \left(-\frac{M_p^2 R}{2} - \xi H^\dagger H R + g^{\mu\nu} D_\mu H^\dagger D_\nu H - \frac{1}{4} F_{\mu\nu} F^{\mu\nu} - V(|H|) - \frac{3\xi^2}{\Omega^2 M_p^2} g^{\mu\nu} \partial_\mu (H^\dagger H) \partial_\nu (H^\dagger H) + \frac{2\xi H^\dagger H}{M_p^2} g^{\mu\nu} D_\mu H^\dagger D_\nu H \right). \quad (6.21)$$

We believe that Eq. (6.21) is the minimal unitarity-conserving action for the Standard Model Higgs doublet with a large non-minimal coupling to gravity. Since the fundamental assumption of Higgs inflation is that inflation is due entirely to the non-minimal coupling of $H^\dagger H$ to gravity, Eq. (6.21) will provide a manifestly unitarity-conserving basis for Higgs inflation.

The non-minimal coupling to R plus the additional terms in Eq. (6.21) may be interpreted as the complete set of terms which must be brought down from the full Planck-scale gravity theory to the scale Λ in order to maintain the quantum consistency of the theory. A non-minimal coupling of the Higgs to gravity is generally expected to exist, but it is usually assumed that $\xi \sim 1$, in which case the associated unitarity violation occurs at $E \sim M_p$. The effect of increasing ξ is to effectively pull down the non-minimal coupling from the Planck-scale gravity theory to the lower mass scale Λ . Unitarity violation can then be interpreted as a sign that other terms from the full gravity theory must accompany the non-minimal coupling in order to maintain the

consistency of the theory.

6.4.2 Cosmology of the unitarity conserving model

Although Eq. (6.21) provides a basis for a unitarity-conserving Higgs inflation model, it is not the same Higgs inflation model as originally proposed in [32]. To compute the predictions of the new model, we analyse it in the Einstein frame, where H has canonical kinetic terms and the model may be treated as a conventional slow-roll inflation model with potential $U(|H|) \equiv V(|H|)/\Omega^4$, just as in Chapter 3. Introducing the physical Higgs field as the inflaton, $H \rightarrow h/\sqrt{2}$, we obtain

$$U(h) = \frac{\lambda h^4}{4 \left(1 + \frac{\xi h^2}{M_p^2}\right)^2}. \quad (6.22)$$

As in the original model, for $h \gg M_p/\sqrt{\xi}$, the potential is flat and slow-roll inflation is possible. With $\tilde{N} = 58$, where $\tilde{N} \approx \frac{\xi h^4}{16M_p^4}$ is the number of e-folding of inflation (from when cosmological scales exit the horizon) in the Einstein frame, the classical value of the spectral index is given by $n = 1 + 2\tilde{\eta} - 6\tilde{\epsilon}$, where

$$\tilde{\epsilon} \equiv \frac{M_p^2}{2} \left(\frac{1}{U} \frac{dU}{dh}\right)^2 \simeq \frac{8M_p^6}{\xi^2 h^6} - \frac{16M_p^8}{\xi^3 h^8} \quad (6.23)$$

and

$$\tilde{\eta} \equiv M_p^2 \left(\frac{d^2 U}{dh^2}\right) \simeq -\frac{12M_p^4}{\xi h^4} + \frac{36M_p^6}{\xi^2 h^6}. \quad (6.24)$$

Therefore,

$$n \approx 1 - \frac{3}{2\tilde{N}} + \frac{3}{8\tilde{N}^{3/2}\sqrt{\xi}} \approx 0.974. \quad (6.25)$$

The tensor to scalar ratio r is given by

$$r \equiv 16\tilde{\epsilon} \simeq \frac{2}{\sqrt{\xi}\tilde{N}^{3/2}} \sim 6 \times 10^{-6}. \quad (6.26)$$

The running of the spectral index α is negligibly small. The curvature perturbation is given by

$$P_\xi = \frac{\lambda \tilde{N}^3}{12\pi^2 \xi^{3/2}}, \quad (6.27)$$

therefore to have a correctly normalised spectrum of density perturbations, $P_\xi^{1/2} = 4.8 \times 10^{-5}$, we require

$$\xi \simeq (3.8 - 6.5) \times 10^5 \quad (6.28)$$

for m_h in the range 114-170 GeV. The predictions are different from the original Higgs inflation model because the slow roll parameters are defined with respect to different canonically normalised fields — χ in the original model and h in the unitarity-conserving model. The predictions may be compared with the original Higgs inflation model, $n \simeq 1 - \frac{2}{\tilde{N}} - \frac{3}{2\tilde{N}^2} = 0.965$, $r \simeq \frac{12}{\tilde{N}^2} = 3.6 \times 10^{-3}$ and $\frac{\lambda}{\xi^2} \simeq \frac{3(0.027)^4}{\tilde{N}^2}$ giving $\xi \simeq 10^4$. These estimates are also based on $\tilde{N} = 58$. As the model contains only Standard Model parameters, it is in principle possible to determine the reheating temperature and hence \tilde{N} precisely. Therefore the model has no free parameters.

6.4.3 Radiative corrections favour S -type inflation model

So far we have considered the model only at tree-level, without quantum corrections to the inflaton potential. The structure of Eq. (6.20) is equivalent to the Standard Model gauge and Higgs fields plus a potential $V(|H|)/\Omega^4$. This suggests that the 1-loop Coleman-Weinberg correction due to gauge boson loops in the Einstein frame will have the form $\sim M_W^4 \log M_W^2 \propto |H|^4$, which would spoil the flatness of the potential. In this case a supersymmetric (SUSY) version of the model will be necessary in order to suppress the quantum corrections to the inflaton potential.

However, if the inflaton was not the Higgs, but instead a singlet scalar coupled to the Standard Model only via the potential (such as our S -inflation model), then its couplings would be suppressed by Ω^{-4} in the Einstein frame and radiative corrections should not spoil the flatness of the inflationary potential. Thus, if unitarity is found to be violated in the original Higgs inflation and S -inflation models, then a unitarity-conserving version of S -inflation, along the lines of Eq. (6.20) would be favoured, if we require a minimal model of inflation.

Discussion

We have proposed a new Higgs inflation model based on a unitarity-conserving extension of the original Higgs inflation action. We believe that this is the minimal form of Higgs inflation model which manifestly conserves unitarity in the presence of a non-minimal coupling of the Higgs to gravity. This is based on some assumptions, which we discuss below. As such, it may provide the correct formulation of the model should strong coupling effects fail to eliminate unitarity violation in the original Higgs inflation model.

The unitarity-conserving model is based on the assumptions:

- (i) the non-polynomial potential ($\propto \frac{1}{\Omega^4}$) does not introduce unitarity violation
- (ii) the kinetic terms scaled by $\frac{1}{\Omega^2}$ must be removed because they *do* cause unitarity violation.

These are the conservative assumptions necessary to allow Higgs inflation without unitarity violation — the non-polynomial potential is an essential component of the model. The assumptions seem reasonable. At large values of h the potential tends to a flat potential, whereas terms with derivatives do not have the same cancellation at large h . This is why we expect them to introduce unitarity violation. While these arguments are plausible, there is (as yet) no rigorous proof that the model is both unitarity-conserving and minimal. However, the predictions of the model *can* be tested by observation.

Perhaps the most interesting conclusion is that while unitarity-conserving Higgs inflation is possible, the predictions of the new unitarity-conserving model are quite different from those of the original Higgs inflation model. In particular, the classical spectral index of the new model is $n = 0.974$, which is within the 7-year WMAP $1\text{-}\sigma$ limits on n ($n = 0.963 \pm 0.012$ [7]) but significantly different from the original Higgs inflation model prediction of $n = 0.965$. Therefore it should be possible to observationally distinguish between unitarity-conserving Higgs inflation and the original Higgs inflation model.

A feature that the unitarity-conserving model shares with the original Higgs inflation model is that since all the model parameters are Standard Model parameters, they can be fixed experimentally (with the exception of ξ , which is fixed by the density perturbations). In particular, it will be possible to precisely compute quantum corrections to the spectral index as a function of Higgs mass. This should allow for precision tests of the model once m_h is determined by the LHC and n by PLANCK. A caveat is that such quantum corrections are likely to be large in the case of a non-SUSY Higgs model, in which case a SUSY version following the same strategy will be necessary in order to maintain the flatness of the inflaton potential. A very minimal non-SUSY model may still be possible if the inflaton was instead a singlet scalar with a potential coupling to the Standard Model. We expect that the tree-level predictions of any unitarity-conserving model, being necessarily based on minimal kinetic terms and V/Ω^4 in the Einstein frame, will remain unchanged, giving $n \simeq 1 - \frac{3}{2N}$.

Chapter 7

Conclusions

In this thesis we have presented the S -inflation model and discussed its observational predictions, mechanism for reheating, relationship to Higgs inflation and issues of naturalness. The model consists of the Standard Model plus a stable gauge singlet scalar, S , which is non-minimally coupled to gravity. We have shown that the S scalar can simultaneously serve as the inflaton and as a thermal relic dark matter particle.

The consistency of the model with respect to (i) stability of the electroweak vacuum, (ii) perturbativity of the scalar potential as a function of s and h up to the Planck scale and (iii) the observed spectral index¹, constrains the (λ_{hs}, m_h) parameter space. The coupling λ_{hs} determines the strength of the interaction between S dark matter and ordinary matter. We find $|\lambda_{hs}(m_t)| \lesssim 0.15$ for the WMAP5 1- σ bound ($n < 0.973$), which can increase up to $|\lambda_{hs}(m_t)| \lesssim 0.55$ for small S self-coupling and larger n . The range of Higgs masses is $145 \text{ GeV} \lesssim m_h \lesssim 170 \text{ GeV}$ for $n < 0.973$ and small $\lambda_s(m_t)$, shifting to $130 \text{ GeV} \lesssim m_h \lesssim 170 \text{ GeV}$ for $n \geq 0.980$.

Demanding that the S annihilation rate through $\lambda_{hs}(m_t)$ produces the correct thermal relic S dark matter density translates each $\lambda_{hs}(m_t)$ into a discrete set of possible values of m_s . This determines an allowed range of m_s , which is $50 \text{ GeV} \lesssim m_s \lesssim 750 \text{ GeV}$ for $\lambda_s = 0.025$, with the upper limit increasing to 1 TeV for $\lambda_s(m_t) = 0.2$. For complex S the range of m_s is narrower, $50 \text{ GeV} \lesssim m_s \lesssim 500 \text{ GeV}$ for $\lambda_s(m_t) = 0.025$. The parameter space does not exclude the possibility of producing S pairs at the LHC. As the accuracy of the observed n improves (and if m_h can be measured), the parameter space will become much more tightly constrained, which should allow the consistency of the model to be tested.

A barrier to a precisely predictive model is the dependence on the S self-coupling $\lambda_s(m_t)$, which is not directly observable. In principle, there are five observable quantities: n , m_h , m_s ,

¹The tensor-to-scalar ratio r and the running of the spectral index α are both negligibly small compared with the observational limits.

$\lambda_{hs}(m_t)$ and $\mathcal{P}_\zeta(k_0)$ and five input parameters: m_h , m_s , $\lambda_{hs}(m_t)$, $\xi_s(m_t)$ and $\lambda_s(m_t)$. Therefore n cannot be predicted exactly as there will always be a dependence on $\lambda_s(m_t)$, even if the other parameters of the model are fixed by experiment. However, we find that there are constraints on λ_s from reheating, giving either $\lambda_s > 0.019$ or $\lambda_s > 0.25\lambda_{hs}$.

Nevertheless, the S -inflation model makes a clear prediction, that $n \geq n_{cl}$ for $m_h \gtrsim 130$ GeV, which can distinguish it from Higgs inflation. The spectral index n can be further constrained by vacuum stability and perturbativity constraints. In addition, in the limit of small $\lambda_s(m_t)$, the model could become effectively independent of λ_s . In this case we may be able to predict n if m_h , m_s and $\lambda_{hs}(m_t)$ are fixed by the LHC and by direct dark matter experiments. If we are fortunate enough that S -inflation occurs in this limit, then the model can in principle be completely predictive and testable.

The predictions of S -inflation were made assuming that the relationship $\xi_s \gg \xi_h$ is satisfied. For the values of λ_s that we considered in Chapter 3, this is a reasonable assumption (if it holds at the weak scale, it also holds at the scale of inflation, provided that the running of ξ_h is not too large). However, if λ_s was very small (as discussed in Chapter 6 in the context of avoiding the unitarity bound), then $\xi_s \gg \xi_h$ may not be satisfied, as λ_{hs} could cause the running of ξ_h to be substantial. This would mean that the minimum for large field values is not along the S -direction. However, a study of inflation along a general direction would be difficult, as the fields could not be simultaneously canonically normalised. It should be noted that in order for the model to produce the observed spectrum of curvature perturbations, ξ_s must take a large value ($\sim 10^4$), which may be unnatural. Unlike Higgs inflation, the coupling ξ_s can instead be made $\mathcal{O}(1)$, at the expense of having an unnaturally small value of λ_s .

We have shown that S -inflation makes clear observational predictions, which are generally distinct from those of Higgs inflation. Given that the reheating temperature in both models is well determined, the classical spectral index n_{cl} of both models will be similar. The key difference between the models is that for $m_h \gtrsim 130$ GeV, radiative corrections cause n to *increase* for S -inflation and *decrease* for Higgs inflation. Thus, in this case, a measurement of n close to but above n_{cl} strongly favours S -inflation while a measurement close to but below n_{cl} favours Higgs inflation. Note that the discovery of a gauge singlet scalar with coupling to the Higgs boson rules out pure Higgs inflation but does not provide information about the direction of inflation.

The S -inflation model provides a model for inflation and dark matter which is based purely on weak scale particles and interactions. In order to have a complete model of cosmology, we also need to address the issues of reheating, neutrino masses and the origin of the baryon asymmetry. In the case of S -inflation, a concern is that since the particles are stable, the energy in the inflaton

would not transfer to radiation. In fact, reheating occurs successfully. The primary reheating mechanism is a stochastic resonance to Higgs bosons, which subsequently annihilate to produce relativistic particles. Any remaining energy density in the inflaton field is easily thermalised by scattering with the relativistic background. S dark matter particles are then produced thermally. Reasonable assumptions give the reheating temperature to be $3 \times 10^{13} \text{ GeV} < T_R < 8 \times 10^{14} \text{ GeV}$, corresponding to $59 < \tilde{N} < 60$ (or $58 < \tilde{N} < 61$ once theoretical errors of ± 1 are included). For reheating to complete before the inflaton starts to oscillate in a quartic potential, we require either $\lambda_s > 0.02$ or $\lambda_s > 0.25\lambda_{hs}$.

Baryogenesis could occur via electroweak baryogenesis, which may be possible in scalar extensions of the SM. Additional scalars interacting with the Higgs can produce a sufficiently strong 1st order electroweak phase transition. This usually requires that the gauge singlet scalar gains a vacuum expectation value (vev) after the transition [108], therefore a more complicated model with two or more additional scalars would be required². Additional CP violation will also be necessary, as the Standard Model does not provide enough to generate the observed asymmetry. Neutrino masses and mixings also remain to be explained. As suggested by [75], an $SU(2)$ triplet scalar field could be introduced, which would introduce neutrino masses in a type-II see-saw mechanism [109]. Alternatively, baryogenesis could occur via the oscillating leptogenesis mechanism [28] or low-scale resonant leptogenesis [110] once the SM is extended by sterile neutrinos in order to account for neutrino masses.

S -inflation, as with all non-minimally coupled models involving more than one scalar, may violate unitarity at an energy $E > \Lambda \sim \frac{M_p}{\xi_s}$. The unitarity violation comes from scattering of non-identical scalars $\phi_1\phi_2 \rightarrow \phi_1\phi_2$ via graviton exchange (for the case $\phi_1\phi_1 \rightarrow \phi_1\phi_1$, there is a cancellation and no unitarity violation occurs). If unitarity violation occurs, new terms would need to be added to the action, which *may* spoil the naturalness and predictiveness of this type of theory. One possibility is that these new terms enter only through derivative terms, so do not affect the scalar potential. In this case, a small self coupling λ_s could avoid the unitarity bound.

Working under the assumption that unitarity *is* violated, we suggested a new unitarity conserving model of Higgs inflation. The central assumptions of the model are: (i) inflation is caused by the non-minimal coupling of the Higgs to gravity and (ii) the non-polynomial potential is *not* a source of unitarity violation. In this model, the kinetic terms are canonically normalised without being rescaled. This is the origin of the difference between the predictions of the new model, $n \approx 1 - \frac{3}{2\tilde{N}} = 0.974$, and the predictions of the original model, $n \simeq 1 - \frac{2}{\tilde{N}} - \frac{3}{2\tilde{N}^2} = 0.965$ (both tree level, with $\tilde{N} = 58$). Radiative corrections in the Higgs inflation version of this model would

²We note that it may be possible to evade this if the scalar has an expectation value prior to and during the electroweak phase transition but its vev vanishes in the vacuum after the transition [42].

spoil the flatness of the potential, because the one-loop Coleman Weinberg potential due to gauge boson loops in the Einstein frame is not suppressed by Ω^{-4} , as it is in the original Higgs inflation model. Therefore, a non-SUSY version of the model strongly favours an S -inflation version, as in this case the scalar couplings originate from the potential and *are* suppressed by Ω^{-4} . An alternative would be to consider a SUSY version of the model.

However, the occurrence of unitarity violation has not been proven. The apparent unitarity violation could instead be an artefact of using perturbation theory in a non-perturbative regime. If so, then no modification of the theory is required and the inflaton potential is unaltered. In general, a full, non-perturbative analysis would be necessary to determine whether or not the model violates unitarity. Given the clear experimental predictions of the model, we propose it is sensible to let experiment and observation lead the way in favouring or ruling out the model.

There are a number of issues arising from this thesis which would merit further work. These include scattering from the non-polynomial potential — an unsolved problem in field theory and not specific to this work. Further work could be done towards proving whether or not non-minimally coupled models violate unitarity, and if so, at which scale. (Although as this seems to require non-perturbative calculations, it may be an unrealistic aim.) If SUSY is discovered at the LHC, SUSY versions of the model will become particularly interesting to develop. Some attempts at this have already been made for the case of Higgs inflation [106, 111, 112]. The radiative corrections for the unitarity conserving model in Chapter 6 remain to be calculated — they will be large for a Higgs-inflation model, but are expected to be small for an S -inflation version. Also, the case of small λ_s (in the original S -inflation model) should be investigated further. It is particularly interesting because the self-coupling will be determined by λ_{hs} , through loop corrections. Thus all parameters could, in principle, be determined by experiment. (It is likely that reheating would need to be reconsidered in this case.)

The most important piece of future work will be to compare the findings of Planck, LHC and direct detection experiments to the predictions in this thesis. In contrast to many inflation models, S -inflation is notable for the close relationship it implies between the observables of inflation (in particular, the spectral index), particle physics (in particular, the Higgs mass and Higgs decay width) and the direct detection of dark matter. It can therefore be directly tested by the experimental and observational advances which are anticipated in the near future as the LHC, Planck satellite and future direct dark matter detection experiments come to fruition.

Appendix: Deriving the RG equations for scalar couplings

In this appendix, we explain the derivation of the scalar RG equations. We are interested in the modification to the Standard Model RG equations due to the additional scalar S . In a set of papers by Machacek and Vaughn [70, 71, 72], hereafter referred to as MV, the RG equations for a general theory with scalars are given to two-loops in the $\overline{\text{MS}}$ scheme. The anomalous dimensions and β -functions are expressed in terms of real (reducible) representations of the scalar fields and Majorana spinors. Thus we must formulate our theory in these terms to apply the general results of MV.

Representation of scalars

We express the Higgs doublet and gauge singlet scalars as a set of six real scalar fields, ϕ_i ($i = 1\dots 6$), where

$$H = \frac{1}{\sqrt{2}} \begin{pmatrix} \phi_1 + i\phi_2 \\ \phi_3 + i\phi_4 \end{pmatrix} \quad \text{and} \quad S = \frac{1}{\sqrt{2}} (\phi_5 + i\phi_6) . \quad (\text{A-1})$$

For the case of real S , $\phi_6 = 0$. The potential is given by

$$V = \frac{1}{4!} \lambda_{abcd} \phi_a \phi_b \phi_c \phi_d . \quad (\text{A-2})$$

If n, m represent the Higgs scalars and p, q the S scalars, then $\lambda_{nnnn} = 6\lambda_h$, $\lambda_{nnmm} = 2\lambda_h$, $\lambda_{nnpp} = \lambda_{hs}$, $\lambda_{pppp} = 3\lambda_s$ and $\lambda_{ppqq} = 2\lambda_s$. Additionally, a factor of c_s accompanies ϕ_5 and c_h accompanies ϕ_3 .

Writing the scalars as a real representation in the form $(\phi_1, \phi_2, \phi_3, \phi_4, \phi_5, \phi_6)^T$, the $SU(2)_L$

generators (θ_{ab}^A in the notation of MV) are

$$\theta^1 = \frac{1}{2} \begin{pmatrix} 0 & 0 & 0 & i & 0 & 0 \\ 0 & 0 & -i & 0 & 0 & 0 \\ 0 & i & 0 & 0 & 0 & 0 \\ -i & 0 & 0 & 0 & 0 & 0 \\ 0 & 0 & 0 & 0 & 0 & 0 \\ 0 & 0 & 0 & 0 & 0 & 0 \end{pmatrix}, \quad \theta^2 = \frac{1}{2} \begin{pmatrix} 0 & 0 & -i & 0 & 0 & 0 \\ 0 & 0 & 0 & -i & 0 & 0 \\ i & 0 & 0 & 0 & 0 & 0 \\ 0 & i & 0 & 0 & 0 & 0 \\ 0 & 0 & 0 & 0 & 0 & 0 \\ 0 & 0 & 0 & 0 & 0 & 0 \end{pmatrix}$$

and

$$\theta^3 = \frac{1}{2} \begin{pmatrix} 0 & i & 0 & 0 & 0 & 0 \\ -i & 0 & 0 & 0 & 0 & 0 \\ 0 & 0 & 0 & -i & 0 & 0 \\ 0 & 0 & i & 0 & 0 & 0 \\ 0 & 0 & 0 & 0 & 0 & 0 \\ 0 & 0 & 0 & 0 & 0 & 0 \end{pmatrix}. \quad (\text{A-3})$$

The $U(1)_Y$ generator is

$$\theta^Y = i \begin{pmatrix} 0 & Y & 0 & 0 & 0 & 0 \\ -Y & 0 & 0 & 0 & 0 & 0 \\ 0 & 0 & 0 & Y & 0 & 0 \\ 0 & 0 & -Y & 0 & 0 & 0 \\ 0 & 0 & 0 & 0 & 0 & 0 \\ 0 & 0 & 0 & 0 & 0 & 0 \end{pmatrix} \quad (\text{A-4})$$

where $Y = 1/2$ is the hypercharge of the complex fields in the Higgs doublet.

Representation of the top quark

The only Yukawa coupling we consider is the top quark Yukawa coupling. In 4-component spinor notation this is (in the notation of MV)

$$\bar{q} \underline{H} \phi^{\dagger c} q + h.c. , \quad (\text{A-5})$$

where \underline{H} is the Yukawa coupling matrix, $q = (u_L, d_L)^T$ is the $SU(2)_L$ quark doublet and ϕ is the Higgs doublet. In our case

$$\bar{q} \underline{H} \phi^{\dagger c} q \equiv \bar{t}_R y_t t_L \phi^0 - \bar{t}_R y_t b_L \phi^+ . \quad (\text{A-6})$$

(In this we have suppressed colour indices.) We define a reducible representation ψ_i (in the notation of MV) by $(\psi_1, \psi_2, \psi_3) = (t_R^c, t_L, b_L)$, where t_L , b_L and t_R^c are the two-component spinors which form the Dirac spinors in the chiral representation ($t \equiv (t_L, t_R)^T$ etc), with $t_R^c = -i\sigma_2 t_R^*$. The Yukawa coupling can then be written as

$$Y_{ij}^a \psi_i \xi \psi_j \phi_a + h.c. \quad (a = 1, 2, 3, 4) \quad (\text{A-7})$$

where

$$Y^1 = \frac{1}{\sqrt{2}} \begin{pmatrix} 0 & y_t & 0 \\ y_t & 0 & 0 \\ 0 & 0 & 0 \end{pmatrix}, \quad Y^2 = \frac{i}{\sqrt{2}} \begin{pmatrix} 0 & y_t & 0 \\ y_t & 0 & 0 \\ 0 & 0 & 0 \end{pmatrix}, \quad Y^3 = \frac{1}{\sqrt{2}} \begin{pmatrix} 0 & 0 & -y_t \\ 0 & 0 & 0 \\ -y_t & 0 & 0 \end{pmatrix},$$

and

$$Y^4 = \frac{i}{\sqrt{2}} \begin{pmatrix} 0 & 0 & -y_t \\ 0 & 0 & 0 \\ -y_t & 0 & 0 \end{pmatrix}. \quad (\text{A-8})$$

The corresponding $SU(2)_L$ generators t^A acting on ψ are

$$t^1 = \frac{1}{2} \begin{pmatrix} 0 & 0 & 0 \\ 0 & 0 & 1 \\ 0 & 1 & 0 \end{pmatrix}, \quad t^2 = \frac{1}{2} \begin{pmatrix} 0 & 0 & 0 \\ 0 & 0 & -i \\ 0 & i & 0 \end{pmatrix} \quad \text{and} \quad t^3 = \frac{1}{2} \begin{pmatrix} 0 & 0 & 0 \\ 0 & 1 & 0 \\ 0 & 0 & -1 \end{pmatrix}. \quad (\text{A-9})$$

The $U(1)_Y$ generator is

$$t^Y = \begin{pmatrix} -\frac{2}{3} & 0 & 0 \\ 0 & \frac{1}{6} & 0 \\ 0 & 0 & \frac{1}{6} \end{pmatrix}. \quad (\text{A-10})$$

(Suppressed colour indices should be summed over when taking traces in the formulae of MV.)

Finally, $\kappa = 1/2$ should be used since ψ_i are two-component spinors.

Calculating RG equations

With these definitions of θ^A , Y^a and t^A , the formulae of MV can be used to compute the RG equations to two-loop order as a function of the t-quark Yukawa coupling, gauge couplings and the scalar couplings. The suppression factors are inserted by hand, following the procedure in Section 3.2.2.

We demonstrate the calculation of β_{λ_s} . From [72],

$$16\pi^2\beta_{\lambda_{abcd}} = \frac{1}{8} \sum_{perms} \lambda_{abef} \lambda_{efcd} \quad (\text{A-11})$$

(all other terms are zero in this case). For the case of λ_s , this simplifies to

$$\begin{aligned} 16\pi^2\beta_{\lambda_s} &= \frac{1}{6} \frac{24}{8} \sum_e \lambda_{55ee} \lambda_{ee55} \\ &= \frac{1}{2} (3\lambda_{hs}^2 + c_h^2 \lambda_{hs}^2 + c_s^2 (6\lambda_s)^2 + (2\lambda_s)^2), \end{aligned} \quad (\text{A-12})$$

which is equivalent to Eq. (3.29). The other equations are calculated in a similar manner, although the expressions are more complicated.

Bibliography

- [1] R. N. Lerner and J. McDonald, “Gauge singlet scalar as inflaton and thermal relic dark matter,” *Phys. Rev.* **D80** (2009) 123507, [arXiv:0909.0520 \[hep-ph\]](#).
- [2] R. N. Lerner and J. McDonald, “Higgs Inflation and Naturalness,” *JCAP* **1004** (2010) 015, [arXiv:0912.5463 \[hep-ph\]](#).
- [3] R. N. Lerner and J. McDonald, “A Unitarity-Conserving Higgs Inflation Model,” [arXiv:1005.2978 \[hep-ph\]](#). Accepted for publication in PRD.
- [4] E. Hubble, “A Relation between Distance and Radial Velocity among Extra-Galactic Nebulae,” *Proceedings of the National Academy of Science* **15** (Mar., 1929) 168–173.
- [5] **WMAP** Collaboration, E. Komatsu *et al.*, “Five-Year Wilkinson Microwave Anisotropy Probe Observations: Cosmological Interpretation,” *Astrophys. J. Suppl.* **180** (2009) 330–376, [arXiv:0803.0547 \[astro-ph\]](#).
- [6] A. A. Penzias and R. W. Wilson, “A Measurement of excess antenna temperature at 4080- Mc/s,” *Astrophys. J.* **142** (1965) 419–421.
- [7] E. Komatsu *et al.*, “Seven-Year Wilkinson Microwave Anisotropy Probe Observations: Cosmological Interpretation,” [arXiv:1001.4538 \[astro-ph.CO\]](#).
- [8] D. H. Lyth and A. R. Liddle, *The Primordial Density Perturbation*. Cambridge University Press, 2009.
- [9] G. N. Felder, L. Kofman, and A. D. Linde, “Instant preheating,” *Phys. Rev.* **D59** (1999) 123523, [arXiv:hep-ph/9812289](#).
- [10] G. N. Felder *et al.*, “Dynamics of symmetry breaking and tachyonic preheating,” *Phys. Rev. Lett.* **87** (2001) 011601, [arXiv:hep-ph/0012142](#).
- [11] A. D. Sakharov, “Violation of CP Invariance, C Asymmetry, and Baryon Asymmetry of the Universe,” *Pisma Zh. Eksp. Teor. Fiz.* **5** (1967) 32–35.
- [12] **Boomerang** Collaboration, A. Melchiorri *et al.*, “A measurement of Omega from the North American test flight of BOOMERANG,” *Astrophys. J.* **536** (2000) L63–L66, [arXiv:astro-ph/9911445](#).
- [13] **Supernova Search Team** Collaboration, A. G. Riess *et al.*, “Observational Evidence from Supernovae for an Accelerating Universe and a Cosmological Constant,” *Astron. J.* **116** (1998) 1009–1038, [arXiv:astro-ph/9805201](#).
- [14] **Supernova Cosmology Project** Collaboration, S. Perlmutter *et al.*, “Measurements of Omega and Lambda from 42 High-Redshift Supernovae,” *Astrophys. J.* **517** (1999) 565–586, [arXiv:astro-ph/9812133](#).
- [15] M. Markevitch *et al.*, “Direct constraints on the dark matter self-interaction cross-section from the merging galaxy cluster 1E0657-56,” *Astrophys. J.* **606** (2004) 819–824, [arXiv:astro-ph/0309303](#).
- [16] D. Clowe *et al.*, “A direct empirical proof of the existence of dark matter,” *Astrophys. J.* **648** (2006) L109–L113, [arXiv:astro-ph/0608407](#).

- [17] V. Springel *et al.*, “Simulating the joint evolution of quasars, galaxies and their large-scale distribution,” *Nature* **435** (2005) 629–636, [arXiv:astro-ph/0504097](#).
- [18] V. C. Rubin, N. Thonnard, and W. K. Ford, Jr., “Rotational properties of 21 SC galaxies with a large range of luminosities and radii, from NGC 4605 /R = 4kpc/ to UGC 2885 /R = 122 kpc/,” *Astrophys. J.* **238** (1980) 471.
- [19] B. Moore *et al.*, “Dark matter substructure within galactic halos,” *Astrophys. J.* **524** (1999) L19–L22.
- [20] W. J. G. de Blok, S. S. McGaugh, A. Bosma, and V. C. Rubin, “Mass Density Profiles of LSB Galaxies,” *Astrophys. J.* **552** (2001) L23–L26, [arXiv:astro-ph/0103102](#).
- [21] W. J. G. de Blok, A. Bosma, and S. McGaugh, “Simulating observations of dark matter dominated galaxies: towards the optimal halo profile,” *MNRAS* **340** (Apr., 2003) 657–678, [arXiv:astro-ph/0212102](#).
- [22] B. W. Lee and S. Weinberg, “Cosmological lower bound on heavy-neutrino masses,” *Phys. Rev. Lett.* **39** (1977) 165–168.
- [23] J. Bernstein, “KINETIC THEORY IN THE EXPANDING UNIVERSE,” CAMBRIDGE, USA: UNIV. PR. (1988) 149p.
- [24] J. McDonald, “Gauge Singlet Scalars as Cold Dark Matter,” *Phys. Rev.* **D50** (1994) 3637–3649, [arXiv:hep-ph/0702143](#).
- [25] M. Shaposhnikov, “Is there a new physics between electroweak and Planck scales?,” [arXiv:0708.3550 \[hep-th\]](#).
- [26] T. Asaka, S. Blanchet, and M. Shaposhnikov, “The ν MSM, dark matter and neutrino masses,” *Phys. Lett.* **B631** (2005) 151–156, [arXiv:hep-ph/0503065](#).
- [27] T. Asaka and M. Shaposhnikov, “The ν MSM, dark matter and baryon asymmetry of the universe,” *Phys. Lett.* **B620** (2005) 17–26, [arXiv:hep-ph/0505013](#).
- [28] E. K. Akhmedov, V. A. Rubakov, and A. Y. Smirnov, “Baryogenesis via neutrino oscillations,” *Phys. Rev. Lett.* **81** (1998) 1359–1362, [arXiv:hep-ph/9803255](#).
- [29] M. Shaposhnikov, “A possible symmetry of the ν MSM,” *Nucl. Phys.* **B763** (2007) 49–59, [arXiv:hep-ph/0605047](#).
- [30] M. Shaposhnikov and I. Tkachev, “The ν MSM, inflation, and dark matter,” *Phys. Lett.* **B639** (2006) 414–417, [arXiv:hep-ph/0604236](#).
- [31] A. Anisimov, Y. Bartocci, and F. L. Bezrukov, “Inflaton mass in the ν MSM inflation,” *Phys. Lett.* **B671** (2009) 211–215, [arXiv:0809.1097 \[hep-ph\]](#).
- [32] F. L. Bezrukov and M. Shaposhnikov, “The Standard Model Higgs boson as the inflaton,” *Phys. Lett.* **B659** (2008) 703–706, [arXiv:0710.3755 \[hep-th\]](#).
- [33] F. Bezrukov, D. Gorbunov, and M. Shaposhnikov, “On initial conditions for the Hot Big Bang,” *JCAP* **0906** (2009) 029, [arXiv:0812.3622 \[hep-ph\]](#).
- [34] F. L. Bezrukov, A. Magnin, and M. Shaposhnikov, “Standard Model Higgs boson mass from inflation,” *Phys. Lett.* **B675** (2009) 88–92, [arXiv:0812.4950 \[hep-ph\]](#).
- [35] F. Bezrukov and M. Shaposhnikov, “Standard Model Higgs boson mass from inflation: two loop analysis,” *JHEP* **07** (2009) 089, [arXiv:0904.1537 \[hep-ph\]](#).
- [36] A. O. Barvinsky, A. Y. Kamenshchik, and A. A. Starobinsky, “Inflation scenario via the Standard Model Higgs boson and LHC,” *JCAP* **0811** (2008) 021, [arXiv:0809.2104 \[hep-ph\]](#).
- [37] A. O. Barvinsky, A. Y. Kamenshchik, C. Kiefer, A. A. Starobinsky, and C. Steinwachs, “Asymptotic freedom in inflationary cosmology with a non-minimally coupled Higgs field,” *JCAP* **0912** (2009) 003, [arXiv:0904.1698 \[hep-ph\]](#).

- [38] A. De Simone, M. P. Hertzberg, and F. Wilczek, “Running Inflation in the Standard Model,” *Phys. Lett.* **B678** (2009) 1–8, [arXiv:0812.4946 \[hep-ph\]](#).
- [39] J. Garcia-Bellido, D. G. Figueroa, and J. Rubio, “Preheating in the Standard Model with the Higgs-Inflaton coupled to gravity,” *Phys. Rev.* **D79** (2009) 063531, [arXiv:0812.4624 \[hep-ph\]](#).
- [40] S. C. Park and S. Yamaguchi, “Inflation by non-minimal coupling,” *JCAP* **0808** (2008) 009, [arXiv:0801.1722 \[hep-ph\]](#).
- [41] V. Silveira and A. Zee, “Scalar Phantoms,” *Phys. Lett.* **B161** (1985) 136.
- [42] J. McDonald, “Electroweak baryogenesis and dark matter via a gauge singlet scalar,” *Phys. Lett.* **B323** (1994) 339–346.
- [43] C. P. Burgess, M. Pospelov, and T. ter Veldhuis, “The minimal model of nonbaryonic dark matter: A singlet scalar,” *Nucl. Phys.* **B619** (2001) 709–728, [arXiv:hep-ph/0011335](#).
- [44] M. C. Bento, O. Bertolami, and R. Rosenfeld, “Cosmological constraints on an invisibly decaying Higgs boson,” *Phys. Lett.* **B518** (2001) 276–281, [arXiv:hep-ph/0103340](#).
- [45] M. Peskin and D. Schroeder, *An introduction to Quantum Field Theory*. Westview Press, 1995.
- [46] M. Maggiore, *A Modern Introduction to Quantum Field Theory*. Oxford University Press, 2005.
- [47] S. O. I.L. Buchbinder and I. Shapiro, *Effective Action in Quantum Gravity*. Institute of Physics Publishing, 1992.
- [48] W. N. Cottingham and D. Greenwood, *An introduction to the Standard Model of Particle Physics*. Cambridge University Press, 2007.
- [49] S. Dawson, “Introduction to electroweak symmetry breaking,” [arXiv:hep-ph/9901280](#).
- [50] S. R. Coleman and E. J. Weinberg, “Radiative Corrections as the Origin of Spontaneous Symmetry Breaking,” *Phys. Rev.* **D7** (1973) 1888–1910.
- [51] M. Sher, “Electroweak Higgs Potentials and Vacuum Stability,” *Phys. Rept.* **179** (1989) 273–418.
- [52] C. Ford, D. R. T. Jones, P. W. Stephenson, and M. B. Einhorn, “The Effective potential and the renormalization group,” *Nucl. Phys.* **B395** (1993) 17–34, [arXiv:hep-lat/9210033](#).
- [53] G. ’t Hooft, “Dimensional regularization and the renormalization group,” *Nucl. Phys.* **B61** (1973) 455–468.
- [54] S. Weinberg, “New approach to the renormalization group,” *Phys. Rev.* **D8** (1973) 3497–3509.
- [55] M. Sher and H. W. Zaglauer, “Cosmic Ray Induced Vacuum Decay in the Standard Model,” *Phys. Lett.* **B206** (1988) 527.
- [56] J. R. Espinosa, G. F. Giudice, and A. Riotto, “Cosmological implications of the Higgs mass measurement,” *JCAP* **0805** (2008) 002, [arXiv:0710.2484 \[hep-ph\]](#).
- [57] E. E. Flanagan, “The conformal frame freedom in theories of gravitation,” *Class. Quant. Grav.* **21** (2004) 3817, [arXiv:gr-qc/0403063](#).
- [58] A. Ashtekar and A. Corichi, “Non-minimal couplings, quantum geometry and black hole entropy,” *Class. Quant. Grav.* **20** (2003) 4473–4484, [arXiv:gr-qc/0305082](#).
- [59] Y. Fujii and T. Nishioka, “MODEL OF A DECAYING COSMOLOGICAL CONSTANT,” *Phys. Rev.* **D42** (1990) 361–370.

- [60] M. C. Bergere and Y.-M. P. Lam, “Equivalence Theorem and Faddeev-Popov Ghosts,” *Phys. Rev.* **D13** (1976) 3247–3255.
- [61] A. Blasi, N. Maggiore, S. P. Sorella, and L. C. Q. Vilar, “Renormalizability of nonrenormalizable field theories,” *Phys. Rev.* **D59** (1999) 121701, [arXiv:hep-th/9812040](#).
- [62] D. I. Kaiser, “Frame independent calculation of spectral indices from inflation,” [arXiv:astro-ph/9507048](#).
- [63] E. W. Kolb, D. S. Salopek, and M. S. Turner, “Origin of density fluctuations in extended inflation,” *Phys. Rev.* **D42** (1990) 3925–3935.
- [64] T. E. Clark, B. Liu, S. T. Love, and T. ter Veldhuis, “The Standard Model Higgs Boson-Inflaton and Dark Matter,” *Phys. Rev.* **D80** (2009) 075019, [arXiv:0906.5595 \[hep-ph\]](#).
- [65] D. S. Salopek, J. R. Bond, and J. M. Bardeen, “Designing Density Fluctuation Spectra in Inflation,” *Phys. Rev.* **D40** (1989) 1753.
- [66] A. De Simone and A. Riotto, “On Resonant Leptogenesis,” *JCAP* **0708** (2007) 013, [arXiv:0705.2183 \[hep-ph\]](#).
- [67] **Particle Data Group** Collaboration, C. Amsler *et al.*, “Review of particle physics,” *Phys. Lett.* **B667** (2008) 1. And 2009 partial update for the 2010 edition.
- [68] D. H. Lyth and A. Riotto, “Particle physics models of inflation and the cosmological density perturbation,” *Phys. Rept.* **314** (1999) 1–146, [arXiv:hep-ph/9807278](#).
- [69] E. F. Bunn, A. R. Liddle, and M. J. White, 1, “Four-year COBE normalization of inflationary cosmologies,” *Phys. Rev.* **D54** (1996) 5917–5921, [arXiv:astro-ph/9607038](#).
- [70] M. E. Machacek and M. T. Vaughn, “Two Loop Renormalization Group Equations in a General Quantum Field Theory. 1. Wave Function Renormalization,” *Nucl. Phys.* **B222** (1983) 83.
- [71] M. E. Machacek and M. T. Vaughn, “Two Loop Renormalization Group Equations in a General Quantum Field Theory. 2. Yukawa Couplings,” *Nucl. Phys.* **B236** (1984) 221.
- [72] M. E. Machacek and M. T. Vaughn, “Two Loop Renormalization Group Equations in a General Quantum Field Theory. 3. Scalar Quartic Couplings,” *Nucl. Phys.* **B249** (1985) 70.
- [73] I. L. Buchbinder and S. D. Odintsov, “ASYMPTOTICAL PROPERTIES OF NONABELIAN GAUGE THEORIES IN EXTERNAL GRAVITATIONAL FIELDS,” *Sov. J. Nucl. Phys.* **40** (1984) 848.
- [74] I. L. Buchbinder, “QUANTUM FIELD THEORY RENORMALIZATION IN CURVED SPACE-TIME AND RENORMALIZATION GROUP EQUATIONS,” *Fortsch. Phys.* **34** (1986) 605–628.
- [75] N. Okada and Q. Shafi, “WIMP Dark Matter Inflation with Observable Gravity Waves,” [arXiv:1007.1672 \[Unknown\]](#).
- [76] V. Barger, P. Langacker, M. McCaskey, M. J. Ramsey-Musolf, and G. Shaughnessy, “LHC Phenomenology of an Extended Standard Model with a Real Scalar Singlet,” *Phys. Rev.* **D77** (2008) 035005, [arXiv:0706.4311 \[hep-ph\]](#).
- [77] W.-L. Guo and Y.-L. Wu, “The real singlet scalar dark matter model,” [arXiv:1006.2518 \[hep-ph\]](#).
- [78] C. E. Yaguna, “Gamma rays from the annihilation of singlet scalar dark matter,” *JCAP* **0903** (2009) 003, [arXiv:0810.4267 \[hep-ph\]](#).

- [79] **CDF and D0** Collaboration, T. Aaltonen *et al.*, “Combination of Tevatron searches for the standard model Higgs boson in the $W+W-$ decay mode,” *Phys. Rev. Lett.* **104** (2010) 061802, [arXiv:1001.4162 \[hep-ex\]](#).
- [80] **CDF** Collaboration, D. Benjamin, “Searches for a High Mass Higgs Boson at the Tevatron,” [arXiv:0906.1403 \[hep-ex\]](#).
- [81] X.-G. He, T. Li, X.-Q. Li, J. Tandean, and H.-C. Tsai, “Constraints on Scalar Dark Matter from Direct Experimental Searches,” *Phys. Rev.* **D79** (2009) 023521, [arXiv:0811.0658 \[hep-ph\]](#).
- [82] J. L. Bourjaily, “Determining the actual local density of dark matter particles,” *Eur. Phys. J.* **C40N6** (2005) 23–30, [arXiv:astro-ph/0410470](#).
- [83] Gaitskell, Mandic, and Filippini, “DM Tools Beta.” Website, August, 2010. <http://dmttools.brown.edu>.
- [84] S. Davidson and S. Sarkar, “Thermalisation after inflation,” *JHEP* **11** (2000) 012, [arXiv:hep-ph/0009078](#).
- [85] M. S. Turner, “Coherent Scalar Field Oscillations in an Expanding Universe,” *Phys. Rev.* **D28** (1983) 1243.
- [86] L. Kofman, A. D. Linde, and A. A. Starobinsky, “Towards the theory of reheating after inflation,” *Phys. Rev.* **D56** (1997) 3258–3295, [arXiv:hep-ph/9704452](#).
- [87] J. F. Donoghue, E. Golowich, and B. R. Holstein, *Dynamics of the standard model (Volume 2)*. Camb. Monogr. Part. Phys. Nucl. Phys. Cosmol., 1992.
- [88] E. Kolb and M. Turner, *The Early Universe*. Westview Press, 1994.
- [89] G. Huetsi, “Power spectrum of the SDSS luminous red galaxies: constraints on cosmological parameters,” *Astron. Astrophys.* **459** (2006) 375–389, [arXiv:astro-ph/0604129](#).
- [90] A. R. Liddle and S. M. Leach, “How long before the end of inflation were observable perturbations produced?,” *Phys. Rev.* **D68** (2003) 103503, [arXiv:astro-ph/0305263](#).
- [91] A. Ringwald, “EVOLUTION EQUATION FOR THE EXPECTATION VALUE OF A SCALAR FIELD IN SPATIALLY FLAT RW UNIVERSES,” *Ann. Phys.* **177** (1987) 129.
- [92] E. Elizalde and S. D. Odintsov, “Renormalization group improved effective potential for gauge theories in curved space-time,” *Phys. Lett.* **B303** (1993) 240–248, [arXiv:hep-th/9302074](#).
- [93] K. Ishikawa, “GRAVITATIONAL EFFECT ON EFFECTIVE POTENTIAL,” *Phys. Rev.* **D28** (1983) 2445.
- [94] J. Ellis, J. R. Espinosa, G. F. Giudice, A. Hoecker, and A. Riotto, “The Probable Fate of the Standard Model,” *Phys. Lett.* **B679** (2009) 369–375, [arXiv:0906.0954 \[hep-ph\]](#).
- [95] J. L. F. Barbon and J. R. Espinosa, “On the Naturalness of Higgs Inflation,” *Phys. Rev.* **D79** (2009) 081302, [arXiv:0903.0355 \[hep-ph\]](#).
- [96] C. P. Burgess, H. M. Lee, and M. Trott, “Power-counting and the Validity of the Classical Approximation During Inflation,” *JHEP* **09** (2009) 103, [arXiv:0902.4465 \[hep-ph\]](#).
- [97] S. R. Huggins and D. J. Toms, “ONE GRAVITON EXCHANGE INTERACTION OF NONMINIMALLY COUPLED SCALAR FIELDS,” *Class. Quant. Grav.* **4** (1987) 1509.
- [98] M. P. Hertzberg, “On Inflation with Non-minimal Coupling,” [arXiv:1002.2995 \[hep-ph\]](#).
- [99] C. P. Burgess, H. M. Lee, and M. Trott, “On Higgs Inflation and Naturalness,” *JHEP* **07** (2010) 007, [arXiv:1002.2730 \[hep-ph\]](#).

- [100] T. Han and S. Willenbrock, “Scale of quantum gravity,” *Phys. Lett.* **B616** (2005) 215–220, [arXiv:hep-ph/0404182](#).
- [101] J. Gomis and S. Weinberg, “Are Nonrenormalizable Gauge Theories Renormalizable?,” *Nucl. Phys.* **B469** (1996) 473–487, [arXiv:hep-th/9510087](#).
- [102] Y. B. Zeldovich and A. A. Starobinsky, “Particle production and vacuum polarization in an anisotropic gravitational field,” *Sov. Phys. JETP* **34** (1972) 1159–1166.
- [103] N. D. Birrell, P. C. W. Davies, and L. H. Ford, “EFFECTS OF FIELD INTERACTIONS UPON PARTICLE CREATION IN ROBERTSON-WALKER UNIVERSES,” *J. Phys.* **A13** (1980) 961–968.
- [104] L. H. Ford, “Gravitational Particle Creation and Inflation,” *Phys. Rev.* **D35** (1987) 2955.
- [105] E. Tomboulis, “1/N Expansion and Renormalization in Quantum Gravity,” *Phys. Lett.* **B70** (1977) 361.
- [106] S. Ferrara, R. Kallosh, A. Linde, A. Marrani, and A. Van Proeyen, “Superconformal Symmetry, NMSSM, and Inflation,” [arXiv:1008.2942 \[hep-th\]](#).
- [107] C. Rovelli, “Loop quantum gravity,” *Living Rev. Rel.* **11** (2008) 5.
- [108] V. Barger, P. Langacker, M. McCaskey, M. Ramsey-Musolf, and G. Shaughnessy, “Complex Singlet Extension of the Standard Model,” *Phys. Rev.* **D79** (2009) 015018, [arXiv:0811.0393 \[hep-ph\]](#).
- [109] I. Gogoladze, N. Okada, and Q. Shafi, “Higgs boson mass bounds in a type II seesaw model with triplet scalars,” *Phys. Rev.* **D78** (2008) 085005, [arXiv:0802.3257 \[hep-ph\]](#).
- [110] A. Pilaftsis and T. E. J. Underwood, “Electroweak-scale resonant leptogenesis,” *Phys. Rev.* **D72** (2005) 113001, [arXiv:hep-ph/0506107](#).
- [111] M. B. Einhorn and D. R. T. Jones, “Inflation with Non-minimal Gravitational Couplings in Supergravity,” *JHEP* **03** (2010) 026, [arXiv:0912.2718 \[hep-ph\]](#).
- [112] S. Ferrara, R. Kallosh, A. Linde, A. Marrani, and A. Van Proeyen, “Jordan Frame Supergravity and Inflation in NMSSM,” *Phys. Rev.* **D82** (2010) 045003, [arXiv:1004.0712 \[hep-th\]](#).